

University of
Strathclyde
Glasgow

Department of Pure and Applied Chemistry

**Through Barrier Detection Using Surface Enhanced Spatially
Offset Raman Spectroscopy**

Fay Nicolson

A thesis submitted to the Department of Pure and Applied Chemistry,
University of Strathclyde, in fulfilment of the requirements for degree of
Doctor of Philosophy.

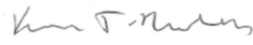
2018

The thesis is the result of the author's original research. This thesis incorporates published work which is the result of the author's original research. It has been composed by the author and has not been previously submitted for examination which has led to the award of a degree.'

Signed (Author):

Date:

Signed (Supervisor)*:



Date:

*Confirming author was primarily responsible for the composition of the published material within the thesis.

ACKNOWLEDGMENTS

Firstly I would like to start by thanking my supervisors Professor Karen Faulds and Professor Duncan Graham for the input, guidance and support you have given me throughout my PhD. Karen despite what you say, I learnt the resting bitch face from you – thanks for helping me to perfect it so well! Duncan, keep lunging and stay away from dancing on tables...I will continue to search for the full version of the clothes show! Jokes aside, thank you for everything – I've had some amazing opportunities during my PhD and for that I am incredibly grateful. I would also like to thank my supervisor, Professor Neil Shand at DSTL. Without your investment I simply would not have the results presented in this thesis. Thank you so much for all the instrumentation, as well as your valued knowledge, advice and support. I'll be in touch if I ever get a job at Red Bull! I would also like to extend my thanks to Konstantinos Plakas and Professor Mike Detty at University at Buffalo for all of the dye molecules. Furthermore, I would like to acknowledge EPSRC and DSTL for funding my PhD as well as the funding bodies that have provided me with grants to attend conferences; The RSC, Wiley and The ABS trust.

Huge thanks to the members of the Centre for Nanometrology (old and new) for all the fun - you have all made the last three and a half years incredible. Special thanks to Dr Lauren Jamieson and Dr Sam Mabbott for all of your help and support, I couldn't have done it without you both. Thanks to Dr Hayleigh May for all the helpful discussions. Additionally, thanks to Sam and Sureyya for your friendship and for taking my side in the farm simulator debate..."just seal with it". Shout out to Rachel Norman, Sian Sloan-Dennison, Craig Ward, Laura Frame, Ryan Kane and Alex Girard (Vegas) for the office banter and incredible SciX trips! Kirsty Milligan, Emma O'Connor and Rachael Cameron for always being up for wine...Rachael I still don't know how you do it!

Thank you to Professor Rohit Bhargava for the opportunity to work in your lab and to Rachel and Scott for looking after me...."Scott's Skinnies for life"! Additional thanks to WestCHEM for the financial support. Special thanks to Stuart Bonthron at Cobalt Light Systems for all the help with software and to Scott Rudder, Andrew Whitely and Tina Gong for the amazing Spring SciX trip! To Debbie for understanding what it's like to have a "thing" and for being a formatting queen, you're the best! To Rebekah for your friendship and tea trips, thank you.

Most importantly, I would like to thank my mum and dad for all their emotional and financial support throughout my education. It wouldn't have been possible without you both and I hope I have made you proud. Finally, thanks to Joe. Even though you have been on a ship for the last five months, I appreciate everything you do for me – at sea or in Glasgow. Thanks for your endless support, tolerating my sass, canoeing expertise and for always making me smile. I am truly grateful for everything.

ABSTRACT

In the fields of security and biomedical imaging there is a significant need to non-invasively probe through barriers, e.g. plastic, glass or tissue. Raman spectroscopy provides a means to solving this challenge since it provides a unique chemical fingerprint without the need to destroy the sample. In spite of this, conventional Raman can be limited by sample volume and thickness, often failing to probe beneath the surface or through samples obscured by an opaque barrier. Spatially offset Raman spectroscopy provides a means of overcoming the limitation associated with conventional Raman spectroscopy since it is capable of providing a unique chemical fingerprint of the analyte under study, even when obscuring barriers such as plastic or tissue are present. Furthermore, by combining the depth penetration benefits of SORS with the signal enhancing capabilities of SERS, SESORS is capable of achieving sample interrogation at even greater depth. Therefore, the focus of this research is to probe through barriers, specifically plastic and tissue, using both handheld CR and SORS instruments. The ability of both techniques to detect Raman and SERS analytes through barriers is explored and compared for applications involving security and biomedicine.

The use of conventional Raman and SORS to detect ethanol through varying thicknesses of plastic is investigated. Raman signals from an ethanol solution through plastic was detected through thicknesses of up to 21 mm using SORS in combination with multivariate analysis. SORS was compared to conventional Raman, where through barrier detection of ethanol took place through depths up to 9 mm.

Using a handheld SORS spectrometer, the detection of *ex vivo* breast cancer tumour models containing SERRS active nanotags through 15 mm of porcine tissue is demonstrated. In addition, SERRS-active nanotags were tracked through porcine tissue to depths of up to 25 mm. To date, this is the largest thickness that SERRS nanotags have been tracked through using a backscattering approach. This unprecedented performance is due to the use

of red-shifted chalcogenpyrylium-based Raman reporters to demonstrate the novel technique of surface enhanced spatially offset resonance Raman spectroscopy (SESORRS) for the first time. The same *ex vivo* tumour models are also used to demonstrate a multiplexed imaging system through depths of 10 mm using back scattering SESORRS.

The benefit of using red-shifted chalcogenpyrylium based Raman reporters for probing through large thicknesses of plastic and tissue barriers using SERS is also highlighted. Raman signals were collected from SERRS active nanotags through plastic thicknesses of up to 20 mm. The detection of SERRS-active nanotags taken up into *ex vivo* tumour models through depths of 5 mm of tissue is also shown. The advantages of applying multivariate analysis for through barrier detection when discriminating analytes with similar spectral features as the barrier is also clearly demonstrated.

Finally, resonant chalcogenpyrylium nanotags were used to demonstrate the benefit of using a resonant Raman reporter for superior low-level limits of detection using SESORS. Nanotags containing chalcogenpyrylium dye were observed at concentrations as low as 1 pM through 5 mm of tissue. This is compared to the non-resonant small molecule Raman reporter BPE which could only be detected at concentrations of 11 pM. Calculated limits of detection suggest that these SERRS nanotags can be detected at concentrations as low as 104 fM using SESORRS.

ABBREVIATIONS

Azopyridine	AZPY
Conventional Raman	CR
Gold Nanoparticles	AuNPs
Limit of detection	LOD
Localised surface plasmon resonance	LSPR
Mucin1	MUC1
Multicellular tumour spheroids	MTS
Nanoparticle	NP
Near infrared	NIR
Photothermal ablation therapy	PTA
Poly(methyl methacrylate)	PMMA
Polyethylene terephthalate	PET
Polypropylene	PP
Principal component analysis	PCA
Resonance Raman scattering	RRS
Spatially offset Raman spectroscopy	SORS
Surface enhanced Raman spectroscopy	SERS
Surface enhanced resonance Raman scattering	SERRS
Surface enhanced spatially offset Raman scattering	SESORS
Surface enhanced spatially offset resonance Raman spectroscopy	SESORS
<i>trans</i> -1,2-bis(4-pyridyl)-ethylene	BPE

Contents

Acknowledgements.....	ii
Abstract.....	iii
Abbreviations.....	v
Contents	6
1 Introduction.....	10
1.1 Nanoparticles.....	10
1.1.1 Nanoparticle synthesis	10
1.1.2 Localised Surface Plasmon Resonance.....	11
1.2 Raman Spectroscopy.....	14
1.2.1 Raman Scattering.....	15
1.2.2 Resonance Raman Scattering	18
1.2.3 Surface Enhanced Raman Scattering	19
1.2.4 Surface Enhanced Resonance Raman Scattering	20
1.2.5 Spatially Offset Raman Spectroscopy	22
1.2.6 Surface Enhanced Spatially Offset Raman Spectroscopy.....	28
1.3 Introductory Conclusions and Project Aims	30
1.4 References	32
2 Through Barrier Detection of Ethanol using Handheld Raman Spectroscopy - Conventional Raman versus Spatially Offset Raman Spectroscopy (SORS).....	37
2.1 Abstract.....	38
2.2 Introduction	39
2.3 Experimental.....	41
2.3.1 Instrumentation.....	41
2.3.2 Through barrier detection.....	41

2.3.3	Data processing	42
2.4	Results and Discussion.....	43
2.5	Conclusion	59
2.6	References	60
3	Through Tissue Imaging of a Live Breast Cancer Tumour Model Using Handheld Surface Enhanced Spatially Offset Resonance Raman Spectroscopy	62
3.1	Abstract.....	63
3.2	Introduction	64
3.3	Experimental.....	67
3.4	Results and Discussion.....	69
3.5	Conclusions	75
3.6	References	76
4	Multiplex Imaging of Live Breast Cancer Tumour Models Through Tissue Using Handheld Surface Enhanced Spatially Offset Resonance Raman Spectroscopy (SESORRS)	78
4.1	Abstract.....	79
4.2	Introduction	80
4.3	Experimental.....	83
4.4	Results and Discussion.....	84
4.5	Conclusions	90
4.6	References	92
5	Point and Shoot – The Benefit of Resonant Raman Reporters for Probing Through Plastic and Tissue Barriers Using Handheld Surface Enhanced Raman Spectroscopy (SERS)	94
5.1	Abstract.....	95
5.2	Introduction	96

5.3	Experimental.....	99
5.3.1	Synthesis of SERS nanotags	99
5.3.2	SERS measurements.....	100
5.3.3	Through barrier detection using plastic	100
5.3.4	Cell culture	100
5.3.5	Through barrier detection using tissue	101
5.3.6	Data processing	102
5.4	Results and discussion	102
5.5	Conclusions	115
5.6	References	116
6	Towards establishing a minimal nanoparticle concentration for applications involving surface enhanced spatially offset Raman spectroscopy (SESORS) in vivo	118
6.1	Abstract.....	119
6.2	Introduction	120
6.3	Experimental.....	123
6.4	Results and Discussion.....	126
6.5	Conclusion	132
6.6	References	133
7	Conclusions	135
8	Future work.....	141
9	Appendix.....	143
9.1	Materials and Methods.....	143
9.2	Instrumentation	143
9.2.1	Extinction Spectroscopy	143
9.2.2	Dynamic Light Scattering	143

9.2.3	NanoSight	143
9.2.4	SEM Measurements.....	143
9.2.5	Raman and SERS Measurements	143
9.2.6	SORS and SESORS Measurements.....	144
9.3	Data Analysis.....	144
9.4	Experimental.....	145
9.4.1	Nanoparticle Synthesis.....	145
9.4.2	Dye Preparation	145
9.4.3	Nanoparticle Functionalisation	145
9.4.4	Raman and SORS Measurements Involving Plastic Barriers .	146
9.4.5	Raman and SORS Measurements Involving Tissue Barriers .	146
9.4.6	Cell culture and Nanoparticle Incubation.....	148
9.5	Supporting information - Through Barrier Detection of Ethanol using Handheld Raman Spectroscopy - Conventional Raman versus Spatially Offset Raman Spectroscopy (SORS).....	149
9.6	Supporting information - Through Tissue Imaging of a Live Breast Cancer Tumour Model Using Handheld Surface Enhanced Spatially Offset Resonance Raman Spectroscopy	157
9.7	Supporting information - Multiplex Imaging of Live Breast Cancer Tumour Models Through Tissue Using Handheld Surface Enhanced Spatially Offset Resonance Raman Spectroscopy (SESORRS)	162
9.8	Supporting information - Point and Shoot – The Benefit of Resonant Raman Reporters for Probing Through Plastic and Tissue Barriers Using Handheld Surface Enhanced Raman Spectroscopy (SERS)	165
9.9	Supporting information - Towards establishing a minimal nanoparticle concentration for applications involving surface enhanced spatially offset Raman spectroscopy (SESORS) <i>in vivo</i>	168
10	Publications and Presentations.....	169

1 Introduction

The study of metallic nanoparticles (NPs) is an area of intense scientific research. The concept of nanotechnology was first introduced by Richard P. Feynman when he stated that 'There is plenty of room at the bottom', referring to the idea that key biological problems would be solved on the atomic scale.¹ Today, NPs are prevalent in a multitude of applications including cosmetics², electronics³ and diagnostics.⁴ Examples include the use of silver based NPs as antimicrobial and antibacterial agents due to their activity against a broad range of microbes and bacteria.^{5,6} Zinc oxide and titanium dioxide NPs are increasingly used in sunscreens due to their favourable cosmetic properties over micro-sized particles.⁷

1.1 Nanoparticles

NPs are defined as particles of any shape with at least one dimension in the range of 1-100 nm.⁸ Commonly synthesised metal nanoparticles include copper (Cu),⁹ silver (Ag)¹⁰ and gold (Au)⁸ which exhibit different physical and chemical properties to that of their bulk metal. Historically NPs were used to colour glass and ceramics, with the most famous example being the Lycurgus cup. The cup is made from glass containing Au and Ag NPs and appears green in reflected light but red in transmitted light.¹¹

1.1.1 Nanoparticle synthesis

Nanometer-sized gold nanoparticles (AuNPs) are of great interest since their chemical, electronic and optical properties can be exploited in a number of applications. The synthesis of colloidal gold can be traced back to 1857 when Michael Faraday outlined the formation of gold colloid by the aqueous reduction of chloroaurate (AuCl_4^-).⁴ He noted that the optical properties of the bulk material (solid) differed from that of colloidal gold. Upon reaction with a reducing agent, chloroaurate changes within minutes from yellow to the characteristic ruby red colour associated with gold colloid. Faraday reasoned

that the gold was now dispersed in the liquid in a very finely divided metallic state.¹² It is probable that this discovery formed the basis of metal nanoparticle research.

Formation of colloidal gold is a relatively easy process, requiring the mixing of reagents under well-controlled external conditions.¹³ Proposed in 1951, the Turkevich method produces AuNPs in the 10-20 nm range. In this method, AuNPs are produced by the reduction of chloroauric acid (HAuCl₄) at 100 °C with citric acid being used as both the reducing and stabilising agent. The negatively charged citrate ions coat the NPs with a negative charge, therefore creating electrostatic repulsion between the NPs and allowing them to remain stable in solution. Advancements in the Turkevich method came from Frens *et al.* in 1973, who also demonstrated that it was possible to control the AuNP size by varying the feed ratio of gold salt to sodium citrate.¹⁴ Reduction of sodium citrate concentration consequently diminishes the overall citrate ion concentration available for particle stabilisation. Thus, by lowering the concentration of citrate, it is possible to synthesize larger gold NPs.¹⁴

Properties of AuNPs are dependent on their size, shape, and surface composition, all of which can be controlled and easily manipulated during the synthetic process.¹³ Other NP shapes include rods,¹³ stars,¹⁵ and hollow AuNPs¹⁶, all of which are particularly interesting due to their ability to specifically tune their localised surface plasmon resonance (LSPR) into the near infrared (NIR) region during the synthetic process.

1.1.2 Localised Surface Plasmon Resonance

AuNPs display different properties from that of bulk gold. Their physical properties are strongly dependent on particle size, interparticle distance, nature of capping agent and shape of NP.¹⁷ Termed localised surface plasmon resonance (LSPR), the specific optical properties of gold can be attributed to the collective oscillation of electrons at the surface of a spherical

nanoparticle that are coupled with the electromagnetic field of incoming light. Such oscillations are induced by certain wavelengths of light depending on the size of the NP. NPs have sizes smaller than the wavelength of light and interact fully with the incident light, hence the electron cloud of the NPs are completely displaced by the electric field.¹⁸ As shown in Figure 1.1, all free electrons become polarised by the incident light and are thus drawn to the surface of the NP where they accumulate on opposite ends of the particle.¹³

When a sample of homogeneous nanoparticles is irradiated with a beam of light, the light is absorbed and scattered by the electrons. The sum of these two processes is known as extinction and the resulting extinction spectrum consists of a sharp absorption band, specific to that of the LSPR.¹⁹ This effect is described as “Mie theory” and was first reported in 1908.⁴ It describes the light scattering of absorbing and non-absorbing materials, and can therefore be applied to AuNPs to describe their properties due to the collective oscillation of free electrons in the conduction band.¹⁷

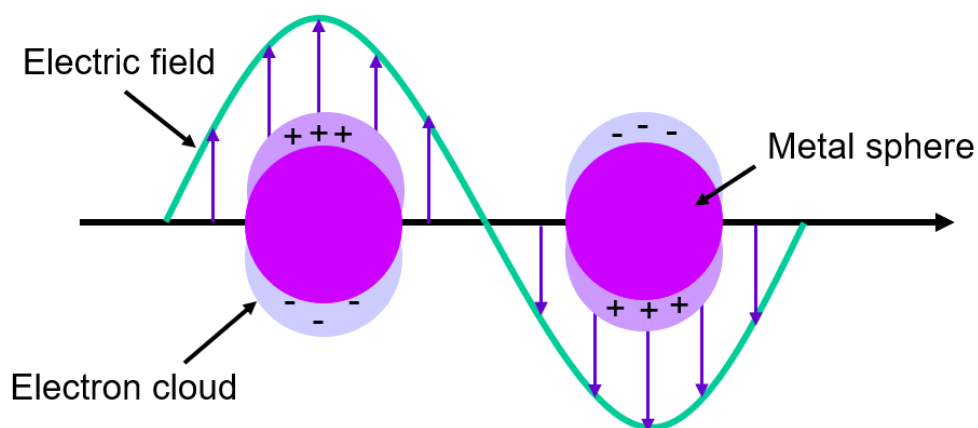


Figure 1.1 Schematic of the oscillation of electrons of spherical nanoparticles in an electromagnetic field. The electrons become polarised and are drawn to the surface of the metal NP.¹⁸

Spherical AuNPs with a size in the region of 20 nm have a characteristic ruby red colour. Colourmetric properties of AuNPs are dependent on the spectral position of the LSPR, thus solvents, capping agent, shape and size can all have an influence on the position of the LSPR.^{13,16} As the size of the AuNP increases, the position of the spectral band changes to a longer wavelength and is also referred to as a red shift.^{11,17} It is this shift which accounts for the colour change from red to purple of AuNPs as particle size increases. A change in dielectric constant of the medium surrounding the particle, which can also occur through surface modification with a biomolecule, will also induce a red shift.¹³

By monitoring changes in the LSPR, NPs can be used for biosensing applications since the LSPR is largely influenced by properties of the local environment.²⁰ It is therefore possible to monitor adsorbate-induced changes to the NP by observing the change in the extinction spectrum wavelength.²⁰ This was shown by Mirkin *et al.*, who attached non-complementary DNA oligonucleotides to gold NPs. Upon addition of complementary “sticky ended” oligonucleotide duplexes the AuNP solution changed from red to purple as they aggregated in solution. The transition from red to purple was a consequence of changes in the local dielectric environment of the NP caused by gold nanoparticle aggregation.²¹

NPs have been used in multiple applications including diagnostics,²² imaging,²³ drug delivery²⁴ and the treatment of cancer.²⁵ In recent years, red shifted nanomaterials have attracted increasing interest due to their potential for use in applications involving photothermal ablation therapy (PTA). This technique involves inducing hyperthermia through the use of red-shifted nanomaterials that absorb NIR light, which in turn, elevates the environmental temperature of the cells and induces cell death of malignant cells.²⁶ The use of dual-photothermal approaches, such as NPs functionalised with targeting biomolecules such as antibodies²⁷ or drug molecules²⁸ is particularly promising as it allows photo energy to be delivered directly to tumours with minimal damage and systemic effects to healthy cells and tissue.^{29,30} Furthermore, this technique offers up a potential alternative to common cancer treatments such as chemotherapy and radiotherapy^{31,32} which not only damage cancerous but also healthy cell.

1.2 Raman Spectroscopy

Raman spectroscopy is a form of vibrational spectroscopy which provides molecularly specific patterns of molecules in a range of samples, e.g. pharmaceutical or cellular.³³ Raman spectroscopy is a scattering process which relies on the inelastic scattering of incident light. It was first suggested in 1923 by Smekal,³⁴ and was subsequently observed experimentally by Raman and Krishnan in 1928 when they successfully demonstrated the scattering effect in a series of liquid and vapours.³⁵ Today Raman spectroscopy is a widely used analytical tool which has been implemented in many applications including pharmaceutical,²⁸ security,³⁶ biosensing,³⁷ and mineralogy.³⁸ More specifically, advancements in instrumentation has allowed for the translation of the Raman technique into handheld spectrometers for use in the field,³⁹ as well as benchtop mapping devices which make it possible to analyse and image the whole surface area of the analyte of interest using Raman spectroscopy.³³

1.2.1 Raman Scattering

When incident light interacts with a molecule it can be absorbed, scattered or transmitted. If the energy of the incident photon coincides with the band gap energy of an electronic transition within the molecule, the molecule is promoted from the ground state to an excited state. The loss of energy of the incident light, due to the absorption, can be measured. For scattering to occur, the photon does not need to have an energy that matches an energy level of the molecule. Instead, when incident light interacts with a molecule, distortion and polarisation of the electron cloud centred around the molecule takes place. This creates a short lived virtual state. Relaxation of the electron cloud results in the release of light in the form of scattered radiation.^{33,40}

The majority of scattered radiation does not change in frequency; this is known as Rayleigh scattering. It is termed elastic scattering since the scattered light has the same frequency as that of the incident light. Weaker, inelastic scattering processes can also take place.³³ In this instance, the energy is transmitted from the incident photon to the molecule, or vice versa, and the scattered photon differs in energy from the incident photon by one vibrational unit.^{33,40} This phenomenon is known as Raman scattering with two potential processes taking place; Stokes or anti-Stokes.³³

For Stokes scattering to occur, molecules in the ground vibrational state are excited to a virtual energy level by the incident light. They then scatter photons with a lower energy than that of the incident photons.^{33,40} Consequently, molecules are promoted to a higher vibrational energy than the original ground state since the molecules relax to an excited vibrational state. In contrast, anti-Stokes scattering occurs when molecules already in an excited vibrational state and are excited to a virtual energy level. They then scatter photons are scattered to a lower vibrational energy. All three scattering processes; Rayleigh, Stokes and anti-Stokes are illustrated in the Jablonski diagram, Figure 1.2. The difference in energy between the incident and scattered photons is represented by the lengths of the arrows.^{40,41}

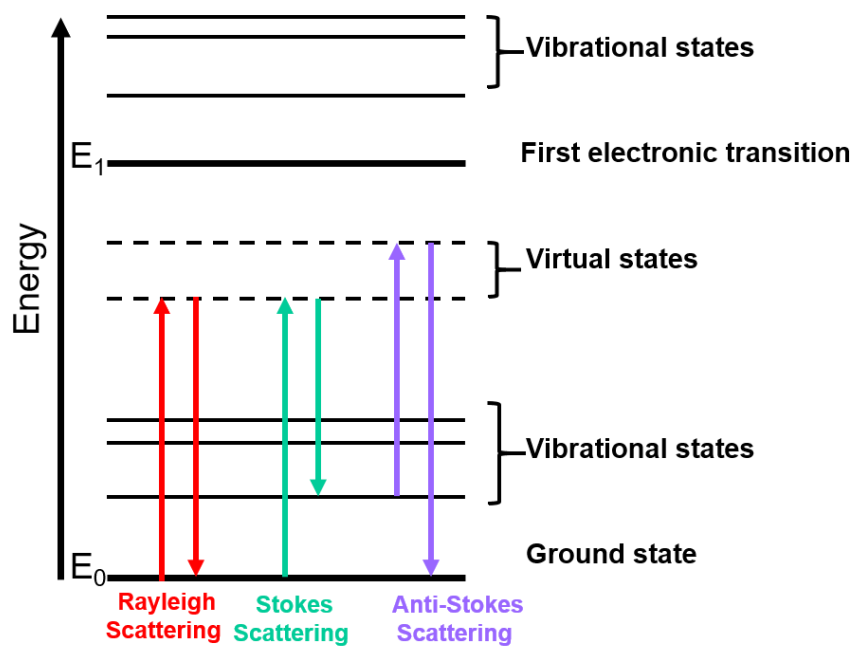


Figure 1.2 Jablonski Diagram depicting the three scattering processes; Rayleigh, Stokes and anti-Stokes.

The proportion of photons that will be Stokes or anti-Stokes scattered is dependent on the population of the excited state. As shown in Equation 1, the Boltzmann equation can be used to determine the number of molecules that are in their ground or excited vibrational state, where N_n is the number of molecules in the excited vibrational energy levels, N_m is the number of molecules in the ground vibrational levels, g is the degeneracy of the energy levels, $E_n - E_m$ is the difference between the vibrational energy levels, E_n and E_m , k is the Boltzmann constant (1.3807×10^{-23}) and (T) is the temperature.

Equation 1

$$\frac{N_n}{N_m} = \frac{g_n}{g_m} \exp \left[\frac{-(E_n - E_m)}{kT} \right]$$

Prior to interaction with the laser, the majority of molecules will be at rest and are most likely to be in the ground vibrational state at room temperature.

Thus, the majority of Raman scattering is observed as Stokes scattering. At higher temperatures, a larger proportion of photons will be anti-Stokes scattered since a larger proportion of molecules will be in a vibrationally excited state.^{33,42}

The Raman shift, given in wavenumbers (cm^{-1}), is the difference in energy between the initial and final vibrational levels ($\bar{\nu}$) is calculated in Equation 2, in which λ represents the wavelength of the incident and scattered photons respectively.⁴³ This is what is plotted on the spectrum.

Equation 2

$$\bar{\nu} = \frac{1}{\lambda_{\text{Incident}}} - \frac{1}{\lambda_{\text{Scattered}}}$$

Although Raman spectroscopy is both qualitative and quantitative, it is a relatively weak analytical process with only one in every $10^6 - 10^8$ scattered photons being Raman scattered.³³ The intensity of the Raman scattering is described in Equation 3, where I is the Raman intensity, K is a constant, l is the power of the laser, α is the polarizability and ν the frequency.

Equation 3

$$I = Kl\alpha^2\nu^4$$

Since intensity is proportional to the fourth power of the laser frequency, the intensity of Raman signal can be improved through the use of a shorter laser excitation wavelength.⁴⁴ However, by using a laser with a higher frequency, there is a higher potential for burning and sample degradation as most molecules absorb light at these wavelengths. One of the major advantages of Raman spectroscopy is the ability to derive label-free and non-destructive spectral information with minimal sample preparation however, the signal obtained is often inherently weak.⁴⁵ Therefore, several approaches can be used to improve the sensitivity of Raman spectroscopy including resonance Raman scattering and surface enhanced Raman scattering.³³

1.2.2 Resonance Raman Scattering

Resonance Raman scattering (RRS) utilises a laser which corresponds to an electronic transition in the molecule of interest, which in turn, enhances the Raman scattering of photons. Enhancements of 10^6 have been observed,³³ but enhancements in the order of 10^3 - 10^4 are more commonly reported.⁴⁶ RRS can be used in the identification of biological compounds, particularly if they possess chromophores.³³ For example, RRS has been used extensively for the study of malaria infections most commonly via the detection of hemozoin⁴⁷ or studying haeme containing proteins.⁴⁸

As shown in Figure 1.3, RRS results from the absorption of a photon to an excited virtual state within the first electronic state, whereas in Raman scattering the photon is excited to a virtual energy level between the ground and the first excited vibrational electronic state. As a result, the vibrations associated with the electronic state are greatly enhanced and RRS allows for a more intense Raman spectrum to be obtained.

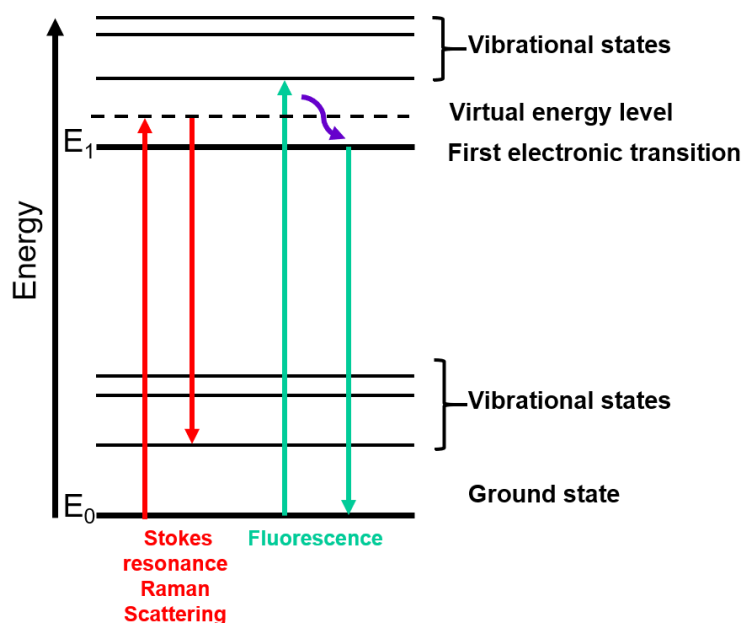


Figure 1.3 Jablonski diagram demonstrating Stokes resonance Raman scattering and fluorescence processes. The arrows demonstrate the transition between energy levels when the laser is in resonance with an electronic transition.

When the laser energy matches an electronic transition in the molecule of interest, competing electronic processes such as fluorescence can also occur (Figure 1.3).⁴⁵ In this instance, the molecule first absorbs a high energy photon to the lowest vibrational state of the excited electronic state. Then, then slow vibrational relaxation of the system occurs, followed by the emission of the photon to a longer wavelength.³³ Fluorescence backgrounds can obscure Raman peaks, however each process occurs on different time scales with fluorescence process typically occurring in nanoseconds while Raman scattering is faster and completed in picoseconds or less. Pulsed lasers can be used to try and separate these two effects on the time scale, thus minimising the amount of fluorescence that occurs.⁴⁹ Fluorescence can also be overcome through the use of NPs which are known to quench the fluorescent background⁵⁰ or by moving away from the resonance condition through the use of a longer excitation wavelength.³³

1.2.3 Surface Enhanced Raman Scattering

Raman scattering can be further enhanced when the analyte of interest is adsorbed onto a roughened metal surface in a technique known as surface enhanced Raman spectroscopy (SERS). SERS was originally observed by Fleischmann *et al.*, in 1974 when an enhancement in Raman signal from pyridine was observed in the presence of a silver electrode.⁵¹ Such observations led to different theories emerging on the origin of the SERS effect with Jeanmarie and Van Duyne⁵² suggesting that the enhancement was due to electromagnetic effects and Albrecht and Creighton proposing that it was due to a charge transfer effect.^{53,54}

The electromagnetic enhancement theory attributes SERS enhancement to the idea that when an analyte is adsorbed onto, or in close proximity to a metal surface, an interaction takes place between the analyte and the LSPR.⁵⁵ When energy from the incident laser light interacts with a sample of NPs, oscillation of the electrons in the conduction band takes place, thus

increasing the local field experienced by the analyte adsorbed onto the metal NP surface. Consequently, the analyte molecule experiences greater polarisation and significant enhancement in Raman scattering is observed.^{55,56} Substantial enhancement in SERS signal is observed when NPs are in close proximity to each other, resulting in an interaction between surface plasmons on neighbouring particles. As a result, regions known as “hot spots” are created, owing to the fact that a large electric field is generated at the junctions between the NPs thus resulting in a strong SERS enhancement.^{56,57}

The charge transfer effect relies upon the formation of a bond between the analyte and the metal's surface atoms, thus forming a charge transfer complex.^{33,56} Enhancement in Raman signal is believed to proceed via the creation of new electronic states, which arise from bond formation between the analyte and metal surface, subsequently creating a new state that is in resonance with the laser excitation wavelength.⁵⁸ Analytes with loosely bound electrons, for example conjugated systems or aromatic compounds, have greater sensitivity to charge transfer interactions. Although the charge transfer effect plays a part in SERS enhancement, it is generally believed that the electromagnetic effect plays a much more significant role.^{33,58}

1.2.4 Surface Enhanced Resonance Raman Scattering

Surface enhanced resonance Raman scattering (SERRS) combines both RRS and SERS to generate a signal enhancement of up to 10^{14} - 10^{15} orders of magnitude.^{59,60} SERRS is achieved when the analyte adsorbed onto the metal surface has an electronic transition that corresponds to the frequency of the laser excitation.^{55,61} One of the main advantages of SERRS is that it can be used to reduce fluorescence backgrounds commonly observed in Raman spectra due to quenching of fluorescence by the metal surface.^{55,62} This in turn, allows reduced laser powers to be used which can ultimately reduce sample degradation. Excellent Raman scattering can be obtained

from both fluorescent and non-fluorescent molecules. The main criteria for effective SERRS is that a good chromophore exists and that the dye adheres strongly to the metal NP surface.^{55,63}

SERRS holds particular promise over conventional fluorescence methods, specifically in multiplexing applications.⁶⁴ Techniques involving fluorescence typically produce broad emission bands, thus providing very little structural information and large spectral overlap occurs when multiple molecules are present in a sample. As a result, multiple excitation wavelengths are often required when multiple fluorophores are present.⁶⁴ Conversely, SERRS provides a sharp fingerprint spectrum, even when multiple analyte molecules exist, making it extremely useful for multiplexed applications.^{65,66} Using SERRS, Faulds *et al.*, reported the multiplexed detection of six labelled oligonucleotides in combination with a chemometric approach.⁶⁴ Reports in the literature also demonstrate the possibility to distinguish between five dye labelled DNA sequences using two different laser excitations that specifically match an electronic transition of a particular subset of Raman reporters.⁶⁷ Gracie *et al.*, quantified three meningitis pathogens in a multiplex assay and reported picomolar limits of detection, thus eliminating the need for current time consuming culture based methods.²²

NPs can be functionalised with a Raman reporter to create a “nanotag”. Gambhir *et al.*, successfully multiplexed ten different SERS active nanotags that were injected into a living mouse.²³ Furthermore, nanotags can be used in combination with targeting moieties such as antibodies and thus have the potential to be used in preclinical imaging models.⁶⁸ Such approach typically involves the use of a laser with an excitation wavelength in the NIR region. Penetration of NIR light through tissue is greater than that from a visible source since tissue will scatter more and absorb less at longer wavelengths.^{23,69}

Several groups have explored the use of targeted SERS nanotags for *in vivo* applications. Kircher *et al.*, used dual functionalised Au nanoprobe with a NIR active dye and an EGFR specific antibody to successfully target tumours

in vivo.⁵⁹ Endoscopic imaging of SERS nanotags was demonstrated by Liu *et al.*, who functionalised the SERS nanotags with antibodies to specifically target oesophageal cells over expressing EGFR and HER2 in a rat models.⁷⁰ Furthermore, DNA aptamers have also been explored as an alternative to traditionally used antibody techniques due to their low cost and immunogenicity. DNA aptamer functionalised nanotags have been used in the *in vivo* imaging of mucin1 (MUC1), a glycoprotein over expressed in 90% of breast cancer cases.⁷¹ SERS nanotags specifically targeted MUC1 positive tumours whilst the nanoparticles were not uptaken into MUC1 negative tumours. The Raman analysis on both the MUC1 positive and negative expressing tumours was then carried out *ex vivo*, perhaps due to the depth limitations of confocal Raman spectroscopy. As such, whilst several reports in the literature demonstrate the potential to target and image cells⁷² and tumors^{60,71,73} *in vivo* using functionalised nanoparticles, little knowledge exists on the ability to detect tumours at clinically relevant and significant depths. Therefore, in order to bring the technique of Raman spectroscopy closer to clinical translation, other Raman imaging approaches must be explored in order to detect nanotags at notable depth.

1.2.5 Spatially Offset Raman Spectroscopy

Raman spectroscopy is a frequently used research technique in the biomedical^{22,74} and defence fields.^{36,39,75} When applied in the backscattering geometry, Raman spectroscopy is a promising analytical technique, generating a unique chemical fingerprint which gives chemical and molecularly specific, sensitive sample evaluation. Despite this, conventional Raman (CR) and SERS can be limited by sample volume and thickness, often failing to provide a non-destructive means capable of adequately determining the chemical composition of subsurface layers in turbid media.⁷⁶ Conversely, spatially offset Raman spectroscopy (SORS) provides a means

of subsurface analysis, even when obscuring barriers such as plastic or tissue are present.⁷⁶

The diffuse component of light is capable of penetrating turbid media through depths of several centimetres. It is formed as a result of scattering effects which completely randomise photon direction. Therefore, SORS relies on the fact that deeper photons are more likely to migrate laterally before they reach their point of collection, and diffuse in multiple directions compared to surface photons.^{76,77} As depicted in Figure 1.4, by varying the distance of the collection probe from the point of laser excitation (typically in the region of a few mm) it is therefore possible to acquire Raman contributions from the subsurface layers. As a result, signals collected close to the point of laser excitation will be made up of a higher proportion of surface signal, however as the spatial offset increases, deeper layer photons will begin to dominate the spectra.^{76,78}

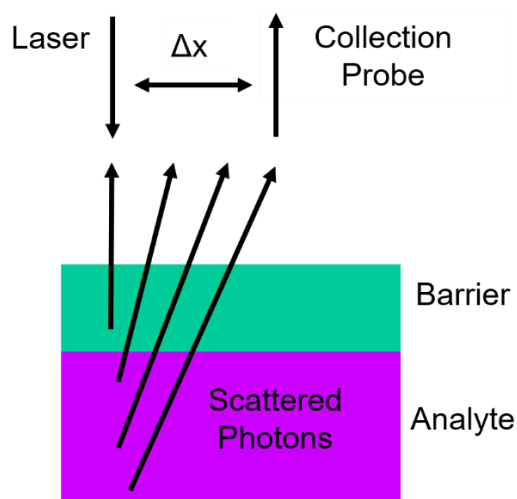


Figure 1.4 Principal of SORS using a back-scattering geometry. As the collection point is moved further away from the point of laser excitation Δx , photons from the deeper layers begin to dominate the acquired spectra.

Transmission Raman is considered a special case of SORS, relying on an extreme spatial offset. In such instance, the laser beam and collection zone are on opposite sides of the sample. Unlike SORS, which can provide information on the various layers within a sample, transmission Raman

scattering can generate volumetric information on the entire sample. It is therefore useful in detecting specific signals at an unknown location in a sample.⁷⁷⁻⁷⁹

SORS was first demonstrated by Matousek *et al.*, where the authors utilised a two-layer sample composed of a 1 mm Poly(methyl methacrylate) (PMMA) layer followed by a 2 mm thick layer of *trans*-stilbene powder using a backscattering configuration.⁷⁶ A set of spectra was then obtained at varying spatial offsets, Figure 1.5. The *trans*-stilbene reference spectrum and the PMMA reference spectrum are shown at the top and bottom respectively of Figure 1.5. As the spatial offset is increased from 0 to 2.5 mm (0.5 mm increments), the contribution of PMMA in the acquired spectra decreases as the spatial offset increases, i.e. a lesser contribution from the surface layer is observed at the largest spatial offset. This therefore demonstrates the potential to extract the chemical composition of subsurface layers using the SORS approach.⁷⁶

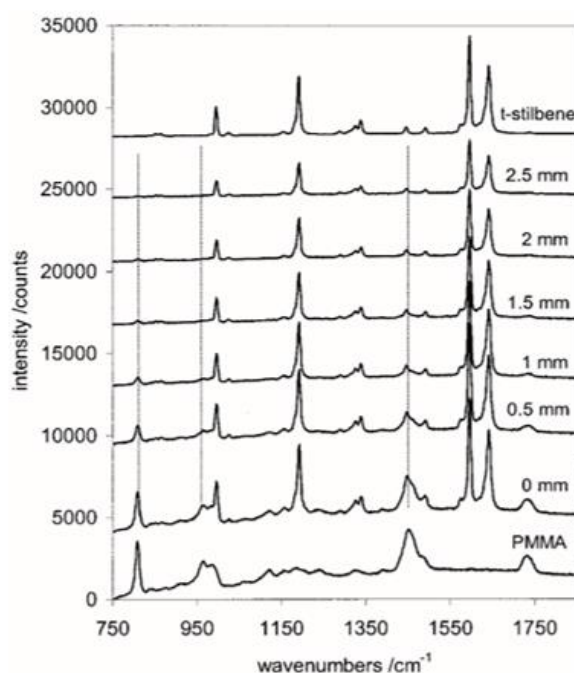


Figure 1.5 A set of SORS spectra from a two-layer system comprised of a 1 mm PMMA layer followed by a 2 mm thick layer of *trans*-stilbene powder. The *trans*-stilbene reference spectrum and the PMMA reference spectrum are at the top and bottom respectively. As the spatial offset is increased from 0 to 2.5 mm (0.5 mm increments), the contribution of the PMMA to the acquired spectra diminishes. Reprinted with permission from *Appl. Spectrosc.* 2005, 59 (4), 393.

Known as inverse SORS, spatially offset Raman measurements can also be deployed using a ring-shape laser illumination geometry.⁸⁰ In this instance, the Raman light can be collected through fibers at centre of a probe and the laser is delivered in the shape of a ring that is centred around the collection zone.^{81,82} As such, the SORS spatial offset can be controlled by simply varying the radius of the ring illumination zone. Furthermore, all of the Raman spectra are subsequently registered on one CCD chip, thus all collected spectra are subjected to the same imaging distortions since they are collected through the same set of CCD pixels.⁷⁹ Such approach can typically generate a higher signal to noise ratio than conventional SORS therefore giving rise to a clearer spectra. Perhaps the most important benefit of this technique is its suitability for *in vivo* imaging applications. Inverse SORS allows a higher laser power to be delivered to the sample since the laser radiation is spread over an extended illumination area, thus permitting the delivery of a higher laser power to the tissue sample in situations where laser intensities must be considered, e.g. *in vivo* applications.^{80,81}

In recent years, the SORS approach has been applied to a number of applications including pharmaceutical analysis,⁸³ security⁸⁴ and disease diagnostics.⁸² Security applications include the probing of powders held in envelopes,⁸⁰ the detection of explosives through plastic containers,⁸⁴ and alcohol through up to 4 mm of coloured glass.⁸⁵ More specifically, the detection of hydrogen peroxide, a critical component of liquid explosives, was demonstrated by Eliasson *et al.*,⁸⁴ through a range of plastic and glass containers. Bloomfield *et al.*, successfully detected ammonium nitrate through 4.5 mm of pearl polypropylene as well as alcohol through 4 mm of coloured glass.⁸⁶ The authors highlighted the benefit of using SORS over conventional Raman techniques for through barrier detection, particularly when similar spectral features are present in both the analyte and barrier spectrum. The SORS technique has also been demonstrated at a laser excitation of 1064 nm where the advantage of a longer wavelength to overcome fluorescence issues, associated with the presence of glass barriers, was discussed.⁸⁷ SORS has also been shown to be useful for the stand-off

detection of explosives through containers at located at distances of 12 m and greater.^{88,89} As such, the applicability of SORS for non-invasive screening methods related to the has advanced to the deployment of benchtop SORS instruments in several airports worldwide for the screening of liquids, e.g. cosmetics or medicines.⁸¹

Other areas where SORS methods have been adopted include the assessment of food quality,⁹⁰ pharmaceutical analysis,^{83,91} the detection of counterfeit alcohol.⁹² Goodacre *et al.*, utilised SORS for the detection of counterfeit alcohol through glass bottles. In combination with multivariate analysis, methanol was detected at concentrations well below the maximum tolerable level for human consumption.⁹² Using SORS, Bloomfield *et al.*, demonstrated the advantage of using SORS for the non-invasive inspection of chemicals using in the pharmaceutical manufacturing process.⁹³ The non-invasive nature of this technique allows for the safe inspection of chemicals as well as limiting the risk of cross contamination and exposure to external environmental conditions.⁹³ SORS has also been used in the monitoring the quality of red blood cells,⁹⁴ again demonstrating that the spectroscopic technique can be used to retrieve chemical information without compromising the sterility of the system.

The introduction of SORS has also opened up new avenues for medical applications; namely non-invasive disease diagnostics.⁷⁸ Examples include the analysis of bone^{82,95,96} and cancerous tissue.^{78,97,98} Currently, the non-invasive diagnosis of osteoporosis is performed using dual energy x-ray absorptiometry however, it is limited in part, by its inability to measure the inorganic component of bone, mainly collagen. As such, only 60-70% of fracture risks are predicted using methods involving dual energy x-ray absorptiometry.^{95,82} SORS has been shown to be capable of generating information on both the inorganic and organic components of bone from chicken and human bone.^{95,82} SORS has been used to measure subcortical bone tissue and depth-resolved biochemical variability in intact, exposed murine bones. Furthermore, the technique was applied to study a mouse model of the bone disorder *osteogenesis imperfecta*.⁹⁶ The results implied

that SORS is more sensitive to disease-related biochemical differences in subcortical trabecular bone and marrow compared to CR spectroscopy. SORS was also investigated for the spectral depth profiling of two common types of bone tissue engineering scaffolds, bioactive glass foams and biodegradable poly(lactic-co-glycolic acid) (PLGA), which are often difficult to measure using confocal techniques due to the depth limitations associated with such measurements.⁹⁶ In order to mimic *in situ* detection of bone mineralization in the subsurface regions of the scaffolds, layered samples of scaffold and hydroxyapatite (HA) powder were analysed. Detection of HA was achieved through layers of up to 2.3 mm and the results demonstrated the feasibility of using SORS as tool for non-destructive characterisation of scaffold-based tissue engineering constructs.

Using transmission SORS, cancerous calcifications in breast tissue have also been identified.^{97,98} The authors reported the ability to detect clinically relevant concentrations of calcium hydroxyapatite and calcium oxalate monohydrate at depths of 20 mm.⁹⁸ The depth penetration achieved using the SORS approach was approximately two orders of magnitude higher than that achieved using CR.⁷⁸ However, the clinical depth used in wider mammographic screening programmes is 50 mm, thus further increases in penetration depth is required. This can be achieved by further enhancing the quality of the detected Raman signal by increasing its intensity through the incident laser power, however safety illumination levels limit this approach for use in human studies.⁹⁸ In spite of this, Ghita *et al.*, recently reported the detection of calcium hydroxyapatite at clinically relevant concentrations and depths of 40 mm in tissue mimics. Such penetrations depths were obtained by increasing the power of the incident laser light over a larger illumination area and also by increasing the slit width and grating dispersion to achieve higher signal to noise ratios through clinically relevant depths, thus bringing the SORS technique one step closer to clinical translation.⁹⁹

Other methods to increase depth penetration include enhanced data processing methods such as multivariate analysis tools,⁷⁸ and the

combination of both the SERS and SORS techniques to yield surface enhanced spatially offset Raman spectroscopy.

1.2.6 Surface Enhanced Spatially Offset Raman Spectroscopy

Surface enhanced spatially offset Raman spectroscopy (SESORS) combines the depth penetration benefits of SORS with the signal enhancing capabilities of SERS to achieve greater sample interrogation at significant depth.¹⁰⁰ By functionalising nanoparticles with a reporter molecule, biomolecule, or both, the SESORS technique allows signal to be detected at depths superior to traditional CR and SERS approaches.¹⁰¹ The SESORS technique is demonstrated in 2010 by Stone *et al.*¹⁰¹ Silver NPs were functionalised with a NIR active dye and inserted into a tissue specimen with a thickness of 25 mm. Further depth penetration was achieved through optimisation of both instrumentation and choice of nanotag which allowed Stone *et al.* to demonstrate the ability to detect signal from nanotags buried at depths of 45 – 50 mm in tissue.¹⁰⁰ In both instances, signal was collected using a benchtop system with a transmission optical approach, 830 nm laser excitation wavelength. In contrast to the initial study,¹⁰¹ silver NPs were replaced by gold NPs which were then functionalised with Raman reporters such as *trans*-1,2-bis(4-pyridyl)-ethylene (BPE) and encapsulated in a silica shell. At the time of publication, these nanotags were commercially available under the tradename “Cabot”. The same study also showed the possibility to distinguish between four different commercially available SERS nanotags buried at depths of 20 mm. In this instance, the four individual nanotags were injected into each corner of a tissue section. Since the spectral fingerprint of the four nanotags was significantly different for each Raman reporter, the authors were able to assign a specific peak in each of the four spectra to enable the spatial multiplex detection using SESORS through depths of 20 mm.¹⁰⁰

Using a transmission geometry and a 830 nm excitation wavelength, Xie *et al.*, functionalised the same commercially available nanotags used in a

previous report,¹⁰⁰ with bisphosphonates and tracked them through 20 mm of tissue.¹⁰² Bisphosphonates, a class of drugs used in the treatment of osteoporosis, specifically bind to calcium phosphate salts and thus through the use of a SERS active nanotag, provide specific identification of bisphosphonate location.

SESORS has been used in biosensing applications including the detection of glucose.¹⁰³ SERS active substrates were implanted into rats to monitor glucose concentration in the interstitial fluid of six rats. The concentration was measured using a backscattering optical approach, and the authors reported the ability to perform quantitative *in vivo* glucose sensing for up to 17 days using SESORS.¹⁰⁴ Using the same optical set-up, the ability to detect low levels of bio-analytes through the skull was also investigated by Sharma *et al.*, who demonstrated the detection of Cabot nanotags through 8 mm of bone.¹⁰⁵ The same nanotags used in a previous report by Stone *et al.*,¹⁰⁰ were injected into tissue and detected through varying thicknesses of bone (3 – 8 mm).¹⁰⁵ Spectra were collected using a 785 nm laser as the excitation source and a custom made fiber bundle to collect the scattered Raman photons. The same study investigated the concentration of nanotags required to obtain a SERS signal through 3 mm of bone using SORS. The stock nanotags were detected at a 40 x dilution ($\sim 2 \times 10^{12}$) and the results were validated using a chemometric approach. In addition, the same SERS nanotags were spin coated onto glass slides and tracked through 6.5 mm of porcine tissue.¹⁰⁶ Measurements were performed using a 785 nm laser which was coupled to one of two fiber optic probes. The probes were angled at 90° to each other. For surface measurements, the collection probe coupled to the laser was used for both excitation and collection measurements. Both probes were used for SORS measurements, i.e. probe one was used for laser excitation whereas probe two was used to collect that Raman signal at spatial offsets up to 6.37 mm.¹⁰⁶

SESORS has also been utilised for the detection of neurotransmitters through the skull.¹⁰⁷ In this instance gold nanoparticles were used to enhance

the Raman scattering properties of three neurotransmitters. The authors successfully measured melatonin, epinephrine, and serotonin concentrations at levels as low as 100 μM in a brain tissue mimic through a cat skull using the SESORS approach. The brain tissue mimic was modified with neurotransmitters. Principal component analysis was used to spectrally differentiate between the bone surface layer and the subsurface tissue layer, and using the same multivariate analysis approach, successful identification of each individual neurotransmitter was achieved.

The medical application of SESORS *in vivo* is hindered by potential toxicity issues, associated with the introduction of SERS nanoparticles into a living system. To date, these have not been fully addressed.⁷⁸ However, combined with targeted delivery of nanoparticles to diseased cells using a specific biomolecule such as an antibody, as well as the potential to also deliver a therapeutic response e.g. through drug release, it is reasoned that the SESORS technique holds notable potential for applications in the field of biomedicine. Multiple groups have explored the use of targeted SERS nanotags for *in vivo* imaging applications in mouse models,^{60,71} as well as for use in multiplexing applications,^{23,108} however they have been limited in their ability to probe through clinically relevant depths. As such the SESORS technique presents several advantages over conventional Raman and SERS approaches, namely the possibility to simultaneously diagnose and treat disease at depth, thus further facilitating the potential translation of Raman spectroscopy into the clinic.

1.3 Introductory Conclusions and Project Aims

The potential to detect Raman and SERS analytes through barriers is an area of intense interest due to its applicability to a number of fields including security and biomedicine. More specifically, if the SERS technique is to advance as a medical imaging tool, the ability to image the accumulation of SERS nanotags at clinically relevant depths must be investigated if the use of NPs as an imaging tool is to advance into the clinic. To date, there are very

few reports on the use of SORS for the detection of SERS analytes through plastic and tissue barriers and even less reports of the use of SESORS utilising a back-scattering configuration.

The basis of this work presented here was to explore the use of handheld conventional Raman and SORS instruments to detect Raman and SERS analytes through plastic and tissue barriers. The ability to detect ethanol through plastic barriers by means of CR and SORS is investigated and the suitability of both techniques for probing through plastic barriers will be discussed. In addition, the use of multivariate analysis tools for probing through large depths will also be applied.

The use of various small molecule Raman reporters for through barrier detection applications in the field of both security and biomedicine will be investigated using both SERS and SESORS techniques. The maximum thickness of plastic and tissue that these nanotags can be tracked through will also be studied. Following this, using either SERS or SESORS, the ability to detect the SERRS nanotags taken up into *ex vivo* tumour models through varying thicknesses of tissue barriers will be assessed. Specifically, the aim is to demonstrate the advantage of using chalcogenpyrylium-based Raman reporters, with tunable resonances into the NIR for superior levels of through barrier detection using SERS or SESORS. A multiplexing imaging system will also be developed using the SESORS approach. Finally, the use of resonant nanotags for will be investigated for superior low limits of detection with the aim of demonstrating the advantage of using a resonant Raman reporter molecule over a non-resonant reporter for improved limits of detection through tissue barriers.

This work, involving the detection of both Raman and SERS analytes through plastic and tissue barriers provides the basis for future investigation in a number of fields, most significantly in the field of biomedical imaging and disease detection.

1.4 References

- 1 R. P. Feynman, *Eng. Sci.*, 1960, **23**, 22–36.
- 2 P. Pimpang and S. Choopun, *Chiang Mai J. Sci.*, 2011, **38**, 31–38.
- 3 A. P. Alivasatos, *Science (80-.)*, 1996, **271**, 933–937.
- 4 K. Saha, S. S. Agasti, C. Kim, X. Li and V. M. Rotello, *Chem. Rev.*, 2012, **112**, 2739–2779.
- 5 B. Le Ouay and F. Stellacci, *Nano Today*, 2015, **10**, 339–354.
- 6 A. Hebeish, M. H. El-Rafie, M. A. EL-Sheikh, A. A. Seleem and M. E. El-Naggar, *Int. J. Biol. Macromol.*, 2014, **65**, 509–515.
- 7 T. G. Smijs and S. Pavel, *Nanotechnol. Sci. Appl.*, 2011, **4**, 95–112.
- 8 N. L. Rosi and C. A. Mirkin, *Chem Rev*, 2005, **105**, 1547.
- 9 N. A. Dhas, C. P. Raj and a. Gedanken, *Chem. Mater.*, 1998, **10**, 1446–1452.
- 10 P. C. Lee and D. Meisel, *J. Phys. Chem.*, 1982, **86**, 3391–3395.
- 11 M. Hu, J. Chen, Z.-Y. Li, L. Au, G. V Hartland, X. Li, M. Marquez and Y. Xia, *Chem. Soc. Rev.*, 2006, **35**, 1084–1094.
- 12 M. Faraday, *Philos. Trans. R. Soc. London*, 1857, **147**, 145–181.
- 13 C. Louis and O. Pluchery, *Gold Nanoparticles for Physics, Chemistry and Biology*, Imperial College Press, 2012.
- 14 G. Frens, *Nat. Phys. Sci.*, 1973, **241**, 20–22.
- 15 S. Laing, L. E. Jamieson, K. Faulds and D. Graham, *Nat. Rev. Chem.*, 2017, **1**, 0060.
- 16 A. M. Schwartzberg, T. Y. Olson, C. E. Talley and J. Z. Zhang, *J. Phys. Chem. B*, 2006, **110**, 19935–19944.
- 17 M. C. Daniel and D. Astruc, *Chem. Rev.*, 2004, **104**, 293–346.
- 18 K. A. Willets and R. P. Van Duyne, *Annu. Rev. Phys. Chem.*, 2007, **58**, 267.
- 19 J. Olson, S. Dominguez-Medina, A. Hoggard, L.-Y. Wang, W.-S. Chang and S. Link, *Chem. Soc. Rev.*, 2015, **44**, 40–57.
- 20 P. K. Jain, X. Huang, I. H. El-Sayed and M. a. El-Sayed, *Plasmonics*, 2007, **2**, 107–118.
- 21 C. A. Mirkin, R. L. Letsinger, R. C. Mucic and J. J. Storhoff, *Nature*, **382**, 607.
- 22 K. Gracie, E. Correa, S. Mabbott, J. a. Dougan, D. Graham, R. Goodacre and K. Faulds, *Chem. Sci.*, 2014, **5**, 1030.
- 23 C. L. Zavaleta, B. R. Smith, I. Walton, W. Doering, G. Davis, B. Shojaei, M. J. Natan and S. S. Gambhir, *Proc. Natl. Acad. Sci. U. S. A.*, 2009, **106**, 13511–13516.
- 24 J. You, Z. Guodong and C. Li, *ACS Nano*, 2010, **4**, 1033–1041.
- 25 X. Li, M. Takashima, E. Yuba, A. Harada and K. Kono, *Biomaterials*, 2014, **35**, 6576–6584.
- 26 H. Yuan, C. G. Khoury, C. M. Wilson, G. a. Grant, A. J. Bennett and T. Vo-Dinh,

- Nanomedicine Nanotechnology, Biol. Med.*, 2012, **8**, 1355–1363.
- 27 I. H. El-Sayed, X. Huang and M. A. El-Sayed, *Cancer Lett.*, 2006, **239**, 129–135.
- 28 H. J. Lee, Y. Liu, J. Zhao, M. Zhou, R. R. Bouchard, T. Mitcham, M. Wallace, R. J. Stafford, C. Li, S. Gupta and M. P. Melancon, *J. Control. Release*, 2013, **172**, 152–158.
- 29 M. P. Melancon, M. Zhou and C. Li, *Acc. Chem. Res.*, 2011, **44**, 947–956.
- 30 J. Z. Zhang, *J. Phys. Chem. Lett.*, 2010, **1**, 686–695.
- 31 W. Lu, C. Xiong, G. Zhang, Q. Huang, R. Zhang, J. Z. Zhang and C. Li, *Clin. Cancer Res.*, 2009, **15**, 876–86.
- 32 W. Lu, M. P. Melancon, C. Xiong, Q. Huang, A. Elliott, S. Song, R. Zhang, L. G. Flores, J. G. Gelovani, L. V. Wang, G. Ku, R. J. Stafford and C. Li, *Cancer Res.*, 2011, **71**, 6116–6121.
- 33 E. Smith and G. Dent, *Modern Raman Spectroscopy: A Practical Approach*, Wiley, 2005.
- 34 A. Smekat, *Naturwissenschaften*, 1923, **11**, 873–875.
- 35 C. V. Raman and K. S. Krishnan, *Nature*, 1928, **121**, 501–502.
- 36 D. S. Moore and R. J. Scharff, *Anal. Bioanal. Chem.*, 2009, **393**, 1571–1578.
- 37 D. I. Ellis, D. P. Cowcher, L. Ashton, S. O'Hagan and R. Goodacre, *Analyst*, 2013, **138**, 3871.
- 38 H. G. M. Edwards, S. E. J. Villar, J. Jehlicka and T. Munshi, *Spectrochim. Acta - Part A Mol. Biomol. Spectrosc.*, 2005, **61**, 2273–2280.
- 39 N. C. Shand, *SPIE Eur. Secur. Def.*, 2008, **7119**, 71190J–71190J–12.
- 40 P. J. LARKIN, *Infrared and Raman spectroscopy: Principles and spectral interpretation*, Elsevier, 2011.
- 41 K. J. I. Ember, M. A. Hoeve, S. L. McAughtrie, M. S. Bergholt, B. J. Dwyer, M. M. Stevens, K. Faulds, S. J. Fobers and C. J. Campbell, *Regen. Med.*, 2017, **2**, 1–12.
- 42 B. Gardner, P. Matousek and N. Stone, *Anal. Chem.*, 2015, **88**, 832–837.
- 43 Kaiser Optical Systems, http://www.kosi.com/na_en/products/raman-spectroscopy/raman-technical-resources/raman-tutorial.php, (accessed 4 January 2018).
- 44 O. Stevens, I. E. Iping Petterson, J. C. C. Day and N. Stone, *Chem. Soc. Rev.*, 2016, **45**, 1919–1934.
- 45 H. J. Butler, L. Ashton, B. Bird, G. Cinque, K. Curtis, J. Dorney, K. Esmonde-white, N. J. Fullwood, B. Gardner, P. L. Martin-Hirsch, M. J. Walsh, M. R. Mcainsh, N. Stone and F. L. Martin, *Nat. Protoc.*, 2016, **11**, 664–687.
- 46 L. Jensen, L. L. Zhao and G. C. Autschbach, *J. Phys. Chem. C*, 2005, **123**, 174110.
- 47 L. Frame, J. Brewer, R. Lee, K. Faulds and D. Graham, *Analyst*, 2017.
- 48 T. Yamamoto and G. Palmer, *J. Biol. Chem.*, 1973, **248**, 5211–2313.
- 49 P. Matousek, M. Towrie, C. Ma, M. Kwok, D. Phillips, W. Toner and A. Parker, *J. Raman Spec.*, 2001, **32**, 983–988.
- 50 X. Huang and M. a. El-Sayed, *J. Adv. Res.*, 2010, **1**, 13–28.

- 51 M. Fleischmann, P. J. Hendra and A. J. McQuilla, *Chem. Phys. Lett.*, 1974, **26**, 163–166.
- 52 D. L. Jeanmarie and Van Duyne R P, *J. Electroanal. Chem. and Interfacial Electrochem.*, 1977, 1–20.
- 53 L. Landau, *J. Am. Chem. Soc.*, 1977, 5215–5217.
- 54 L. Guerrini and D. Graham, *Chem. Soc. Rev.*, 2012, **41**, 7085.
- 55 G. McNay, D. Eustace, W. E. Smith, K. Faulds and D. Graham, *Appl. Spectrosc.*, 2011, **65**, 825–837.
- 56 M. Moskovits, *Rev. Mod. Phys.*
- 57 H. N. Xie, I. a. Larmour, V. Tileli, A. L. Koh, D. W. McComb, K. Faulds and D. Graham, *J. Phys. Chem. C*, 2011, **115**, 20515–20522.
- 58 P. Vandenabeele, *Practical Raman Spectroscopy - An Introduction*, John Wiley and Sons LTD, 2013.
- 59 S. Harmsen, M. A. Bedics, M. A. Wall, R. Huang, M. R. Detty and M. F. Kircher, *Nat. Commun.*, 2015, **6**, 6570.
- 60 X. Qian, X.-H. Peng, D. O. Ansari, Q. Yin-Goen, G. Z. Chen, D. M. Shin, L. Yang, A. N. Young, M. D. Wang and S. Nie, *Nat. Biotechnol.*, 2008, **26**, 83–90.
- 61 S. McAughtrie, K. Faulds and D. Graham, *J. Photochem. Photobiol. C Photochem. Rev.*, 2014, **21**, 40–53.
- 62 S. Schlucker, *Angew. Chemie - Int. Ed.*, 2014, **53**, 4756–4795.
- 63 D. Cunningham, R. E. Littleford, W. E. Smith, P. J. Lundahl, I. Khan, D. W. McComb, D. Graham and N. Laforest, 2006, 135–145.
- 64 K. Faulds, R. Jarvis, W. E. Smith, D. Graham and R. Goodacre, *Analyst*, 2008, **133**, 1505.
- 65 C. McHugh, F. . Docherty, D. Graham and W. E. Smith, *Analyst*, 2003, **129**, 69.
- 66 S. I. Stoeva, J.-S. C. Lee, S. Thaxton and C. A. Mirkin, *Angew. Chemie - Int. Ed.*, 2006, **45**, 3303.
- 67 K. Faulds, F. Mckenzie, W. E. Smith and D. Graham, *Angew. Chemie - Int. Ed.*, 2007, 1829–1831.
- 68 A. I. Henry, B. Sharma, M. F. Cardinal, D. Kourouski and R. P. Van Duyne, *Anal. Chem.*, 2016, **88**, 6638–6647.
- 69 A. M. Smith, M. C. Mancini and S. Nie, *Nat. Nanotechnol.*, 2009, **4**, 710.
- 70 Y. W. Wang, S. Kang, A. Khan, P. Q. Bao and J. T. C. Liu, *Biomed. Opt. Express*, 2015, **6**, 3714.
- 71 S. Pal, S. Harmsen, A. Oseledchyk, H.-T. Hsu and M. F. Kircher, *Adv. Funct. Mater.*, 2017, **27**, 1606632.
- 72 S. McAughtrie, K. Lau, K. Faulds and D. Graham, *Chem. Sci.*, 2013, **4**, 3566–3572.
- 73 A. Oseledchyk, C. Andreou, M. A. Wall and M. F. Kircher, *ACS Nano*, 2017, **11**, 1488.
- 74 C. A. Lieber, S. K. Majumder, D. L. Ellis, D. D. Billheimer and A. Mahadevan-Jansen, *Lasers Surg. Med.*, 2009, **40**, 461–467.

- 75 J. C. Carter, S. M. Angel, M. Lawrence-Snyder, J. Scaffidi, R. E. Whipple and J. G. Reynolds, *Appl. Spectrosc.*, 2005, **59**, 769–775.
- 76 P. Matousek, I. P. Clark, E. R. C. Draper, M. D. Morris, a E. Goodship, N. Everall, M. Towrie, W. F. Finney and A. W. Parker, *Appl. Spectrosc.*, 2005, **59**, 393–400.
- 77 A. Macleod, N and P. Matousek, *Appl. Spectrosc.*, 2008, **62**, 291–304.
- 78 P. Matousek and N. Stone, *Chem. Soc. Rev.*, 2016, **45**, 1794–1802.
- 79 P. Matousek, *Chem. Soc. Rev.*, 2007, **36**, 1292–1304.
- 80 P. Matousek, *Appl. Spectrosc.*, 2006, **60**, 1341–1347.
- 81 P. Matousek, *TrAC Trends Anal. Chem.*, 2018, **103**, 209–214.
- 82 P. Matousek, E. Draper, A. Goodship, I. Clark, K. Ronayne and A. W. Parker, 2006, **60**, 758–763.
- 83 J. Griffen, A. Owen and P. Matousek, *J. Pharm. Biomed. Anal.*, 2015, 115, 277–282.
- 84 C. Eliasson, N. a Macleod and P. Matousek, *Anal. Chem.*, 2007, **79**, 8185–9.
- 85 P. W. Loeffen, G. Maskall, S. Bonthron, M. Bloomfield, C. Tombling and P. Matousek, *Proc. SPIE*, 2011, **8189**, 81890C–1–81890C–10.
- 86 M. Bloomfield, P. W. Loeffen and P. Matousek, *Proc. SPIE*, 2010, **7838**, 783808-1-783808–15.
- 87 R. J. Hopkins, S. H. Pelfrey and N. C. Shand, *Analyst*, 2012, **137**, 4408–4410.
- 88 B. Zachhuber, C. Gasser, E. T. H. Chrysostom and B. Lendl, *Anal. Chem.*, 2011, 83, 9438–9442.
- 89 E. L. Izake, B. Cletus, W. Olds, S. Sundarajoo, P. M. Fredericks and E. Jaatinen, *Talanta*, 2012, 94, 342–347.
- 90 N. K. Afseth, M. Bloomfield, J. P. Wold and P. Matousek, *Appl. Spectrosc.*, 2014, 68, 255–262.
- 91 C. Eliasson and P. Matousek, *Anal. Chem.*, 2007, 79, 1696–1701.
- 92 D. I. Ellis, R. Eccles, Y. Xu, J. Griffen, H. Muhamadali, P. Matousek, I. Goodall and R. Goodacre, *Sci. Rep.*, 2017, 7, 12082.
- 93 M. Bloomfield, D. Andrews, P. Loeffen, C. Tombling, T. York and P. Matousek, *J. Pharm. Biomed. Anal.*, 2013, 76, 65–69.
- 94 K. Buckley, C. G. Atkins, D. Chen, H. G. Schulze, D. V Devine, M. W. Blades and R. F. B. Turner, *Analyst*, 2016, **141**, 1678.
- 95 M. V Schulmerich, K. a Dooley, M. D. Morris, T. M. Vanasse and S. a Goldstein, *J. Biomed. Opt.*, 2015, **11**, 060502.
- 96 G. Feng, M. Ochoa, J. R. Maher, H. A. Awad and A. J. Berger, *J. Biophotonics*, 2017, **10**, 990–996.
- 97 N. Stone, R. Baker, K. Rogers, A. W. Parker and P. Matousek, *Analyst*, 2007, **132**, 899–905.
- 98 N. Stone and P. Matousek, *Cancer Res.*, 2008, **68**, 4424–4430.
- 99 A. Ghita, P. Matousek and N. Stone, *J. Biophotonics*, , DOI:10.1002/jbio.201600260.
- 100 N. Stone, M. Kerssens, G. R. Lloyd, K. Faulds, D. Graham and P. Matousek, *Chem. Sci.*, 2011, **2**, 776–780.

- 101 N. Stone, K. Faulds, D. Graham and P. Matousek, *Anal. Chem.*, 2010, **82**, 3969–3973.
- 102 H. N. Xie, R. Stevenson, N. Stone, A. Hernandez-Santana, K. Faulds and D. Graham, *Angew. Chemie - Int. Ed.*, 2012, **51**, 8509–8511.
- 103 J. M. Yuen, N. C. Shah, J. T. Walsh, M. R. Glucksberg and R. P. Van Duyne, *Anal. Chem.*, 2010, **82**, 8382–8385.
- 104 K. Ma, J. M. Yuen, N. C. Shah, J. T. Walsh, M. R. Glucksberg and R. P. Van Duyne, *Anal Chem*, 2011, **83**, 9146–9152.
- 105 B. Sharma, K. Ma, M. R. Glucksberg and R. P. Van Duyne, *J. Am. Chem. Soc.*, 2013, **135**, 17290–17923.
- 106 S. M. Asiala, N. C. Shand, K. Faulds and D. Graham, *ACS Appl. Mater. Interfaces*, 2017, **9**, 25488–25494.
- 107 A. S. Moody, P. C. Baghernejad, K. R. Webb and B. Sharma, *Anal. Chem.*, 2017, **89**, 5688–5692.
- 108 U. S. Dinish, G. Balasundaram, Y. T. Chang and M. Olivo, *Sci. Rep.*, 2014, 4.

2 Through Barrier Detection of Ethanol using Handheld Raman Spectroscopy - Conventional Raman versus Spatially Offset Raman Spectroscopy (SORS)

Accepted manuscript

Nicolson et al., *J Raman Spectrosc.*, 2017, **48**, 1828–1838

Contributing authors and their roles:

Lauren E. Jamieson¹ – Helped with data processing

Samuel Mabbott¹ – Helped with data processing

Neil C. Shand² – Provided access to SORS instrumentation and PhD supervisor of FN

Duncan Graham¹ – Co-collaborator and PhD supervisor of FN

Karen Faulds¹ – Principal investigator

1. Department of Pure and Applied Chemistry, Technology and Innovation Centre, University of Strathclyde, 99 George Street, Glasgow G1 1RD, UK.
2. DSTL, Porton Down, Salisbury, SP4 0JQ, UK.

The supporting information can be found in chapter 9.5

2.1 Abstract

Spatially offset Raman spectroscopy (SORS) provides chemical analysis at depth even when obscuring barriers such as plastic or tissue are present. As the collection probe is moved further away from the point of laser excitation, scattered photons from deeper layers begin to dominate the acquired spectra, thus giving rise to through barrier detection. Here we demonstrate the potential of conventional Raman (CR) and SORS for through barrier detection using handheld spectrometers. We report the collection of Raman signals from an ethanol solution through plastic at thicknesses of up to 21 mm using SORS in combination with multivariate analysis. SORS is compared to conventional Raman, where we also demonstrate impressive through barrier detection of ethanol at depths up to 9 mm. We also highlight the advantage of applying multivariate analysis for through barrier detection using CR or SORS, particularly when peaks with similar spectral features are present in both the barrier and analyte spectra. In addition, to the best of our knowledge, this is the first report of the assessment of the maximum level of through barrier detection using handheld CR and SORS instruments with a back-scattering geometry.

2.2 Introduction

The literature demonstrates the prevalent use of Raman spectroscopy in the fields of biomedicine¹⁻⁴ and defence applications.⁵⁻⁷ When applied in the backscattering geometry, Raman spectroscopy is a promising analytical technique, generating a unique chemical fingerprint and providing sensitive sample evaluation. In spite of this, conventional Raman (CR) can be limited by sample volume and thickness, often failing to probe beneath the surface or through samples obscured by an opaque barrier.^{8,9} This is particularly true for handheld instruments, where unlike microscope based systems, the focal depth of the instrument is often fixed, thus making it difficult to probe deeper layers. Such drawbacks associated with CR arise from the fact that weak deep-layer Raman scattered photons are swamped by surface scattered photons, which consequently dominate the collected Raman spectrum. Deeper photons have longer to travel to reach their point of collection, and in addition, diffuse in multiple directions compared to surface photons. Consequently, the contribution of sub-surface layers to the collected spectrum is significantly smaller than that from the surface layers.

Spatially offset Raman spectroscopy (SORS) provides a means of subsurface analysis, even when obscuring barriers such as plastic or tissue are present.⁹ By varying the distance of the collection probe from the point of laser excitation (typically in the region of a few mm) it is possible to acquire Raman contributions from the subsurface layers. As a result, signals collected close to the point of laser excitation will be made up of a higher proportion of surface signal, however as the spatial offset increases, deeper layer photons will begin to dominate the spectra.¹⁰

Since first demonstrated by Matousek *et al.*,⁹ SORS has shown promise in a number of applications including the screening of pharmaceutical products obscured by packaging,¹¹ the investigation of obscured liquid explosives¹² and in assessing the quality of transfusable red blood cells stored in plastic bags.¹³ SORS has been applied to the transcutaneous,¹⁴ and *in vivo*,¹⁵ analysis of bone and bone disease, and, in the non-invasive biochemical

analysis of cancerous calcifications in breast tissue.¹⁶ Using an inverse SORS approach, the detection of paracetamol obscured by 2 mm of polyvinylchloride has also been described.¹¹

Bloomfield *et al.*, compared backscattering CR with SORS for the detection of concealed substances.¹⁷ The authors obtained SORS scattering of ammonium nitrate obscured by 4.5 mm of 'pearl' polypropylene and detection of alcohol through 2 – 4 mm of coloured glass.¹⁷ The authors commented on the limitations of CR for through barrier analysis since the collected signal was often swamped by that of the packaging or fluorescence (in the case of glass). They noted that when the contents and packaging spectra do not overlap, it was possible to detect the analyte using CR, however this was inherently difficult and open to interpretation. The SORS technique has also been demonstrated at a laser excitation of 1064 nm where the advantage of a longer wavelength to overcome fluorescence issues, associated with the presence of glass barriers, was discussed.¹⁸ Handheld CR with a 1064 nm laser excitation has also been used for the assessment of packaged food substances susceptible to food fraud including saffron and beef.¹⁹

Currently, benchtop SORS spectrometers are located in several international airports for the detection of liquid explosives.²⁰ Handheld Raman spectrometers have attracted increasing interest in recent years, namely due to their ease of use and portability, with many portable Raman instruments being available on the market.^{6,7,19} Here we present a non-destructive way of obtaining Raman spectra through plastic using handheld spectrometers, thus demonstrating the use of Raman spectroscopy in the field for customs and defence applications. Using a handheld CR instrument and a handheld SORS instrument, the SORS approach is compared with CR spectroscopy for through barrier detection. In both cases, the collection optics for both instruments are on the same side of the sample as the incident laser, i.e. not a transmission geometry. Therefore, we compare two types of Raman spectroscopy in the backscattering configuration for through barrier detection.

2.3 Experimental

2.3.1 Instrumentation

CR measurements were carried out using a handheld CBEx spectrometer, 785 nm laser excitation wavelength, from Snowy Range Instruments. All measurements were obtained using a 3 s integration time, with 5 accumulations. A point and shoot adaptor with a single element lens and a numerical aperture of 0.5 was fitted for through barrier detection using CR. This gave an average laser power of 43 mW. The focal spot of the CBEx was measured using a beam profiler (BeamMap 2 – XYZ scanning slit system 190- 2500 nm, Data-Ray Inc). As shown in Figure S1, supporting information, it appears that the CBEx instrument used in this instance has a spot size of 50 – 60 microns at a focal distance of 0.5 cm. SORS measurements were taken using a handheld Resolve instrument from Cobalt Light Systems (830 nm, average laser power 450 mW). All measurements were carried out using a 2 s integration time, 5 accumulations. The nose cone was fitted to use the instrument in a contact mode setting.

2.3.2 Through barrier detection

Large transparent polyethylene terephthalate (PET) and blue opaque coloured polypropylene (PP) plastic sheets were purchased from a local art store and then cut up into smaller rectangular pieces of (10.5 x 3 cm, thickness 1 mm). The sheets were mounted on a stage and clamped together to create the desired thickness. They were then brought into contact with the laser using either the point and shoot adaptor (CR spectrometer) Figure S2(a), supporting information or the nose cone (SORS spectrometer), Figure S2(b), supporting information. This ensured there was no air/space between the plastic and instrument. A glass vial containing ethanol was placed behind the plastic sheets. The glass vials had a 15 mm diameter, 1 mm thickness and a height of 25 mm (including lid).

To determine the maximum thickness of plastic both instruments could detect ethanol through, measurements were carried out using varying thicknesses of plastic. For all CR measurements, the thickness of plastic was increased by 1 mm for each set of spectral acquisitions. For SORS measurements using PET, sets of spectra were taken at thicknesses of 5 mm increments then at every 1 mm thickness, until the maximum depth for through barrier detection was reached. For blue PP, measurements were taken at thicknesses of 2 mm then at 1 mm additions until the maximum thickness at which the instrument could detect the ethanol analyte was determined. For SORS measurements, at each thickness, the spatial offset was also changed from 1 mm to 8 mm (1 mm increments) to show the influence the spatial offset had on the depth penetration.

2.3.3 Data processing

All spectra were processed using Matlab software (Version 2015a, The MathWorks, Natick, MA, USA). Principal component analysis (PCA) was applied to spectra obtained using CR. 15 spectra (5 replicates, 3 samples) of plastic at a given thickness were obtained followed by 15 spectra (5 replicates, 3 samples) of ethanol obscured by plastic of the same thickness. PCA performed on spectra obtained using SORS was carried out using spectra obtained at the zero position (plastic) and spectra obtained at an offset of 8 mm (plastic and ethanol). Preprocessing involved truncating and scaling the spectra, before applying the first order derivative coupled with Savitzky-Golay smoothing. The first order derivative was used in PCA to remove slight variances in the background which were found to affect the resulting zero order PCA plots.^{21,22}

For SORS spectra, in addition to PCA, a scaled subtraction was also applied. Briefly, spectra were truncated and baselined to remove the fluorescent background. Following this, the surface spectrum (i.e. the signal detected at the zero position) was removed from the subsurface spectrum (i.e. signal detected at the offset position) using a scaled subtraction. Data was subsequently smoothed.

2.4 Results and Discussion

Both handheld instruments (CR and SORS spectrometers) were compared for their ability to detect analytes through plastic barriers and we aim to show the maximum potential of each instrument for through barrier detection. Ethanol was chosen for this comparison since it is a common analytical standard and bottles containing alcohol are frequently subjected to screening in airports. Furthermore, its characteristic and strongest peak was spectrally similar to those found in the plastic barriers, thus allowing us to highlight the advantages of applying multivariate analysis for probing through plastic barriers. The focus of this paper is on the comparison of CR and SORS, and not the detection of specific analytes. It is noted that the depth penetration using both techniques (CR and SORS) will be dependent on the scattering efficiencies of both the analyte and barrier. Therefore, the maximum level of through barrier detection will differ when different plastics and analytes are used. To account for this, clear (PET) and opaque (PP) plastic were chosen to act as barriers.

The probing of ethanol through clear PET plastic using CR spectroscopy is shown in Figure 2.1. Measurements of ethanol were initially taken at each thickness of clear plastic (1-11 mm) to determine the varying contribution of analyte and plastic in the acquired spectra with respect to plastic barrier thickness. The spectrum at the top of Figure 2.1 represents the plastic reference and the bottom spectrum refers to ethanol. At thicknesses of 1 to 3 mm of plastic, the 885 cm^{-1} peak from ethanol clearly dominates the acquired spectra. Beyond a thickness of 3 mm however, signal from the plastic (860 cm^{-1}) begins to appear in the spectrum. This is expected since the working distance of the CR instrument is arguably 2 – 7 mm, Figure S2, supporting information and, unlike a microscope system, has a more relaxed focus, thus explaining why spectral contribution from the plastic is observed at even smaller thicknesses. As the thickness of the plastic barrier is increased, it becomes difficult to visually detect ethanol at thicknesses of 7 mm and

beyond, since the plastic and ethanol peaks become hard to distinguish due to their close proximity to one another.

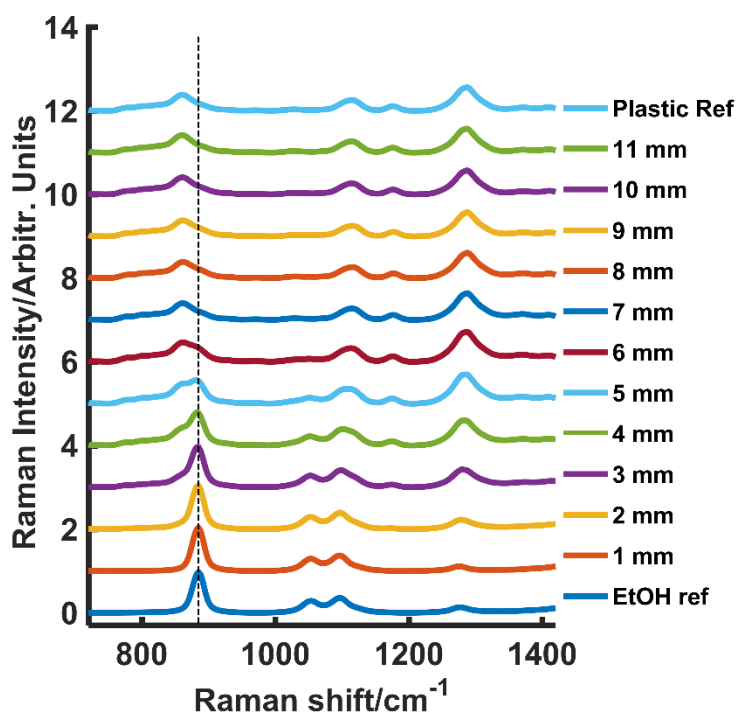


Figure 2.1 – Tracking of ethanol through various thicknesses (1-11 mm) of PET using CR spectroscopy. The spectrum at the top refers to a reference of the plastic and the spectrum at the bottom to that of the ethanol. The dashed line refers to the characteristic ethanol peak at 885 cm⁻¹. Spectra are stacked and normalised for clarity and show the contribution of the analyte and plastic at each thickness. Measurements were performed at a laser excitation wavelength of 785 nm, average laser power 43 mW and 3 s integration time, 5 accumulations.

Multivariate analysis in the form of PCA was applied to distinguish the plastic from the ethanol and determine the depth to which the ethanol could be detected. PCA decomposes the spectra into individual components and reduces the dimensionality of the spectroscopic data, thus aiding in the separation of the two layers.^{21,23} Spectra were truncated and scaled, before the first order derivative coupled with Savitzky-Golay smoothing was applied.

As shown in Figure 2.2, PCA score plots convincingly separate the samples containing ethanol up to thicknesses of 9 mm. This is compared to only 7 mm when detecting a spectral contribution from ethanol by eye. The two clusters represent the plastic reference (e.g. 8 mm thick plastic) and the ethanol

sample obscured by the same thickness of plastic (e.g. 8 mm). As thickness increases, the score for PC1, which indicates the maximum variance, decreases, therefore demonstrating a decline in variability between the two samples, Figure 2.2(a, c). Furthermore, the first derivative was also taken of the raw truncated, unprocessed spectra. Figure 2.2 shows the first order derivative spectra of plastic reference samples at 9 mm, as well as ethanol obscured by plastic at thicknesses of 9 and 10 mm (b) and (d). Samples of ethanol obscured by plastic at thicknesses of 10 mm (Figure 2.2d) show very little spectral difference in the region of 850 to 900 cm^{-1} , thus indicating that the instrument is no longer able to detect the ethanol through the plastic barrier. This is compared to thicknesses of 9 mm in (Figure 2.2b), where the spectral differences in this region are more obvious. Therefore, using CR to detect ethanol through PET, it is possible to detect the analyte visually at thicknesses of 6 mm. More impressively, if multivariate analysis in the form of PCA is applied, ethanol detection is possible up to thicknesses of 9 mm.

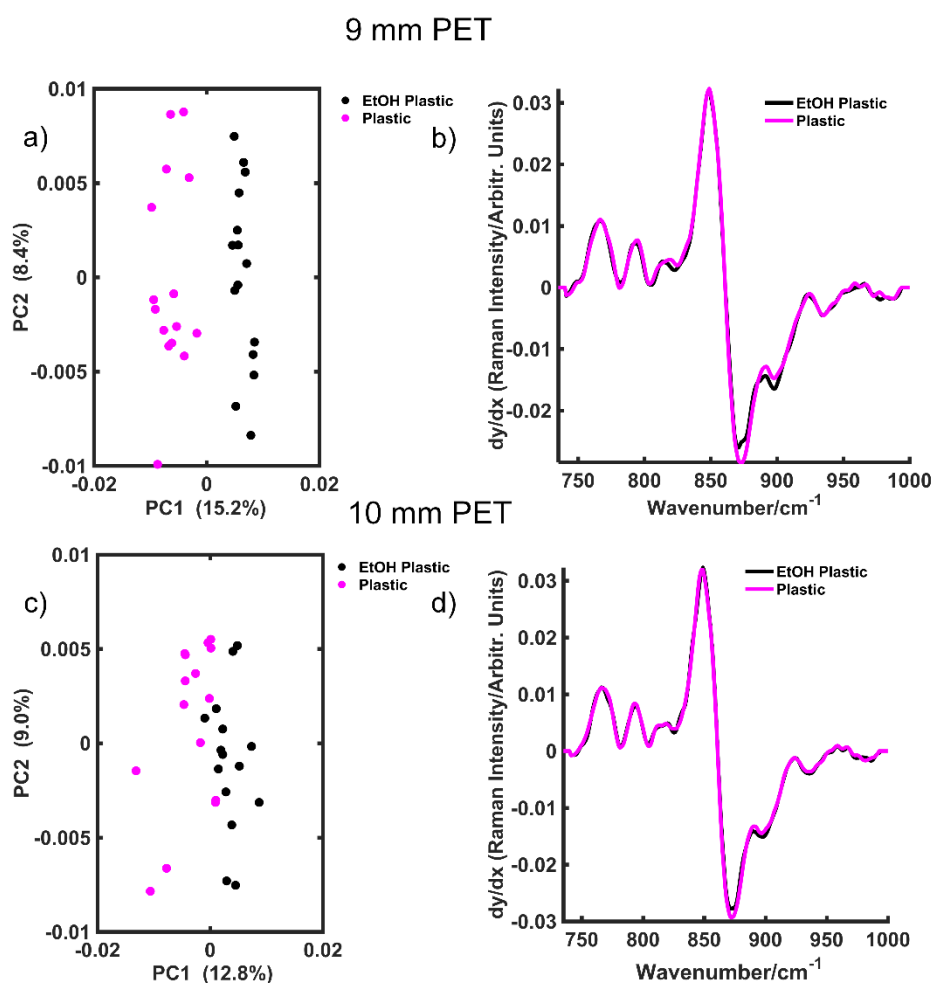


Figure 2.2 – PCA scores plots discriminating between the plastic and ethanol at plastic thicknesses (a) 9 mm and (c) 10 mm using CR spectroscopy. The clusters refer to plastic reference spectra at a given thickness, and ethanol obscured by plastic of the same thickness as the plastic reference. At 9 mm depths, clear separation is seen however, at 10 thicknesses, PCA cannot distinguish between the two sets of spectra. Averaged first order derivative spectra discriminating between the plastic and ethanol at plastic thicknesses of (b) 9 mm and (d) 10 mm using CR spectroscopy. As thickness increases, spectral differences in the region of interest (850 to 900 cm^{-1}) decreases.

The absorption spectra for PET at thicknesses of 1 – 10 mm can be seen in Figure S3 (supporting information). As shown, gradual absorption is taking place as the PET thickness increases. Based on this, it is assumed that not all the incident laser light is being transmitted to the ethanol analyte, particularly when larger thicknesses are involved. However, in comparison to PP of the same thickness, Figure S6 supporting information, PET is still a relatively non-absorbing material. Furthermore, PET is a commonly used

plastic, particularly in the manufacture of plastic bottles, and will therefore be ubiquitous in a range of real world samples.

It is worth noting that the focal distance of the handheld CR instrument was fixed and non-adjustable. In addition, it was not possible to apply a different point and shoot adaptor lens with a greater (or lesser) focal distance. Unlike a microscope, a handheld device is often used in sub-optimal focus and therefore a longer working distance, with a relaxed focus, makes the device easier to use. If a point and shoot adaptor was available with a longer focal distance, it is feasible that through barrier detection would be achieved through even greater thicknesses using CR. This is particularly likely with regards to experiments involving PET since its more transparent nature will allow beam penetration to greater depths.

Through barrier detection was then carried out using a handheld SORS instrument for the detection of ethanol through clear PET plastic. The spatial offset, i.e. the distance of the collection point from that of laser excitation, was changed from 1 to 8 mm, in 1 mm increments, and spectra were obtained at each offset. It is expected that as the spatial offset increases, deeper layer photons i.e. from the ethanol analyte, will dominate the acquired spectra. The results are shown in Figure 2.3 for plastic thicknesses of 5 mm, 10 mm and 15 mm. The data confirms that as the spatial offset is increased, through barrier detection is possible and, furthermore, as the thickness of the barrier increases, a larger spatial offset is also required to obtain through barrier Raman spectra. The offset spectra are stacked for clarity and show the dependence on the increase in spatial offset as the barrier thicknesses increases. Using this instrument, the ethanol specific peaks were observed at 882 cm^{-1} , 1047 cm^{-1} and 1095 cm^{-1} , with the one at 882 cm^{-1} being the most intense and therefore easiest to track as the barrier thickness was increased. In addition, using the SORS instrument, PET peaks were observed at 856 cm^{-1} , 1115 cm^{-1} , 1175 cm^{-1} and 1282 cm^{-1} .

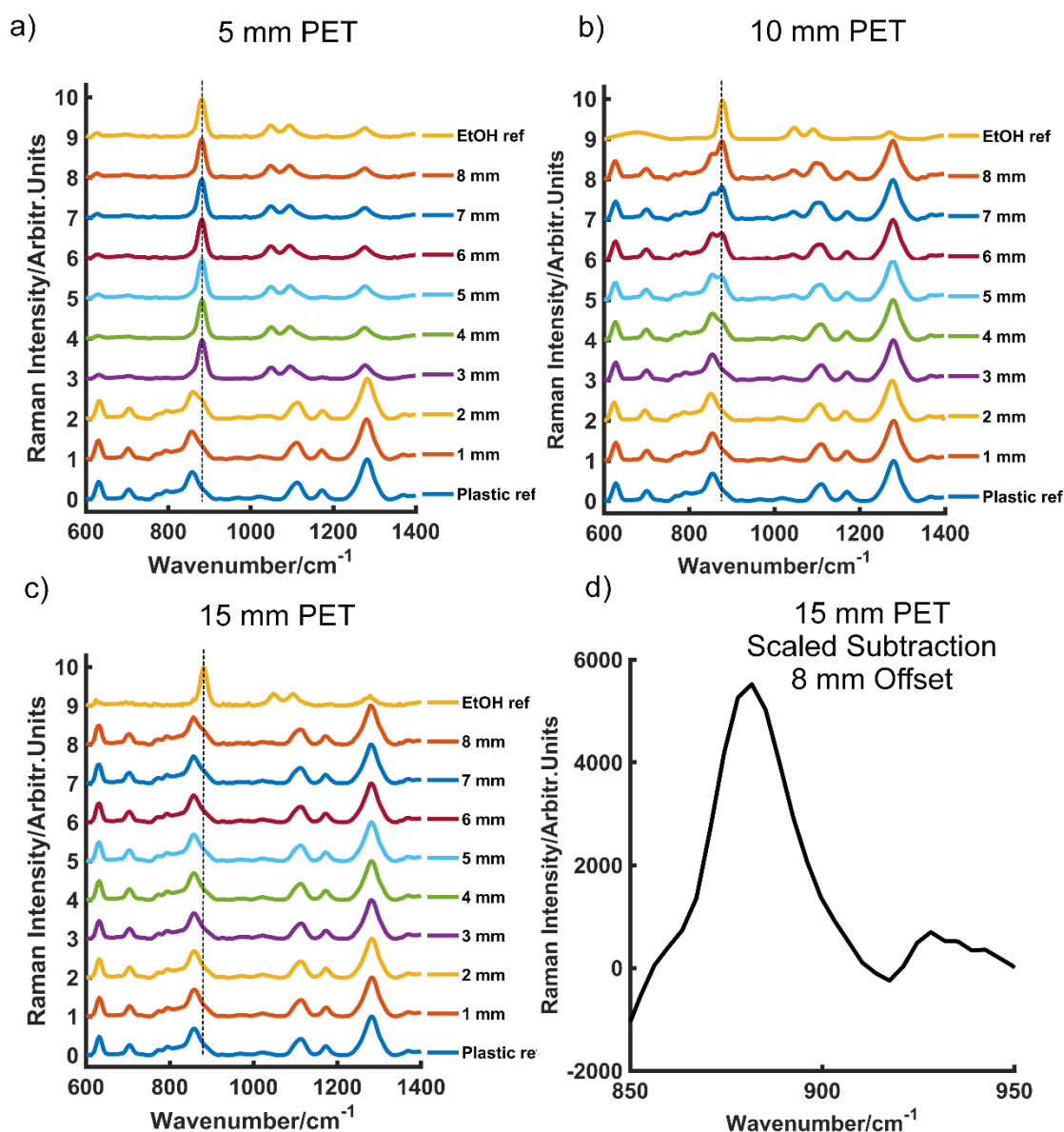


Figure 2.3 – Normalised stacked SORS spectra of ethanol through PET at thicknesses of (a) 5 mm (b) 10 mm and (c) 15 mm. The spatial offset was increased from 1 mm to 8 mm in 1 mm increments and the offset spectra recorded. Spectra are stacked for clarity and the dashed line refers to the characteristic ethanol peak at 882 cm⁻¹. As thickness increases, the spatial offset required to obtain the analyte signal (ethanol) also increases. At a thickness of 5 mm ethanol makes spectral contribution at an offset of 1 mm. At a thickness of 10 mm, ethanol contributes visually to the spectra at a 4 mm offset and at 15 mm thicknesses, an offset of 8 mm is required. The ethanol specific peak at 882 cm⁻¹ is easily distinguishable following a scaled subtraction (d). This approach removes the signal obtained at the zero position (plastic) from that acquired at an 8 mm offset (plastic and ethanol).

At a PET thickness of 5 mm (Figure 2.3a), the characteristic ethanol peak at 882 cm⁻¹ can be seen as a small shoulder at an offset of 1 mm. At an offset of 3 mm and greater, ethanol dominates the acquired spectra, with the plastic

component diminishing dramatically at this offset and beyond. At a thickness of 10 mm and an offset of 4 mm (Figure 2.3b), ethanol begins to contribute visually to the obtained spectra, presenting as a small shoulder in the region of $\sim 882\text{ cm}^{-1}$ due to the presence of the more intense plastic peak at 856 cm^{-1} . At offsets 5 – 8 mm a spectral contribution from the plastic can still be seen, however the peak height ratio of plastic to ethanol decreases at 856 cm^{-1} and increases at 882 cm^{-1} , indicating a greater influence of ethanol in the acquired spectra. Ethanol can be seen most clearly in the spectra obtained at an 8 mm offset; the largest offset possible with the handheld SORS instrument. Therefore, from the graphs in Figure 2.3(a – c) it is evident that as expected, when the barrier thickness is increased, spatial offset must also increase in order for through barrier detection to occur. When PET thickness is increased to 15 mm (Figure 2.3c), a shoulder in the plastic peak at 856 cm^{-1} can be seen in the region of $\sim 882\text{ cm}^{-1}$ at an 8 mm offset. The presence of ethanol at this thickness and spatial offset is confirmed by carrying out a scaled subtraction on the two-layer sample (Figure 2.3d), which shows the presence of the ethanol analyte at 882 cm^{-1} .

As described in the experimental section, a scaled subtraction was applied to data collected at a thickness of 15 mm at the 8 mm offset, Figure 2.3d. Briefly, spectra were truncated and baselined and the spectra collected at the zero position were removed from those collected at the offset using a scaled subtraction. The data was subsequently smoothed. Scaled subtractions are a useful tool, often applied in this instance to remove residual background signal, in this case PET. Whilst a scaled subtraction can usually provide satisfactory identification of the analyte, ethanol in this case, it has potential limitations such as prior knowledge of spectral bands, variations in background and researcher bias. To maintain consistency between spectra obtained using PET as a barrier to ethanol by means of CR or SORS, PCA was performed on the first order derivative spectra obtained by SORS using an offset of 8 mm for spectra collected at thicknesses of 15 mm and beyond. This aimed to establish the true depth to which SORS detection of ethanol

could be achieved, particularly since the plastic and analyte had spectrally similar peaks in the same area.

Figure 2.4 shows that using SORS, in combination with PCA, it is possible to detect ethanol through thicknesses up to 21 mm of PET at a spatial offset of 8 mm. This is compared to that of only 15 mm when visual spectral interpretation is applied. As before, PCA was performed using the first order derivative spectra. Spectra were truncated and scaled, before the first order derivative coupled with Savitzky-Golay smoothing was applied. PCA was carried out on data obtained at an 8 mm offset, since it has been shown at that at this offset maximum through barrier detection takes place (Figure 2.4). Resulting PCA scores plots for thicknesses of 21 mm and 22 mm are shown in Figure 2.4b and d respectively. The loadings for PC1 can be seen in Figure 2.4 (c and f). The PCA scores plot for 21 mm thick plastic shows clear separation of offset spectra (ethanol obscured by PET) from the spectra collected at the zero position (PET). Averaged first order derivative spectra display clear spectral differences in the region of 875 – 885 cm^{-1} . This is supported by the loadings in PC1 (Figure 2.4c). Although plastic signal accounts for the largest separation, a strong proportion of separation is coming from the ethanol peak at around $\sim 880 \text{ cm}^{-1}$, thus suggesting that the portable SORS instrument is capable of seeing ethanol at this depth. Together with a scaled subtraction (Figure. S4a, supporting information) which shows a peak at 882 cm^{-1} , SORS is convincingly capable of detecting ethanol through 21 mm of PET.

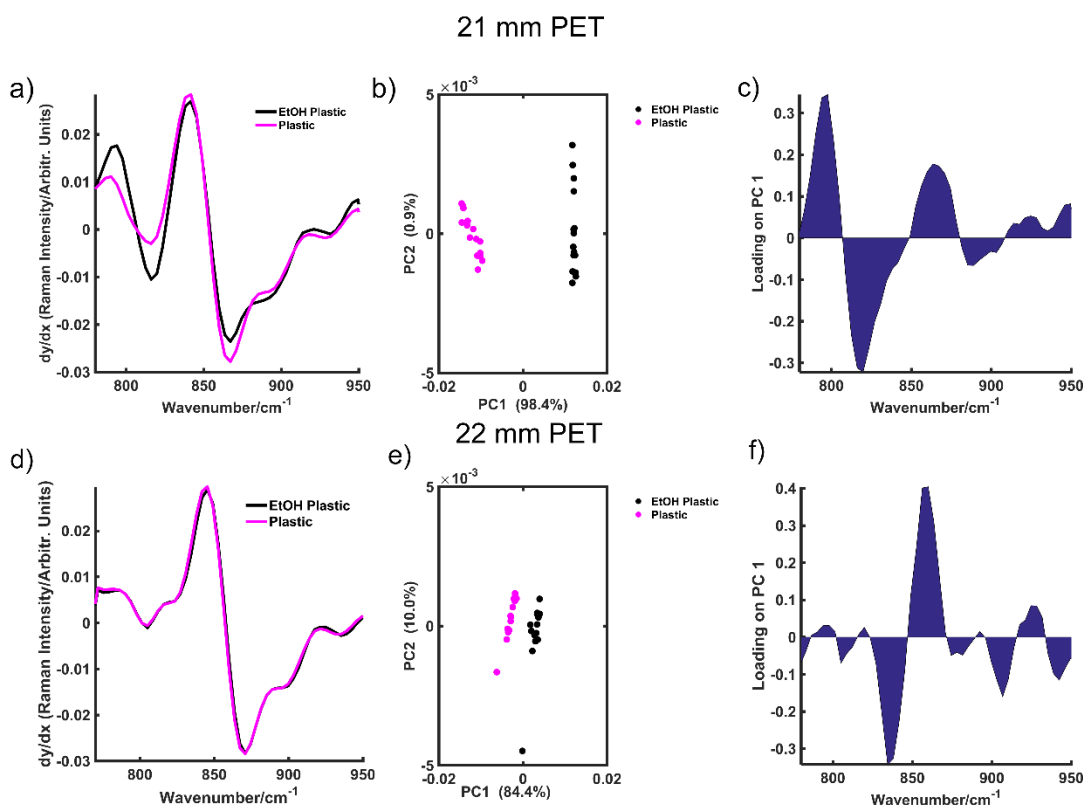


Figure 2.4 – The result of PCA performed using PET as a barrier to ethanol at thicknesses of 21 mm (top, a-c) and 22 mm (bottom, d-f). Average preprocessed first order derivative spectra are shown for (a) 21 mm and (d) 22 mm. This was used to produce PCA plots for thicknesses of (b) 21 mm and (d) 22 mm. PC1 loadings at thicknesses of (c) 21 mm and (f) 22 mm. The loadings on PC1 at 21 mm (c) show a significant contribution from ethanol however at 22 mm plastic (f) the main cause of separation is from the variances in the plastic and not ethanol.

The PCA results through a PET thickness of 22 mm are shown in Figure 2.4d – f. Unlike the first order derivative spectra presented for 21 mm, no spectral differences can be seen in the region of 875 – 885 cm^{-1} . There is however, slight differences in the spectra between 840 – 850 cm^{-1} . These are attributed to the plastic peak which is seen at a maximum in the zero order spectra at 856 cm^{-1} . This peak is displayed as zero-crossing in the first order spectra, Figure 2.4d. Despite evidence of separation between the signal collected at the zero position (plastic) and that collected at the offset (ethanol and plastic), data collected at thicknesses of 22 mm and beyond, suggests SORS is not capable of detecting ethanol. This is also supported in the loadings for PC1 which show a definite separation as a result of variances in signal obtained from the plastic. Zero-crossing exists at 848 cm^{-1} which is

due to the presence of a plastic peak, however no zero-crossing exists at 882 cm^{-1} , thus further suggesting that ethanol isn't being detected by the instrument.

In this instance, separation is most likely due to subtle differences in the plastic spectrum acquired at the zero and offset positions. This is plausible since photons collected at the zero and offset positions will have been scattered differently. Those collected at the offset position will have had further to travel to reach their point of collection and will have passed through several layers of plastic before being collected. This is in comparison to those collected at the zero position in a 180 degree back-scattered mode. Additionally, slight differences in the collection optics at the zero and offset position may also attribute to the small variations in the collected signal. The resulting scaled subtraction at 22 mm (Figure S4b supporting information), produces no definite peak at 882 cm^{-1} with the signal to noise ratio being too low to yield any useful information, further confirming the maximum level to which detection can occur through this type of plastic. PCA was also performed at thicknesses beyond 22 mm e.g. 23 mm. Scores values were in a similar range to that of 22 mm. Additionally, first order derivative spectra show no spectral differences at 882 cm^{-1} , harmonious with those obtained at 22 mm (Figure 2.4d). Coupled with scores plots consistent with the results seen in Figure 2.4d – f, it is believed that slight variations in collected plastic signal are responsible for the separation. It can therefore be said with high confidence, that it is possible to detect ethanol through 9 mm PET using handheld CR and, through PET thicknesses of 21 mm using handheld SORS.

To further assess the potential of CR for handheld through barrier detection, the detection of ethanol through blue PP was also investigated using the same set up. Blue PP was chosen due to its colour and opaque properties. Due to these characteristics, it was predicted that through barrier detection using CR and SORS would be possible, however to a lesser extent to that seen with PET. As shown in Figure 2.5a, the ethanol peak at 885 cm^{-1} can be seen visually to depths of 2 mm. At a thickness of 1 mm, the plastic peak at

875 cm^{-1} begins to become apparent in the acquired spectra. Beyond 2 mm, the ethanol signal is lost to the competing plastic signal with little distinction between the two. Separation between the spectra of PP from that of ethanol obscured by PP at 2 mm is also confirmed in first order derivative PCA scores plots at this thickness, Figure S5 supporting information. Therefore, using CR, ethanol obscured by PP can no longer be detected visually at thickness beyond 1 mm (Figure 2.5a) and at thicknesses beyond 2 mm using PCA (Figure 2.5b).

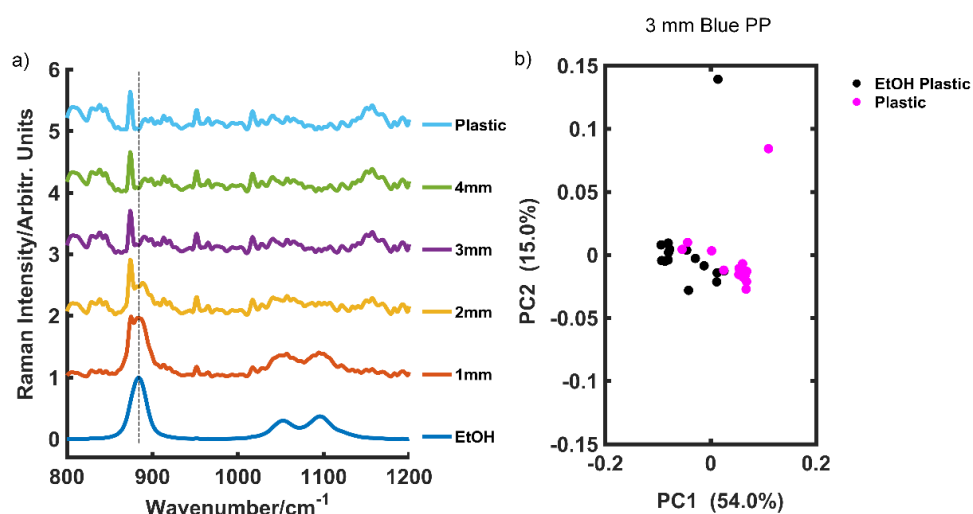


Figure 2.5 – Tracking of ethanol through blue polypropylene through varying thicknesses (1-4 mm) of clear plastic using CR spectroscopy (a). The spectrum at the top refers to a reference of the plastic and the spectrum at the bottom to that of the ethanol. Spectra have been normalised as well as stacked for clarity and show the contribution of the analyte and plastic at each thickness. The dashed line refers to the characteristic ethanol peak at 885 cm^{-1} . PCA scores plots at a plastic thicknesses of 3 mm (b).

The absorption spectra of blue PP is shown in Fig. S6, supporting information. It is apparent that absorption is occurring at 670 nm, which is expected since the sample is blue. In the CR spectra, the characteristic doublet at 810 cm^{-1} and 840 cm^{-1} , which is seen in the PP spectrum collected at 830 nm spectrum (Figure 2.6) is missing. Instead, a sharp peak at 875 cm^{-1} is observed, Figure 2.5. It is believed that the spectra at each PP thickness collected using CR (785 nm) is perhaps a pre-resonance enhanced spectra of the dye with weak PP features superimposed. However, we aim to

compare methods and not wavelengths for through barrier detection and thus see the plastic more simplistically, using it as a barrier to block the Raman signal from ethanol analyte using either CR or SORS. We are able to track the ethanol through the plastic barrier, detecting it spectrally by eye and then by PCA until separation no longer takes place, thus allowing for the assessment of CR for through barrier detection which is the main focus of this paper.

Conventional Raman i.e. barrier surface measurements were also carried out using the SORS instrument at the highest and lowest possible laser powers. At 450 mW, 830 nm, detection of ethanol was achieved through 4 mm of both PET and PP, Figure S7 a and b, supporting information. This was compared to 3 mm PET and PP at a laser power of 60 mW, Figure S7 c and d (supporting Information), thus further demonstrating the advantages of the SORS technique. In this case, the optical properties of the plastic did not influence the level of through barrier detection, i.e. the instrument could see through the similar thickness of clear plastic and blue plastic at each respective laser power. This is believed to be down to the characteristics of the beam used in the CR mode, which is presumed has a very short focal distance. Such optical approach however, is ideal for a SORS set up to ensure maximum discrimination between the barrier and analyte when the measurement at the zero position is carried out. This is discussed in greater detail in the supporting information. Interestingly, at similar laser powers, this set up (SORS in a CR mode) can detect ethanol through fewer thicknesses of PET compared the specific CR spectrometer, thus highlighting the importance of focal distance with regards to through barrier detection using CR.

SORS was also performed on ethanol obscured by blue PP to compare the depth of through barrier detection that could be achieved using CR, Figure 2.6. The contribution of ethanol to the acquired spectrum at thicknesses of 2 mm blue PP (a), 4 mm blue PP (b) and 6 mm blue PP (c) at offsets of 1 -8 mm, are shown in Figure S8, supporting information. Figure 2.6a refers to the spectra acquired at an 8 mm offset at thicknesses of 2, 4 and 6 mm PP. At a

thickness of 2 mm ethanol makes a significant contribution to the spectra with a clearly defined peak at 882 cm^{-1} . As the thickness is increased to 4 mm, ethanol is still visible, however a large contribution from the plastic can also be seen. At a thickness of 6 mm, ethanol is observed as a shoulder at 882 cm^{-1} however, even at this largest possible spatial offset (8 mm) there is little distinction between the plastic and ethanol in this region ($880\text{-}900\text{ cm}^{-1}$). Despite this, the presence of ethanol is confirmed by a scaled subtraction, Figure S8d supporting information, which shows a defined peak at 882 cm^{-1} .

As carried out previously, PCA was performed to establish the maximum thickness of PP through which ethanol could be detected by SORS. Detection of ethanol, combined with the application of PCA, is possible through thicknesses up to 9 mm PP compared to 6 mm visually. Figure 2.6c shows the resulting PC1 loadings a thickness of 9 mm PP, collected at an 8 mm offset. First order derivative spectra (Figure 2.6b) displays spectral differences at 882 cm^{-1} and the PCA scores plot shows separation between the signal collected at the zero position (plastic) and signal collected at the 8 mm offset (ethanol and plastic). The loadings on PC1 (Figure 2.6c) also show that ethanol is contributing strongly to the obtained signal. Furthermore, the resulting scaled subtraction (Figure S9a, supporting information) displays a slight peak at 882 cm^{-1} , with a shoulder at 900 cm^{-1} . This peak at 900 cm^{-1} is a contribution from the plastic, thus highlighting the inconsistencies and variances associated with solely performing a scaled subtraction at depths where there are little differences in the spectra. Nonetheless, it can be determined with conviction that ethanol can be detected through 9 mm of blue PP using SORS.

PCA was also performed on the data collected using 10 mm PP at an offset of 8 mm, Figure 2.6(d,e). As before, with first order derivative spectra using 22 mm PET (Figure 2.4d), it is believed that spectral differences responsible for the PCA separation are only associated with the plastic (Figure 2.6d). In the zero order spectra for plastic (Figure 2.6a), peaks associated with the material can be seen at 809 cm^{-1} and 841 cm^{-1} . As expected, on the first order graph Figure 2.6d, they are displayed as zero-crossing. Slight

fluctuations in the first order spectra can be seen at 832 cm^{-1} and 852 cm^{-1} and are therefore associated with the zero order Raman peak at 842 cm^{-1} . Despite the PCA scores plot indicating separation between signal collected at the zero position and signal collected at the offset, it is once again believed that this is due to subtle differences in the plastic spectra collected at two offsets (0 mm and 8 mm). This is supported in the loadings for PC1 Figure 2.6e, which show that variances in the plastic at 10 mm are responsible for the cause of separation across PC1. Additionally, performing a scaled subtraction produces little valuable information from the ethanol analyte under detection, Figure S9b, supporting information. It is also possible that since the plastic is coloured, signal collected from the deeper layers (8 mm offset) may have absorbed some of the energy from the laser, thus giving rise to a slightly different set of spectra from those obtained at the zero position. Therefore, in summary, it is possible to detect ethanol through 2 mm of blue PP using CR but up to thicknesses of 9 mm using SORS.

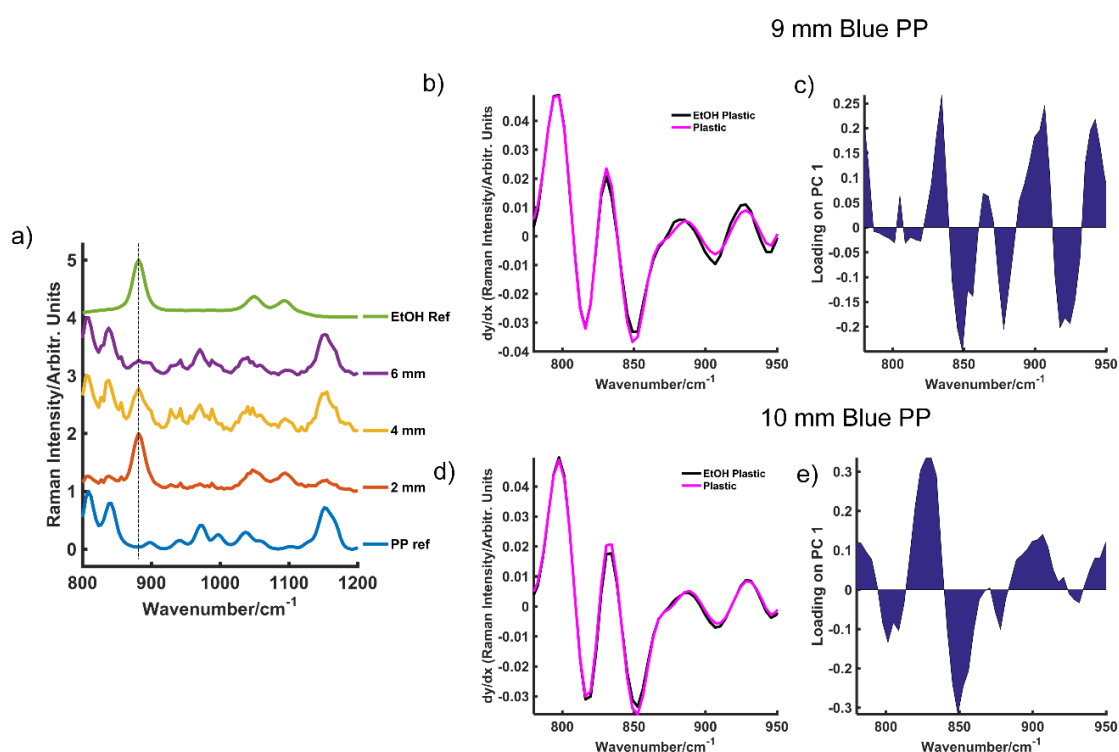


Figure 2.6 – (a) SORS normalised stacked spectra at an 8 mm offset showing the contribution of ethanol obscured by thicknesses of 2 mm, 4 mm and 6 mm thicknesses of PP. Ethanol reference can be seen in the top spectrum and the PP reference in the bottom spectrum. The dashed line refers to the characteristic ethanol peak at 882 cm^{-1} . The resulting PCA performed using blue PP as a barrier to ethanol at thicknesses of 9 mm (top) and 10 mm (bottom). Average pre-processed first order derivative spectra are shown for (b) 9 mm and (d) 10 mm. PC1 loadings at thicknesses of (c) 9 mm and (e) 10 mm. The loadings on PC1 at 9 mm (c) show a significant contribution from ethanol however at 10 mm plastic (e) the main cause of separation is from the variances in the plastic and not ethanol.

To take account of the difference in laser power between the CR and SORS instruments, the laser power on the SORS instrument was lowered to the minimum level possible. This gave an average laser power of 60 mW. Using the SORS technique at a laser power of 60 mW, through barrier detection was possible through thicknesses of 13 mm PET and 6 mm PP, Figure S10 (supporting information). The results of which are discussed further in the supporting information. Nonetheless, the increase in levels of through barrier detection using low power SORS (60 mW) compared to handheld CR show that the SORS technique has a superior advantage. It is acknowledged that the two wavelengths used are different from one another however, handheld instruments with the same wavelength were not available. Furthermore,

rather than comparing specific laser powers and wavelengths, we intended to, and successfully, demonstrate the maximum potential of both Raman techniques for through barrier detection.

2.5 Conclusion

The non-invasive detection of ethanol by means of both CR and SORS has been demonstrated successfully using handheld spectrometers. Impressively, using CR in combination with multivariate analysis, detection of ethanol was possible up to thicknesses of 9 mm through clear PET and 2 mm through blue PP. The SORS approach, also in combination with PCA, allows for even greater through barrier assessment, with detection of ethanol through thicknesses of up to 21 mm of clear PET and 9 mm blue PP. Moreover, when using either CR or SORS, we successfully present the benefits of utilizing PCA for probing through barriers, particularly when both the barrier and analyte have peaks in close proximity to one another. Signals are extracted from greater depths using PCA compared to what can be achieved solely by eye, e.g. using the SORS set up it is possible to visually detect spectral contribution from ethanol up to 15 mm through PET but up to 21 mm using PCA.

Previous work has reported on the use of CR detection through plastic bags and plastic containers. Using benchtop SORS equipment, liquid screening through plastic and has been reported in thicknesses of up 4 mm glass and 4.5 mm PP. This work demonstrates the potential of both CR and SORS for through barrier detection, highlighting the ability of both handheld instruments to see through large thicknesses. In addition, we show the maximum thickness to which through barrier detection can take place and highlight the analytical capabilities of both the instruments for through barrier detection. More specifically, the high degree of sensitivity and capabilities of handheld SORS with back-scattering collection optics is particularly exciting. Both techniques, CR and SORS, demonstrate the applications of handheld Raman in several fields including security. Furthermore, SORS holds notable promise in through barrier detection when obscuring objects such as plastic and glass are present, as well as in a clinical setting, namely disease diagnostics.

2.6 References

- 1 K. Gracie, E. Correa, S. Mabbott, J. a. Dougan, D. Graham, R. Goodacre and K. Faulds, *Chem. Sci.*, 2014, **5**, 1030.
- 2 C. A. Lieber, S. K. Majumder, D. L. Ellis, D. D. Billheimer and A. Mahadevan-Jansen, *Lasers Surg. Med.*, 2008, **40**, 461–467.
- 3 M. J. Baker and K. Faulds, *Chem. Soc. Rev.*, 2016, **45**, 1792–1793.
- 4 A. Jaworska, L. E. Jamieson, K. Malek, C. J. Campbell, J. Choo, S. Chlopicki and M. Baranska, *Analyst*, 2014, **140**, 2321–2329.
- 5 J. C. Carter, S. M. Angel, M. Lawrence-Snyder, J. Scaffidi, R. E. Whipple and J. G. Reynolds, *Appl. Spectrosc.*, 2005, **59**, 769–775.
- 6 N. C. Shand, *SPIE Eur. Secur. Def.*, 2008, **7119**, 71190J–71190J–12.
- 7 D. S. Moore and R. J. Scharff, *Anal. Bioanal. Chem.*, 2009, **393**, 1571–1578.
- 8 A. Macleod, N and P. Matousek, *Appl. Spectrosc.*, 2008, **62**, 291–304.
- 9 P. Matousek, I. P. Clark, E. R. C. Draper, M. D. Morris, a E. Goodship, N. Everall, M. Towrie, W. F. Finney and A. W. Parker, *Appl. Spectrosc.*, 2005, **59**, 393–400.
- 10 P. Matousek and N. Stone, *Chem. Soc. Rev.*, 2016, **45**, 1794–1802.
- 11 P. Matousek, *Appl. Spectrosc.*, 2006, **60**, 1341–1347.
- 12 C. Eliasson, N. a Macleod and P. Matousek, *Anal. Chem.*, 2007, **79**, 8185–9.
- 13 K. Buckley, C. G. Atkins, D. Chen, H. G. Schulze, D. V Devine, M. W. Blades and R. F. B. Turner, *Analyst*, 2016, **141**, 1678.
- 14 M. V Schulmerich, K. a Dooley, M. D. Morris, T. M. Vanasse and S. a Goldstein, *J. Biomed. Opt.*, 2015, **11**, 060502.
- 15 P. Matousek, E. Draper, A. Goodship, I. Clark, K. Ronayne and A. W. Parker, 2006, **60**, 758–763.
- 16 N. Stone, R. Baker, K. Rogers, A. W. Parker and P. Matousek, *Analyst*, 2007, **132**, 899–905.
- 17 M. Bloomfield, P. W. Loeffen and P. Matousek, *Proc. SPIE*, 2010, **7838**, 783808-1-783808–15.

- 18 R. J. Hopkins, S. H. Pelfrey and N. C. Shand, *Analyst*, 2012, **137**, 4408–4410.
- 19 D. L. Ellis, H. Muhamadali, S. A. Haughey, C. . Elliot and R. Goodacre, *Anal. methods*, 2015, **7**, 9401–9414.
- 20 R. J. Stokes, M. Bailey, S. Bonthron, T. Stone, G. Maskall, O. Presly, E. Roy, C. Tombling and P. W. Loeffen, 2016, **9995**, 999506.
- 21 L. E. Jamieson and H. J. Byrne, *Vib. Spectrosc.*
- 22 H. J. Butler, L. Ashton, B. Bird, G. Cinque, K. Curtis, J. Dorney, K. Esmonde-white, N. J. Fullwood, B. Gardner, P. L. Martin-Hirsch, M. J. Walsh, M. R. Mcainsh, N. Stone and F. L. Martin, *Nat. Protoc.*, 2016, **11**, 664–687.
- 23 M. A. Bedics, H. Kearns, J. M. Cox, S. Mabbott, F. Ali, N. C. Shand, K. Faulds, J. B. Benedict, D. Graham and M. R. Detty, *Chem. Sci.*, 2015, **6**, 2302–2306.

3 Through Tissue Imaging of a Live Breast Cancer Tumour Model Using Handheld Surface Enhanced Spatially Offset Resonance Raman Spectroscopy

Accepted manuscript
Nicolson *et al.*, **Chem. Sci.**, 2018, **9**, 3788-3792

Contributing authors and their roles:

Lauren E. Jamieson¹ – Carried out all cell work
Samuel Mabbott¹ – Helped with data processing and preliminary work
Konstantinos Plakas² – Synthesised the dye molecules
Neil C. Shand³ – Provided access to SORS instrumentation and PhD supervisor of FN
Michael R. Detty² – PhD supervisor of Konstantinos Plakas
Duncan Graham¹ – Co-collaborator and PhD supervisor of FN
Karen Faulds¹ – Principal investigator

1. Department of Pure and Applied Chemistry, Technology and Innovation Centre, University of Strathclyde, 99 George Street, Glasgow G1 1RD, UK.
2. Department of Chemistry, University at Buffalo, The State University of New York, New York 14260, USA
3. DSTL, Porton Down, Salisbury, SP4 0JQ, UK.

The supporting information can be found in chapter 9.6

3.1 Abstract

In order to improve patient survival and reduce the amount of unnecessary and traumatic biopsies, non-invasive detection of cancerous tumours is of imperative and urgent need. Multicellular tumour spheroids (MTS) can be used as an *ex vivo* cancer tumour model, to model *in vivo* nanoparticle (NP) uptake by the enhanced permeability and retention (EPR) effect. Surface enhanced spatially offset Raman spectroscopy (SESORS) combines both surface enhanced Raman spectroscopy (SERS) and spatially offset Raman spectroscopy (SORS) to yield enhanced Raman signals at much greater sub-surface levels. By utilizing a reporter that has an electronic transition in resonance with the laser frequency, surface enhanced resonance Raman scattering (SERRS) yields even greater enhancement in Raman signal. Using a handheld SORS spectrometer with back scattering optics, we demonstrate the detection of live breast cancer 3D multicellular tumour spheroids (MTS) containing SERRS active NPs through 15 mm of porcine tissue. False colour 2D heat intensity maps were used to determine tumour model location. In addition, we demonstrate the tracking of SERRS-active NPs through porcine tissue to depths of up to 25 mm. This unprecedented performance is due to the use of red-shifted chalcogenpyrylium-based Raman reporters to demonstrate the novel technique of surface enhanced spatially offset resonance Raman spectroscopy (SESORRS) for the first time. Our results demonstrate a significant step forward in the ability to detect vibrational fingerprints from a tumour model at depth through tissue. Such an approach offers significant promise for the translation of NPs into clinical applications for non-invasive disease diagnostics based on this new chemical principle of measurement.

3.2 Introduction

Non-invasive tumour detection is of vital importance for early cancer diagnosis, resulting in improved patient survival. Multicellular tumour spheroids (MTS) are used as tumour models and mimic *in vivo* tumour physiology. In contrast to traditional 2D monolayer cell cultures, these three dimensional cell models resemble the 3D *in vivo* environment more closely, establishing characteristic concentration gradients in oxygen, nutrients, and metabolites.¹ MTS can be used as an *ex vivo* cancer model, avoiding the need for ethical approval and long term experiments associated with *in vivo* experiments. Termed the enhanced permeability and retention (EPR) effect, tumours retain nanoparticles (NPs) in their microenvironments due to poor lymphatic drainage. Thus, NP uptake is preferential in cancerous cells over healthy cell lines and NPs are frequently used to assist in imaging applications.² MTS can be grown with a uniform distribution of NPs dispersed throughout and can provide a model for NP accumulation in tumours *in vivo*.³ MTS models were used here to develop a Raman imaging technique for effective tumour detection through tissue depths of several millimetres.

Raman spectroscopy has previously been investigated for tumour detection,⁴ but is often limited to biopsy and cellular samples making it unable to non-invasively detect tumours at depth. Spatially offset Raman spectroscopy (SORS) provides a means of non-invasive investigation of tissue samples at depth by offsetting the point of collection from the point of laser excitation typically in the region of a few mm (Δx).^{5,6} Unlike confocal techniques where spectral information can be acquired at a particular depth by focusing the laser to a given distance in the z-axis, SORS makes use of a spatial offset to probe through the barrier/analyte system.⁵ SORS has shown promise in a number of applications including the detection of counterfeit alcohol,⁷ assessment of bone composition^{8,9} and in the analysis of cancerous calcifications in breast tissue.⁴ We have recently reported the use of a handheld SORS spectrometer for the detection of ethanol through up to 21 mm of plastic.¹⁰

When a molecule is adsorbed onto a metal NP surface, enhancement in scattering of the molecularly specific Raman reporter is observed. The surface enhanced Raman scattering (SERS) approach has been shown to yield enhancements several orders of magnitude greater than conventional Raman scattering.¹¹ SERS has been applied in numerous applications including the sensitive detection of DNA,¹² explosives detection,¹³ and in drug delivery sensing.¹⁴ Furthermore, through surface enhanced resonance Raman spectroscopy (SERRS), it is possible to greatly increase the Raman signal generated by the nanotags by using a laser that corresponds to an electronic transition of the Raman analyte to produce enhancements in the order of 10^{10} to 10^{14} .^{15,16}

Surface enhanced spatially offset Raman spectroscopy (SESORS) combines the benefits of SORS with SERS to achieve greater sample interrogation at depth.¹⁷ Using SESORS in a 180° back-scattering configuration, nanotags have been used in glucose sensing,¹⁸ tracked through 6.75 mm of tissue,¹⁹ and up to 8 mm of bone.^{20,21} Using SESORS in a transmission geometry, bisphosphonates have been tracked in bone through 20 mm of tissue²² and Stone *et al.* detected signal from nanotags through 45 – 50 mm of tissue.¹⁷ Several reports in the literature show the potential to target and image tumours *in vivo* using functionalized NPs.^{23,24} Kircher *et al.*, functionalised Au nanoprobe with chalcogenopyrylium based dyes and the EGFR targeting antibody to successfully detect tumours *in vivo* using a mouse model.²⁵ Whilst the authors reported attomolar limits of detection, little knowledge exists on the ability to detect tumours at clinically significant and relevant depths, and therefore the approach presented here provides a model to image and thus demonstrate, NP uptake in cancerous cells at notable depth. Here we report for the first time the use of NPs for the detection of a 3D breast tumour model buried at depths of 15 mm in tissue using a SORS instrument with back scattering optics. This was achieved by growing 3D breast cancer tumour models from cells incubated with SERRS active gold NPs (AuNPs) and then using the signal enhancing benefits of SERRS, combined with the through barrier detection capabilities of SORS, to locate

the tumour model at depth using surface enhanced spatially offset resonance Raman spectroscopy (SESORRS) for the first time. In addition, these SESORRS measurements were carried out using a handheld spectrometer, which could potentially be used in a clinical environment. Furthermore, using the SESORRS approach, we report a penetration depth of up to 25 mm through tissue; the largest thickness to which SERS nanotags have been tracked using a back-scattering configuration.

3.3 Experimental

All chemicals and small molecule Raman reporters were purchased from Sigma Aldrich unless otherwise stated. AuNPs with an average diameter of 83 nm were synthesized using a seeded method and left to stir overnight.²⁶ Briefly, gold seeds of 28 nm were synthesized using the citrate reduction method. Sodium tetrachloroaurate (III) dihydrate (681 μ L, final concentration 0.254M) and sodium citrate trihydrate (528 μ L, final concentration 0.171M) were added to 5.007 ml of 28 nm seeds and made up to 120 ml with dH₂O. The solution was left to stir overnight. NPs were characterized using extinction spectroscopy and had an LSPR of 555 nm. Scanning electron microscope (SEM) images were obtained (Fig.S1, Supporting Information) using a FEI Sirion 200 ultra-high resolution Schottky field emission scanning electron microscope with FEI software.

Chalcogenpyrylium-based dyes were synthesized according to previously reported methods.²⁷ They are named according to the wavelength that they are resonant at. For example, dye 823 is resonant at 823 nm. Dyes 676, 823 and 959 were prepared by dissolving the solid in anhydrous N,N-Dimethylformamide (DMF, 99.8%) to produce a 1 mM stock. Subsequent dilutions were then carried out using DMF and dH₂O (50:50). Raman reporters 1,2-bis(4-pyridyl)ethylene (BPE) and 4,4-azopyridine (AZPY) were prepared by dissolving the solid in ethanol to produce a 10 mM stock. Subsequent dilutions were carried out using dH₂O. Dyes were characterized using extinction spectroscopy (Agilent Cary 60) to determine their λ_{max} . BPE and AZPY are non-resonant Raman reporters.

Measurements were taken using a handheld Resolve instrument from Cobalt Light Systems (830 nm, average laser power 450 mW). All measurements were carried out using a 2 s integration time, 5 accumulations and an 8 mm offset. The nose cone was fitted to use the instrument in a contact mode setting. The handheld instrument used here has a fixed exposure time, therefore it is noted that if longer acquisition times were used, the signal to

noise ratio may have improved. The conventional Raman spectra for each of the five individual Raman reporters used in this work (dye 1-3, BPE and AZPY), can be seen in the Supporting Information (Figure S1). Measurements were carried out using 3 samples. Prior to dye addition, NPs were concentrated by centrifugation (1 mL aliquots, 5000 RPM, 10 mins) and resuspended in 500 μ L of water. Investigation of the nanotags for SESORS applications was carried out by adding each reporter (3 μ L, 300 μ M) to 500 μ L of NPs. The solution was then made up to 1 mL with dH₂O. A final dye concentration of 300 nM was used, thus by keeping the dye concentration as low as possible the benefit of using a Raman reporter which is in resonance with the laser was exploited.

MCF7 human breast cancer cells were cultured in Rosewell Park Memorial Institute medium (RPMI) supplemented with 1% penicillin/streptomycin (10,000 units/mL), 1% fungizone, and 10% heat-inactivated foetal bovine serum (FBS). Cells were incubated at 37 °C and 5% CO₂ in a humidified incubator. Cells at a confluence of ca. 90% growing in a T75 flask were incubated overnight with 571 fM of AuNP (total of 7.092×10^{11} AuNP). The following day, cells were trypsinised and re-suspended in medium to give a concentration of ca. 2.4×10^6 cells/mL. Multicellular tumour spheroids (MTS) were grown using a hanging drop technique by pipetting 20 μ L drops of this cell suspension onto the lid of a petri dish with ca. 12 mL of medium added to the dish. The lid was placed on the dish and MTS grew over a period of 9 days at 37 °C and 5% CO₂ in a humidified incubator. The medium was removed from the drops and replaced after 3 days.

3.4 Results and Discussion

To achieve the detection of the tumour model at depth using the accumulation of NPs within a live 3D tumour model, we used chalcogenpyrylium dyes as resonant Raman reporters in combination with SESORRS detection. The absorbance wavelength of chalcogenpyrylium dyes can be fine-tuned into the near-infrared (NIR) to create a Raman reporter in resonance with the laser excitation wavelength of 830 nm.²⁵ Our previous work has explored the use of red-shifted nanomaterials as SERS probes in the NIR by utilizing large AuNPs in conjunction with chalcogenpyrylium nanotags.²⁸ Chalcogenpyrylium dyes conjugated to large AuNPs have been shown to generate strong SERS responses at picomolar detection levels at 1280 nm²⁷ and 1550 nm laser excitations.²⁸ The chemical structure of each of the five Raman reporters used are shown in Figure 3.1(a-e). The absorbance wavelengths of the highly Raman active chalcogenpyrylium dyes; 676, 823, 959 (Figure 3.1a-c), are tuned by increasing the number of sp² carbons from 1 to 3 to 5 in the aliphatic backbone, thus, the wavelength of absorption is tuned to 676, 823 and 959 nm respectively. ^{28,27} Further fine tuning is achieved through the choice of chalcogen atoms in the ring systems, which causes the absorption maximum to redshift. BPE (d) and AZPY (e) are non-resonant small molecules commonly used for SERS which were used for comparison. SERS spectra for each of these five Raman reporters are shown in the supporting information Figure S2. All measurements were carried out using AuNPs with an average diameter of 83 nm. Each of the five Raman reporters were added to AuNPs to create nanotag solutions with a final dye concentration of 300 nM. The aim was to keep the dye concentration as low as possible by exploiting the benefit of using a Raman reporter that is in resonance with the laser. With regards to the experimental set up, all measurements were carried out using a total exposure time of 10 seconds (2 s integration time, 5 accumulations) at an 8 mm offset. The nose cone was fitted to use the instrument in a contact mode setting. The handheld instrument used here

has a fixed maximum exposure time, therefore it is noted that if longer acquisition times were used, the signal to noise ratio may have improved.

To investigate the advantage of using resonant molecules for *in vivo* applications, nanotag solutions with each reporter were held in a quartz microcuvette. Porcine tissue samples of a 5 mm thickness were placed in front of the cuvette and brought into contact with the laser leaving no space between the nose cone and the sample (supporting information, Figure S3). Spectra were acquired at an 8 mm spatial offset and truncated and baselined prior to processing. We have previously shown that at an 8 mm offset, the greatest level of through barrier detection takes place, which is the maximum capability of the instrument.¹⁰ The height of the most intense peak was then calculated as well as the relative percentage peak intensity (Figure 3.1f). The handheld SORS instrument uses an excitation wavelength of 830 nm and it can be seen clearly in Figure 3.1f that a significant enhancement in signal is generated by the resonant dye 823 compared to the off resonant molecules. Thus, by using a NIR resonant reporter molecule, superior SERRS signal through depth is generated over off resonant reporter molecules and the technique of SESORRS for greater through tissue detection is clearly demonstrated.

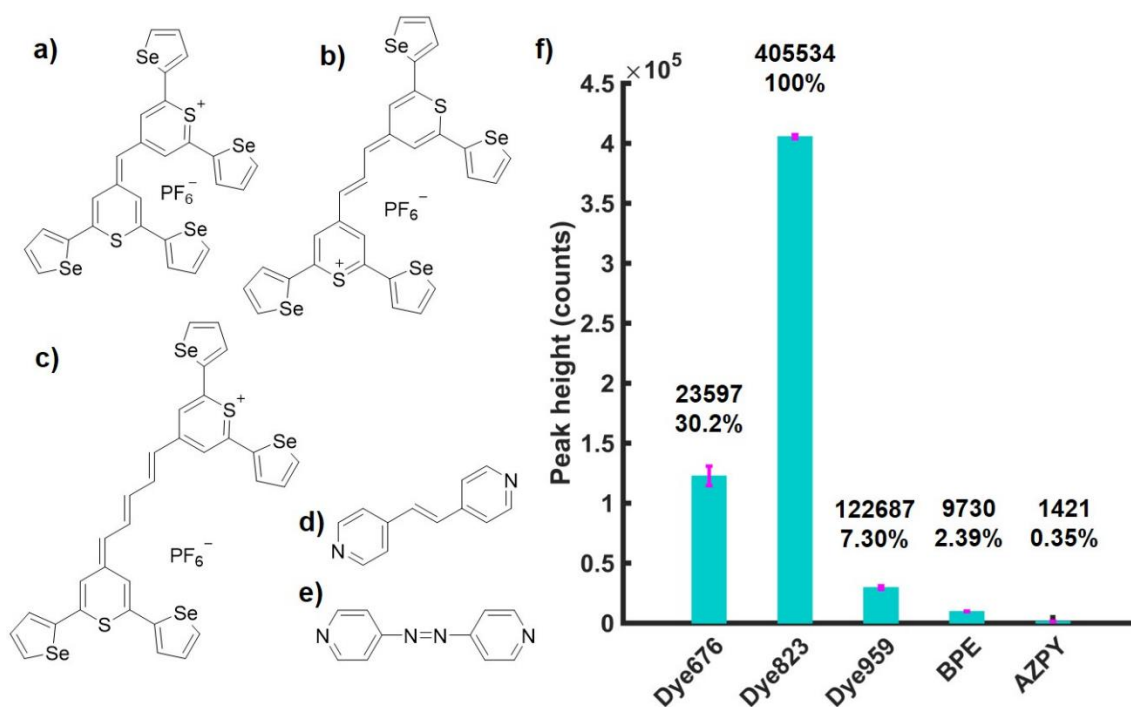


Figure 3.1- (a – e) Chemical structure of dye676, dye823, dye959, BPE and AZPY respectively. (f) Bar chart showing average peak intensities of dye676, dye823, dye959, BPE and AZPY at 1598, 1592, 1572, 1201 and 1162 cm^{-1} respectively, as well as the relative percentage peak intensity, through 5 mm of tissue. Nanotag solutions were held in a cuvette and the cuvette was placed behind tissue samples. Spectra were collected using a handheld SORS instrument with 830 nm laser excitation at an 8 mm offset. Peak intensities were obtained by scanning 3 replicate samples, 5 times (2 second integration, 5 accumulations). The average peak intensity for each of the 5 dyes is shown and error bars represent \pm one standard deviation.

MTS were used as a 3D breast cancer tumour model to demonstrate the clinical significance of SESORRS for *in vivo* diagnostics. MCF7 human breast cancer cells were incubated overnight with the dye 823 nanotag solution (571 fM of AuNps, total of 7.092×10^{11} AuNp) resulting in uptake and accumulation of the nanotags within the cancer cells. MTS were then grown from a suspension of these cells using a hanging drop technique by pipetting 20 μL drops of MCF7 human breast cancer cell suspension onto the lid of a petri dish. They were grown over a period of 9 days at 37 $^{\circ}\text{C}$ and 5% CO_2 in a humidified incubator to a size $<1\text{mm}$. No reduction in growth was observed. It is therefore reasonable to assume that the dyes did not cause cell death since cells need to be alive in order to divide and replicate to form MTS models. Previous reports show that NPs are homogenously dispersed throughout the MTS.³

As described in Figure S4, supporting information, roughly 10 MTS were transferred to a section of tissue (a). A 15 mm section of porcine tissue was then placed on top of the tissue layer upon which the MTS models were positioned (b). This model simulated the detection of SERRS active nanotags in tumours through tissue using the SORS approach. A translational x-y stage with a range of 2.54 cm was used to manoeuvre the tissue samples in steps of 3 mm to create an image of 7 x 7 pixels. As per the experimental set up described in Figure S4, supporting information, the tissue system was brought into contact with the nose cone, and the z-value remained fixed, i.e. the stage was not moved in the z-direction. By fixing the z-direction, and utilising the SORS technique, we were able to probe through the tissue barrier to detect the MTS models through 15 mm of tissue. This was achieved by moving the stage the x-y direction to detect the MTS models through the tissue barrier. A false colour 2D SESORRS heat map of the peak intensity at 1178 cm^{-1} was then constructed, Figure 3.2a. This corresponds to the uptake of dye 823 nanotags into MTS. Clear discrimination is seen between areas where the MTS were present and where they were not (Figure 3.2 a,b). There is a direct correlation between where the MTS models containing the SERRS-active nanotags were placed and the observed area of maximum intensity on the 2D map, i.e. the area of maximum intensity corresponds to the region in which the MTS models were positioned, (Figure S4, supporting information). Similarly, at the point of minimum intensity in areas where the MTS models were not present, there was no spectral contribution from the dye (Figure 3.2). In this instance, the observed spectrum corresponds to that of the tissue. Therefore, since we know the precise location of the spheroids in the tissue, control spectra can be generated on the same image but away from the MTS deposition point. Furthermore, the SERRS-active NPs were contained within the spheroids themselves and therefore their location within in the system was known prior to imaging. The number of NPs present in each MTS was significantly less than for a bulk sample i.e. a nanotag solution held in a cuvette. However,

despite this, the extremely sensitive detection of both dye 823 peaks at 1178 and 1592 cm^{-1} is confirmed in areas where the nanotags, and hence spheroid tumour model, were present (Figure 3.2b), and thus the successful mapping of MTS through 15 mm of tissue using SESORRS was achieved. This proof of concept experiment demonstrates that targeted NPs in combination with SESORRS imaging could potentially be used to locate tumour at depth *in vivo*.

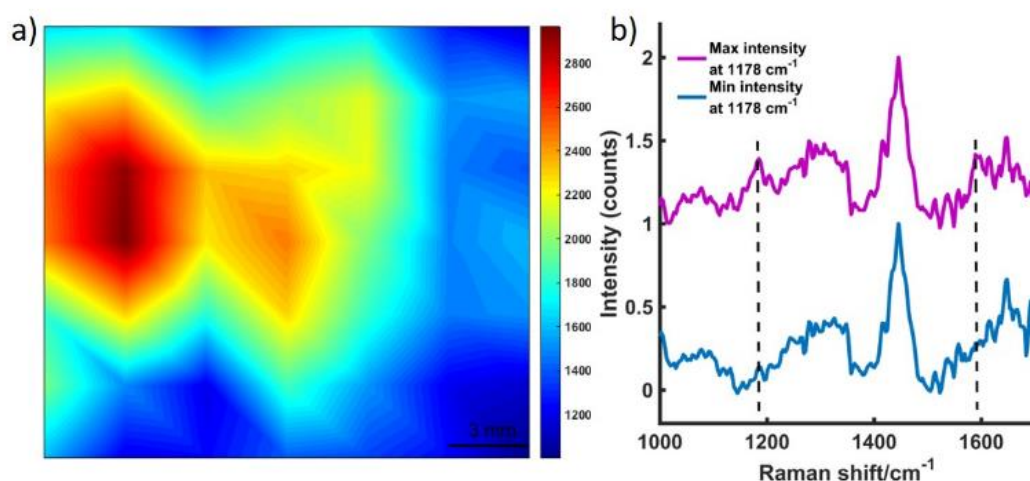


Figure 3.2 (a) A false colour xy-2D heat SESORRS map of MTS containing dye823 through 15 mm of tissue. The map was constructed using the peak intensity at 1178 cm^{-1} . Measurements were carried out using an xy translational stage in step sizes of 3 mm to create an image of 7 x 7 pixels. Spectra were truncated, baselined and smoothed prior to processing. A combination surface/contour false colour was used to generate a 2D heat map and show the tracking of the MTS through 15 mm of tissue. Clear discrimination is seen between spectra collected at the point of maximum intensity where the nanotags were spotted and that collected where the nanotags were not present. **(b)** The corresponding maximum and minimum collected 8 mm offset spectra. All measurements were carried out using a 2 s integration time, 5 accumulations, 830 nm laser excitation wavelength.

In a secondary, but no less significant demonstration of the power of this approach, dye 823 SERRS-active nanotags were detected through 25 mm of tissue. The nanotags were held in a quartz microcuvette (supporting information Figure S3) and placed behind 25 mm of porcine tissue. Figure 3.3 shows the dye 823 reference spectrum and tissue reference spectrum (top and bottom). The middle spectrum refers to SESORRS signal collected using an 8 mm offset. Both characteristic dye 823 peaks (1178 cm^{-1} and

1592 cm^{-1}) are detectable by eye with the peak at 1178 cm^{-1} having greater distinction due to the lack of spectral overlap from the tissue in the 1600 cm^{-1} region. A scaled subtraction was also applied (Figure S5, supporting information). This also confirms the detection of dye 823 demonstrating impressive potential of the SESORRS approach to detect nanotags through 25 mm of tissue using a back-scattering configuration by controlling the SERRS effect to achieve superior depth penetration. In previous collaborations with Stone and Matousek non-resonant SERS nanotags were detected through depths of up to 25 and 50 mm, however this was using a transmission geometry and a benchtop instrument.¹⁷ The results detailed here report the largest thickness that nanotags have been detected through using a back-scattering optical approach. Furthermore, all previous reports of SESORS has involved a benchtop system and this work highlights the ability of a handheld instrument to detect SESORRS signals through large thicknesses of tissue.

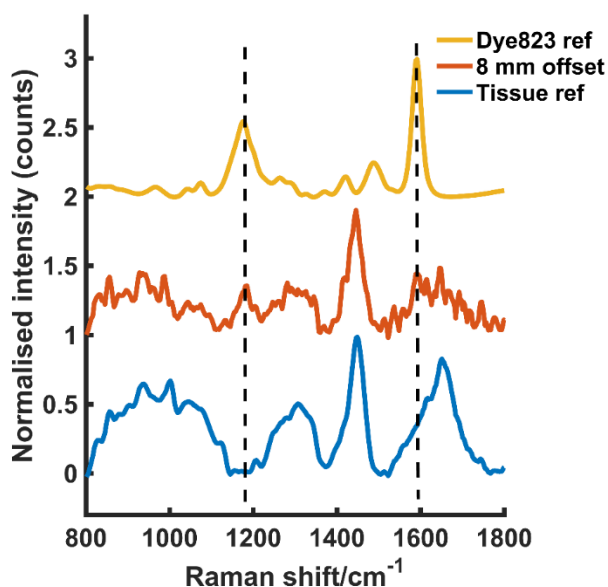


Figure 3.3 - The tracking of dye 823 nanotag solution through 25 mm of tissue. The tissue and dye823 reference spectra are shown at the bottom and top respectively. The middle spectrum represents the Raman signal collected at an 8 mm offset through 25 mm of tissue. The peak at 1178 cm^{-1} is easily detectable by eye and the peak at 1592 cm^{-1} is also detectable, albeit to a lesser extent. All measurements were carried out using a 2 s integration time, 5 accumulations, 830 nm laser excitation wavelength

3.5 Conclusions

Through utilizing powerful chalcogenpyrylium-based Raman reporters for SERRS applications in combination with SORS we present the SESORRS technique for the first time, made possible through the resonant Raman tags, and report the highly significant and successful detection of 3D breast tumour models through 15 mm of tissue. To the best of our knowledge this is the first report of the detection of 3D tumour models using SESORRS. Furthermore, we show it is possible to detect nanotags through up to 25 mm of tissue, which is the largest thickness of through barrier detection reported using a back-scattering geometry, in contrast to a transmission approach. Previous work in the SESORS field has also involved benchtop systems, which are bulky and lack portability. The handheld instrument used in this instance has a fixed accumulation, i.e. the instrument permits only a certain maximum exposure time. Thus, whilst we would expect to achieve larger depth penetration and improved signal to noise with high-end benchtop systems which can facilitate longer acquisition times, particularly when resonant reporter molecules are used, the results described here show the excellent potential of handheld SORS which is more suited to clinical applications. Through the exploitation of the resonance effect, this novel work represents a significant step forward in the detection of vibrational fingerprints through tissue samples. Thus, an important step forward in the use of handheld back-scattering SESORRS for potential clinical applications including non-invasive tumour detection is demonstrated. Future work will focus on targeting and imaging tumours *in vivo* using SESORRS through the use of dual functionalised NPs, i.e NPs functionalised with both a reporter molecule and a biomolecule that specifically targets the tumour *in vivo*. The use of a Raman reporter molecule will then facilitate the imaging of diseased tissue at depth due to accumulation of biofunctionalised NPs at the tumour site. Investigation of tumour depth location is also important and this will be investigated as the imaging capabilities of SORS develops to give a better insight into tumour location *in vivo*.

3.6 References

- 1 L. E. Jamieson, D. J. Harrison and C. J. Campbell, *Analyst*, 2015, **140**, 3910–3920.
- 2 A. B. Chinen, C. M. Guan, J. R. Ferrer, S. N. Barnaby, T. J. Merkel and C. A. Mirkin, *Chem Rev*, 2015, **115**, 10530–10574.
- 3 L. E. Jamieson, V. L. Camus, P. O. Bagnaninchi, K. M. Fisher, G. D. Stewart, W. H. Nailon, D. B. McLaren, D. J. Harrison and C. J. Campbell, *Nanoscale*, 2016, **8**, 16710–16718.
- 4 N. Stone, R. Baker, K. Rogers, A. W. Parker and P. Matousek, *Analyst*, 2007, **132**, 899–905.
- 5 P. Matousek, *Chem. Soc. Rev.*, 2007, **36**, 1292–1304.
- 6 P. Matousek and N. Stone, *Chem. Soc. Rev.*, 2016, **45**, 1794–1802.
- 7 D. I. Ellis, R. Eccles, Y. Xu, J. Griffen, H. Muhamadali, P. Matousek, I. Goodall and R. Goodacre, *Sci. Rep.*, 2017, **7**, 12082.
- 8 G. Feng, M. Ochoa, J. R. Maher, H. A. Awad and A. J. Berger, *J. Biophotonics*, 2017, **10**, 990–996.
- 9 K. Sowoidnich, J. H. Churchwell, K. Buckely, A. E. Goodship, A. W. Parker and P. Matousek, *Analyst*, 2017, **142**, 3219.
- 10 F. Nicolson, L. E. Jamieson, S. Mabbott, N. C. Shand, D. Graham and K. Faulds, *J. Raman Spectrosc.*, 2017, **48**, 1828–1838.
- 11 S. Schlucker, *Angew. Chemie - Int. Ed.*, 2014, **53**, 4756–4795.
- 12 Y. C. Cao, R. Jin and C. A. Mirkin, *Science*, 2002, **297** VN-, 1536–1540.
- 13 S. S. R. Dasary, A. K. Singh, D. Senapati, H. Yu and P. C. Ray, *J. Amer. Chem. Soc.*, 2009, **131**, 13806–13812.
- 14 J. Song, L. Pu, J. Zhou, B. Duan and H. Duan, *ACS Nano*, 2013, **7**, 9947–9960.
- 15 B. Sharma, R. R. Frontiera, A.-I. Henry, E. Ringe and R. P. Van Duyne, *Mater. Today*, 2012, **15**, 16–25.
- 16 S. McAughtrie, K. Faulds and D. Graham, *J. Photochem. Photobiol. C Photochem. Rev.*, 2014, **21**, 40–53.
- 17 N. Stone, M. Kerssens, G. R. Lloyd, K. Faulds, D. Graham and P. Matousek, *Chem. Sci.*, 2011, **2**, 776–780.
- 18 K. Ma, J. M. Yuen, N. C. Shah, J. T. Walsh, M. R. Glucksberg and R. P. Van Duyne, *Anal Chem*, 2011, **83**, 9146–9152.
- 19 S. M. Asiala, N. C. Shand, K. Faulds and D. Graham, *ACS Appl. Mater.*

- Interfaces*, 2017, **9**, 25488–25494.
- 20 B. Sharma, K. Ma, M. R. Glucksberg and R. P. Van Duyne, *J. Am. Chem. Soc.*, 2013, **135**, 17290–17923.
 - 21 A. S. Moody, P. C. Baghernejad, K. R. Webb and B. Sharma, *Anal. Chem.*, 2017, **89**, 5688–5692.
 - 22 H. N. Xie, R. Stevenson, N. Stone, A. Hernandez-Santana, K. Faulds and D. Graham, *Angew. Chemie - Int. Ed.*, 2012, **51**, 8509–8511.
 - 23 X. Qian, X.-H. Peng, D. O. Ansari, Q. Yin-Goen, G. Z. Chen, D. M. Shin, L. Yang, A. N. Young, M. D. Wang and S. Nie, *Nat. Biotechnol.*, 2008, **26**, 83–90.
 - 24 A. Oseledchyk, C. Andreou, M. A. Wall and M. F. Kircher, *ACS Nano*, 2017, **11**, 1488.
 - 25 S. Harmsen, M. A. Bedics, M. A. Wall, R. Huang, M. R. Detty and M. F. Kircher, *Nat. Commun.*, 2015, **6**, 6570.
 - 26 W. Leng, P. Pati and P. J. Vikesland, *Environ. Sci. Nano*, 2015, **2**, 440–453.
 - 27 M. A. Bedics, H. Kearns, J. M. Cox, S. Mabbott, F. Ali, N. C. Shand, K. Faulds, J. B. Benedict, D. Graham and M. R. Detty, *Chem. Sci.*, 2015, **6**, 2302–2306.
 - 28 H. Kearns, M. A. Bedics, N. C. Shand, K. Faulds, M. R. Detty and D. Graham, *Analyst*, 2016, **141**, 5062–5065.

4 Multiplex Imaging of Live Breast Cancer Tumour Models Through Tissue Using Handheld Surface Enhanced Spatially Offset Resonance Raman Spectroscopy (SESORRS)

Accepted to *Chem. Commun.*, 2018, **54**, 8530-8533

Contributing authors and their roles:

Lauren E. Jamieson¹ – Carried out all cell work
Samuel Mabbott¹ – Helped with data processing and preliminary work
Konstantinos Plakas² – Synthesised the dye molecules
Neil C. Shand³ – Provided access to SORS instrumentation and PhD supervisor of FN
Michael R. Detty² – PhD supervisor of Konstantinos Plakas
Duncan Graham¹ – Co-collaborator and PhD supervisor of FN
Karen Faulds¹ – Principal investigator

1. Department of Pure and Applied Chemistry, Technology and Innovation Centre, University of Strathclyde, 99 George Street, Glasgow G1 1RD, UK.
2. Department of Chemistry, University at Buffalo, The State University of New York, New York 14260, USA
3. DSTL, Porton Down, Salisbury, SP4 0JQ, UK.

The supporting information can be found in chapter 9.7

4.1 Abstract

Through utilizing the depth penetration capabilities of surface enhanced spatially offset resonance Raman spectroscopy (SESORRS), multiplexed imaging of three nanotags taken up into breast cancer tumour models is reported for the first time through depths of 10 mm using a handheld SORS instrument.

4.2 Introduction

With the number of new cases of cancer expected to rise by approximately 70% in the next two decades,¹ non-invasive tumour detection is of profound importance for early diagnosis and improved patient survival. Surface enhanced Raman scattering (SERS) has emerged as a promising tool for biomedical imaging.^{2,3} SERS has been deployed in numerous biomedical applications including biosensing⁴ and in the detection of cancer *in vivo*.^{5,6} Surface enhanced resonance Raman scattering (SERRS) utilises a Raman reporter molecule with an electronic transition close to the laser frequency of the Raman instrument, thus generating further enhancement in Raman signal. SERRS holds promise over fluorescence based methods, particularly in multiplexing applications due to the sharp fingerprint spectrum obtained. This allows multiple analyte molecules to be detected simultaneously without the need for separation or multiple excitation wavelengths.⁷ The ability to simultaneously detect multiple biomarkers in a sensitive and non-destructive manner is of profound interest in disease diagnostic applications. Using confocal techniques, the simultaneous detection of multiple SERS nanotags has been reported *in vivo*⁸ as well as the detection of three breast cancer biomarkers in mouse models.³ Here the ability to not only detect and but also classify multiple SERRS nanotags taken up into *ex vivo* tumour models buried at tissue depths of 10 mm is demonstrated using the technique of surface enhanced spatially offset resonance Raman spectroscopy (SESORRS).

Spatially offset Raman spectroscopy (SORS) is an emerging spectroscopic technique that has been deployed for the non-invasive analysis of turbid media. Unlike confocal techniques, SORS is better equipped to probe through depth⁹ and uses a spatial offset between the point of laser excitation and point of collection to obtain Raman signal from the deeper layers within a sample. SORS has been deployed in numerous security¹⁰⁻¹² and biomedical applications including the analysis of bone^{13,14} and in the identification of calcifications associated with breast cancer.¹⁵ Surface enhanced spatially

offset Raman spectroscopy (SESORS) combines the depth penetration benefits of SORS with the signal enhancing capabilities of SERS to achieve greater sample interrogation at significant depth.⁹ Using a back-scattering configuration, SESORS has been used in glucose sensing,¹⁶ to track nanotags through up to 8 mm of bone,¹⁷ and in the detection of neurotransmitters.¹⁸ Using a transmission approach, Stone *et al.* detected signal from nanotags through up to 50 mm of tissue.^{9,19}

To the best of our knowledge, the only report on the use of SESORS for multiplex imaging was in a previous collaboration with Stone *et al.*, where the ability to detect Raman signal from four SERS nanotags through depths of 20 mm was reported.⁹ The individual nanotags were each injected into four corners of a tissue section. Since the spectral fingerprint of the four nanotags was significantly different for each Raman reporter, the authors were able to assign a specific peak in each of the four spectra to enable the spatial multiplex detection using SESORS. However, this approach utilised a benchtop instrument with transmission geometry which could be challenging for some biomedical applications where it may not be possible to collect Raman scattering in a transmission mode.

Using multicellular tumour spheroids (MTS) as *ex vivo* cancer models, the novel technique of SESORRS has been reported. SESORRS couples the signal enhancing capabilities of SERRS with SORS, to yield enhanced signal at even greater depth.²⁰ By exploiting the ability to tune the absorbance wavelength of chalcogenpyrylium dyes into the near-infrared (NIR),²¹ it is possible to create Raman reporters that are in resonance with the laser excitation wavelength of 830 nm to generate greater resonance enhancement. Thus, successful detection single SERRS-active nanotags taken up into MTS breast cancer tumour models using handheld SESORRS through depths of 15 mm of tissue has been reported.²¹ Now, using the same *ex vivo* breast cancer models, the development of a multiplex imaging system capable of detecting a triplex of three SERRS-active NPs present in MTS is reported and the promise of handheld SESORRS with back-scattering optics for multiplex applications is shown. Not only does this work

highlight the ability to detect multiple analytes at depth, it is the first demonstration of the use of chemometrics to classify a triplex of nanotags located at depths using the SESORRS technique in a 3D tumour model. Furthermore, in comparison a previous report,⁸ it represents the ability to carry out multiplex detection using SESORRS in a clinically relevant scenario.

4.3 Experimental

All chemicals were purchased from Sigma Aldrich unless otherwise stated. AuNPs with an average diameter of 78 nm were synthesized using a seeded method and left to stir overnight.²² Briefly, gold seeds of 28 nm were synthesized using the citrate reduction method. Sodium tetrachloroaurate (III) dihydrate (681 μ L, final concentration 0.254M) and sodium citrate trihydrate (528 μ L, final concentration 0.171M) were added to 5.007 ml of 28 nm seeds and made up to 120 ml with dH₂O. The solution was left to stir overnight. NPs were characterized using extinction spectroscopy and had an LSPR of 550 nm.

Chalcogenpyrylium-based dyes were synthesized according to previously reported methods.²¹ They are named according to the wavelength that they are resonant at, e.g. dye823 is resonant at 823 nm. Dyes 810, 813 and 823 were prepared by dissolving the solid in anhydrous N,N-Dimethylformamide (DMF, 99.8%) to produce a 1 mM stock. Subsequent dilutions were then carried out using DMF and dH₂O (50:50). Dyes were characterized using extinction spectroscopy (Agilent Cary 60) to determine their λ_{max} .

SERRS and SESORRS measurements were taken using a handheld Resolve instrument from Cobalt Light Systems (830 nm, average laser power 450 mW). All measurements were carried out using a 2 s integration time, 5 accumulations and an 8 mm offset. The nose cone was fitted to use the instrument in a contact mode setting. Measurements were carried out using 3 samples. Prior to dye addition, NPs were concentrated by centrifugation (1 mL aliquots, 5000 RPM, 10 mins) and resuspended in 500 μ L of water. The Raman reporters were added to the nanoparticles and the solution made up to 1 ml with dH₂O. This produced SERRS nanotags with a final concentration of 300 nM.

MCF7 human breast cancer cells were cultured in Rosewell Park Memorial Institute medium (RPMI) supplemented with 1% penicillin/streptomycin (10,000 units/mL), 1% fungizone, and 10% heat-inactivated foetal bovine serum (FBS). Cells were incubated at 37 °C and 5% CO₂ in a humidified

incubator. Cells at a confluence of ca. 90% growing in a T75 flask were incubated overnight with 13.7 pM of AuNP. The following day, cells were trypsinised and re-suspended in medium to give a concentration of ca. 3.68×10^6 cells/mL. Multicellular tumour spheroids (MTS) were grown using a hanging drop technique by pipetting 20 μ L drops of this cell suspension onto the lid of a petri dish with ca. 12 mL of medium added to the dish. The lid of the petri dish was placed on the dish and MTS grew over a period of 7 days at 37 °C and 5% CO₂ in a humidified incubator. Medium was removed from the drops and replaced after 3 days.

4.4 Results and Discussion

To develop a multiplexed imaging system at depth, gold NPs were synthesised according to previously reported methods.²¹ The resulting particles had an average diameter of 78 nm and were functionalised separately with three different chalcogenpyrylium resonant Raman reporters. These nanotags were then incubated, enabling delivery into live breast cancer tumour models to demonstrate the ability to carry out multiplexed detection at depths of 10 mm in tissue using SESORRS. The chalcogenpyrylium dyes were chosen specifically due to their resonance properties. Previous reports have shown that by exploiting the resonance effect, superior depth penetration can be achieved.²⁰ The absorbance wavelength of the highly Raman active molecules is tuned by controlling the number of sp² carbons in the aliphatic back bone and the chalcogen atoms in the ring system.²¹ The chemical structure of the three Raman reporters used in this work are shown in Figure 4.1 (a-c). Each reporter is named on their absorbance properties, i.e. dye 810 has absorbance maxima at 810 nm. The SERRS spectra for each of the three dyes is also shown in Figure 4.1d.

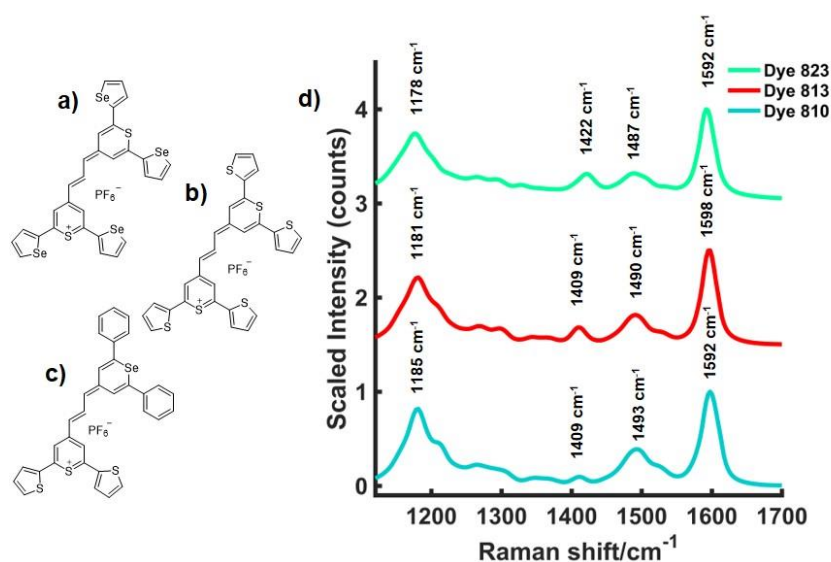


Figure 4.1 – Chemical structure of dye 823 (a), dye 813 (b) and dye810 (c). Dyes were named according to the resonances, i.e. dye823 has an absorbance maximum at 823 nm. (d) SERRS spectra of Dyes 823, 813 and 810. All measurements were carried out using a 2 s integration time, 5 accumulations, 830 nm laser excitation wavelength.

MTS were used as a 3D breast cancer tumour model to demonstrate the clinical significance of SESORRS for *in vivo* multiplex applications. MCF7 human breast cancer cells were incubated overnight with 1 mL of each of the three nanotag solutions containing dye 810, 813 and 823. MCF7 cells were also incubated with a 1 mL triplex solution containing 33% of each of the three SERRS nanotags (13.7 pM of AuNPs), i.e the final number of NPs remained constant. Incubation resulted in the uptake and accumulation of the nanotags within the cancer cells. MTS were then grown from a suspension of these cells using a hanging drop technique. They were grown over a period of 7 days at 37 °C and 5% CO₂ in a humidified incubator to a size <1 mm. Previous reports show that NPs are homogenously dispersed throughout the MTS.²³ The dyes did not cause cell death since the cells divided and replicated in order to form the MTS models.

The experimental set up is described in Figure S1. Approximately 10 MTS containing either a single SERRS nanotag, i.e. dye 823, dye 813 or dye 810, or a triplex of all three nanotags, were transferred to a section of porcine tissue. For example, 10 MTS containing dye 823 were transferred to a single tissue section. Another section of tissue with a 10 mm thickness was then

placed on top of the layer containing the MTS. The same process was applied for the remaining MTS containing the singleplex or triplex nanotags. As such, all MTS models were obscured by 10 mm of tissue. A translational x-y stage with a range of 2.54 cm was used to manoeuvre the tissue samples in steps of 3 mm to create an image of 8 x 8 pixels. The tissue system was brought into contact with the nose cone, and the z-value remained fixed, i.e. the ability to probe through a depth of 10 mm in the z-plane was achieved by using an 8 mm spatial offset. Thus, by utilising, the SESORRS technique, it was possible to detect of each of the four individual MTS models through a 10 mm of tissue barrier.

Using spectra collected at an 8 mm offset, false colour 2D SESORRS heat maps of the peak intensity at 1178 cm^{-1} (dye 823) 1181 cm^{-1} (dye 813), 1185 cm^{-1} (dye 810) and 1181 cm^{-1} (triplex) were then constructed, Figure 4.2. The four peaks were chosen to show the position of the MTS through 10 mm of tissue and correspond to the uptake of both the single nanotags and triplex of nanotags into MTS, rather than the specific contribution of each dye to the acquired spectrum. The false colour images show clear discrimination between areas where the MTS models containing the SERRS-active nanotags were present and where they were not. As such, the areas of maximum intensity in each of the four heat maps correspond to the regions in which the MTS models were positioned (Figure 4.2 a-d). The ability to detect each of the four tumour models containing either the single nanotags or the triplex, is further confirmed in the spectra collected at an 8 mm offset. This can be used as a means to determine if detection of the MTS models has taken place since a SERRS response is observed from the uptake of nanotags into the MTS. The offset spectra collected at the point of maximum intensity, (Figure 4.2 a-d, purple spectra) shows clear detection of MTS containing either single nanotags or a triplex of the three nanotags. The spectra collected at the point of minimum intensity (Figure 4.2 a-d, green) corresponds to the tissue. Thus, by comparing the spectra collected at the point of maximum and minimum intensity through the same barrier thickness

of 10 mm of tissue, successful detection of MTS containing either single or a triplex of varying SERRS nanotags is demonstrated.

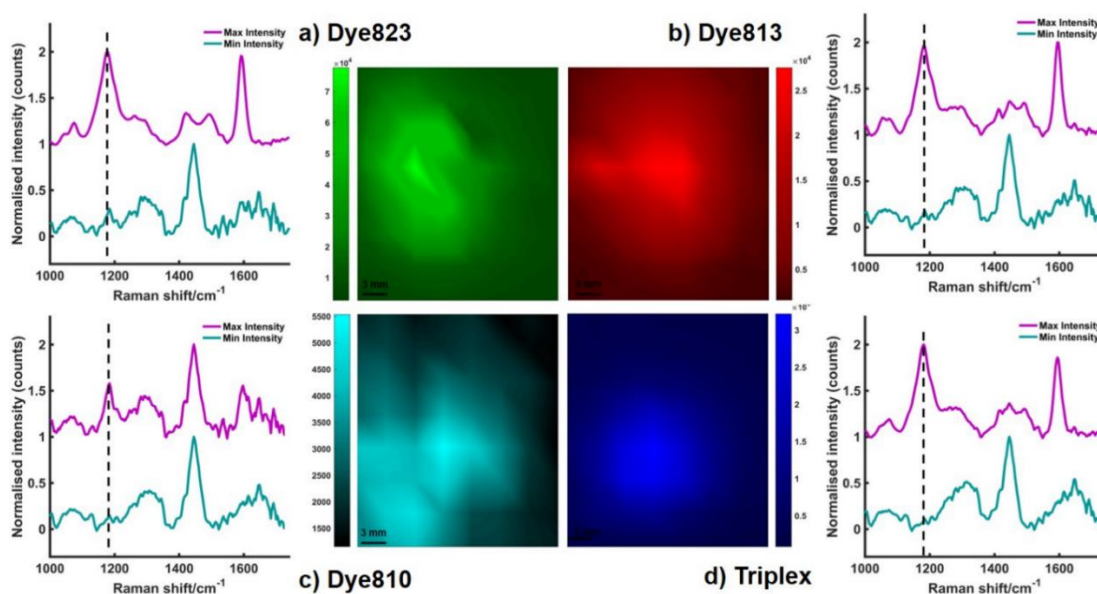


Figure 4.2 – SESORRS False colour 2D heat maps of the peak intensity at (a) 1178 cm^{-1} (dye823), (b) 1181 cm^{-1} (dye813), (c) 1185 cm^{-1} (dye810) and (d) 1181 cm^{-1} (triplex). Measurements were carried out using an xy translational stage in step sizes of 3 mm to create an image of 8 x 8 pixels. 2D heat maps were generated and show the tracking of each of the four MTS models through 10 mm of tissue. Clear discrimination is seen between spectra collected at the point of maximum intensity where the nanotags were spotted and that collected where the nanotags were not present. The corresponding maximum and minimum collected 8 mm offset spectra also confirm the presence of the nanotags in regions where the MTS were spotted (a-d). All measurements were carried out using a 2 s integration time, 5 accumulations, 830 nm laser excitation wavelength.

The focus of the work presented here is to demonstrate the ability to distinguish between multiple nanotags and to specifically spectrally classify single nanotag and a triplex of the three nanotags through depth using SESORRS. Since strong spectral similarity exists between the spectra from the three individual SERRS nanotags and the triplex, principal component analysis (PCA) was applied to analyse the data from the SESORRS multiplex image.²⁴ Offset spectra were acquired at the point of maximum intensity through 10 mm of tissue, i.e. through 10 mm of tissue in the region where the MTS models were present. Sets of spectra were acquired for both the single

nanotags taken up into the MTS models and the MTS models containing the triplex. Reference spectra were also obtained from aqueous solutions of the nanotags containing each of the three single nanotags and a mixture composed of equal amounts of each solution (triplex) were deposited into a quartz microcuvette (path length 1 mm, chamber volume 350 μ L) and placed behind 10 mm of porcine tissue. The final concentration of dye in both the single and triplex solutions was 300 nM. The experimental set up is described in the supplementary information and in Figure S2.

The resulting principal component (PC) scores plots for both the MTS multiplex (a) and the solution multiplex (b) are shown in Figure 4.3. Both plots demonstrate a strong separation between the three single nanotags and the triplex allowing four distinct groupings to be observed. In both the MTS and solution scores plots, the red cluster refers to either MTS models or solutions containing dye813, the teal cluster dye810 and the green cluster dye823. Similarly, the blue cluster refers to either the MTS models or solutions containing the triplex, i.e. equal contributions of dye823, dye813 and dye810. In both scores plots, the SESORRS spectra from the triplex is tightly clustered and clearly separated from the single nanotag samples. Thus, by using the scores plot from the solution multiplex (Figure 4.3b), where the identity of the nanotags and the ratio of the nanotags in the instance of the triplex sample is known, it is possible to use the scores plot as a reference to develop a multiplex imaging system at depth using the SESORRS technique. The PC scores plot allows for not only the successful identification but also impressive discrimination between single and multiplexed SERRS nanotags taken up into tumour models, buried at depths of 10 mm using a handheld SORS spectrometer. The results presented here represent the ability to not only analyze a tissue sample containing SERRS-active nanotags at depth, but also the ability simultaneously classify a sample containing multiple nanotags. The ability to distinguish between multiple SERS analytes has previously been reported using confocal techniques⁸ however the results presented here offer the added advantage of superior depth penetration through the use of backscattering SESORRS. To the best of our knowledge,

this is the first report of the use of PCA in combination with SESORRS to spectrally discriminate between multiple nanotags taken up into *ex vivo* tumour models through depth. Previous work has reported the multiplexing potential of SESORS,⁸ however in that instance, the nanotags were located in different regions of a tissue section, thus a spatial multiplex as was carried out. The work presented here incorporates multiple nanotags into a MTS tumour model, thus representing a step forward in the ability to spectrally classify singleplex nanotags and a triplex of nanotags through 10 mm of tissue. Additionally, since the dyes are so spectrally similar, the potential of SESORRS combined with powerful data analysis to distinguish between multiple analytes through large tissue thicknesses is demonstrated.

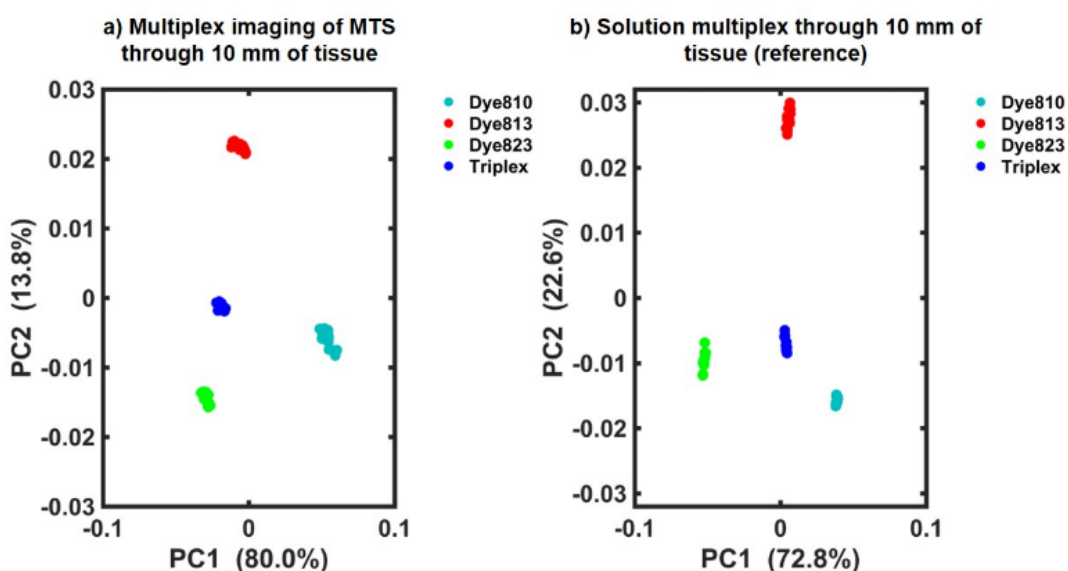


Figure 4.3 – PC scores plots discriminating between the single nanotags and the triplex of all three nanotags uptaken into MTS models (a) and in solution (b) through 10 mm of porcine tissue. In both PC plots, the red cluster refers to the MTS models or solution containing dye 813, the teal cluster dye 810 and the green cluster dye823. Similarly, the blue cluster refers to either the MTS models or solution containing the triplex, i.e. equal contributions of dye 823, dye 813 and dye 810. Distinct separation is seen in both scores plots with the triplex falling in the middle of the three reference single nanotag clusters.

4.5 Conclusions

Through utilising the powerful performance of chalcogenpyrylium-based Raman reporters for superior depth penetration, the ability to identify and discriminate between three different SERRS nanotags taken up into 3D breast cancer tumour models buried at depths of 10 mm is presented. To the best of our knowledge, this is the first report of the use of *ex vivo* breast cancer models for the development of a multiplex imaging system at depth using back-scattering SESORRS. Furthermore, this is the largest thickness to which multiplex detection has been achieved through tissue using not only a handheld back-scattering approach but also the SESORRS technique. Previous work utilising a transmission geometry has shown the potential to multiplex through 20 mm of tissue. However, the results presented here demonstrate the ability to multiplex through the same total thickness using handheld SESORRS using a back-scattering approach. The incident photons reach the MTS models at depths of 10 mm however, following interaction between the nanotags within the MTS models and the incident laser light, the scattered photons are then returned to the collection optics through 10 mm of tissue, thus the total thickness that the photons must travel through is equal to 20 mm. Moreover, previous reports demonstrating SERS multiplexing using a transmission approach have involved benchtop systems which although often bulky, are capable of longer acquisition times and improved signal to noise. The handheld instrument used in this instance is potentially more suited to clinical applications due to improved portability and its user-friendly nature. The ability to simultaneously detect multiple targets *in vivo* is a significant challenge, however through the exploitation of the resonance effect this novel work represents a significant step forward in the ability to detect and discriminate between multiple vibrational fingerprints at depth *in vivo*. Future work will focus on expanding on this proof of concept study by detecting and imaging multiple targets *in vivo* using the SESORRS technique, as well as determining the minimum concentration of NPs required for detection through a given thickness. Future work will focus on

expanding on this proof of concept study by detecting and imaging multiple targets in vivo using the SESORRS technique, as well as determining the minimum concentration of NPs required for detection through a given thickness.

4.6 References

- 1 The World Health Organisation, Cancer Fact Sheet, <http://www.who.int/mediacentre/factsheets/fs297/en/>, (accessed 15 February 2018).
- 2 A. I. Henry, B. Sharma, M. F. Cardinal, D. Kurouski and R. P. Van Duyne, *Anal. Chem.*, 2016, **88**, 6638–6647.
- 3 U. S. Dinish, G. Balasundaram, Y. T. Chang and M. Olivo, *Sci. Rep.*, 2014, **4**.
- 4 R. A. Alvarez-Puebla and L. M. Liz-Marzán, *Small*, 2010, **6**, 604–610.
- 5 X. Qian, X.-H. Peng, D. O. Ansari, Q. Yin-Goen, G. Z. Chen, D. M. Shin, L. Yang, A. N. Young, M. D. Wang and S. Nie, *Nat. Biotechnol.*, 2008, **26**, 83–90.
- 6 A. Oseledchyk, C. Andreou, M. A. Wall and M. F. Kircher, *ACS Nano*, 2017, **11**, 1488.
- 7 S. Schlucker, *Angew. Chemie - Int. Ed.*, 2014, **53**, 4756–4795.
- 8 C. L. Zavaleta, B. R. Smith, I. Walton, W. Doering, G. Davis, B. Shojaei, M. J. Natan and S. S. Gambhir, *Proc. Natl. Acad. Sci. U. S. A.*, 2009, **106**, 13511–13516.
- 9 N. Stone, M. Kerssens, G. R. Lloyd, K. Faulds, D. Graham and P. Matousek, *Chem. Sci.*, 2011, **2**, 776–780.
- 10 C. Eliasson, N. a Macleod and P. Matousek, *Anal. Chem.*, 2007, **79**, 8185–9.
- 11 F. Nicolson, L. E. Jamieson, S. Mabbott, N. C. Shand, D. Graham and K. Faulds, *J. Raman Spectrosc.*, 2017, **48**, 1828–1838.
- 12 D. I. Ellis, R. Eccles, Y. Xu, J. Griffen, H. Muhamadali, P. Matousek, I. Goodall and R. Goodacre, *Sci. Rep.*, 2017, **7**, 12082.
- 13 G. Feng, M. Ochoa, J. R. Maher, H. A. Awad and A. J. Berger, *J. Biophotonics*, 2017, **10**, 990–996.
- 14 K. Sowoidnich, J. H. Churchwell, K. Buckely, A. E. Goodship, A. W. Parker and P. Matousek, *Analyst*, 2017, **142**, 3219.
- 15 N. Stone and P. Matousek, *Cancer Res.*, 2008, **68**, 4424–4430.
- 16 K. Ma, J. M. Yuen, N. C. Shah, J. T. Walsh, M. R. Glucksberg and R. P. Van Duyne, *Anal Chem*, 2011, **83**, 9146–9152.
- 17 B. Sharma, K. Ma, M. R. Glucksberg and R. P. Van Duyne, *J. Am. Chem. Soc.*, 2013, **135**, 17290–17923.
- 18 A. S. Moody, P. C. Baghernejad, K. R. Webb and B. Sharma, *Anal.*

- Chem.*, 2017, **89**, 5688–5692.
- 19 N. Stone, K. Faulds, D. Graham and P. Matousek, *Anal. Chem.*, 2010, **82**, 3969–3973.
 - 20 F. Nicolson, L. E. Jamieson, S. Mabbott, K. Plakas, N. Shand, M. Detty, D. Graham and K. Faulds, *Chem. Sci.*, 2018, **9**, 3788–3792.
 - 21 M. A. Bedics, H. Kearns, J. M. Cox, S. Mabbott, F. Ali, N. C. Shand, K. Faulds, J. B. Benedict, D. Graham and M. R. Detty, *Chem. Sci.*, 2015, **6**, 2302–2306.
 - 22 W. Leng, P. Pati and P. J. Vikesland, *Environ. Sci. Nano*, 2015, **2**, 440–453.
 - 23 L. E. Jamieson, V. L. Camus, P. O. Bagnaninchi, K. M. Fisher, G. D. Stewart, W. H. Nailon, D. B. McLaren, D. J. Harrison and C. J. Campbell, *Nanoscale*, 2016, **8**, 16710–16718.
 - 24 H. Kearns, R. Goodacre, L. E. Jamieson, D. Graham and K. Faulds, *Anal. Chem.*, 2017, **89**, 12666–12673.

5 Point and Shoot – The Benefit of Resonant Raman Reporters for Probing Through Plastic and Tissue Barriers Using Handheld Surface Enhanced Raman Spectroscopy (SERS)

Intention to submit to *Analyst* – subject to approval from DSTL

Contributing authors and their roles:

Lauren E. Jamieson¹ – Carried out all cell work
Samuel Mabbott¹ – Helped with data processing and preliminary work
Konstantinos Plakas² – Synthesised the dye molecules
Neil C. Shand³ – Provided access to SORS instrumentation and PhD supervisor of FN
Michael R. Detty² – PhD supervisor of Konstantinos Plakas
Duncan Graham¹ – Co-collaborator and PhD supervisor of FN
Karen Faulds¹ – Principal investigator

1. Department of Pure and Applied Chemistry, Technology and Innovation Centre, University of Strathclyde, 99 George Street, Glasgow G1 1RD, UK.
2. Department of Chemistry, University at Buffalo, The State University of New York, New York 14260, United States
3. DSTL, Porton Down, Salisbury, SP4 0JQ, UK

The supporting information can be found in chapter 9.8.

5.1 Abstract

The ability to probe through barriers and tissue non-invasively is an urgent unmet need in both the security and biomedical imaging fields. Surface enhanced Raman spectroscopy (SERS) has been shown to yield superior enhancement in signal over conventional Raman techniques. Furthermore, by utilising a resonant Raman reporter to produce surface enhanced resonance Raman spectroscopy (SERRS), even greater enhancement in chemical signal can be generated. Here we show the benefit of using red-shifted chalcogenopyrylium based Raman reporters for probing through large thicknesses of plastic and tissue barriers. Furthermore, the benefit of using a resonant Raman reporter for superior levels of through barrier detection is demonstrated. Raman signals were collected from SERRS active nanotags through plastic thicknesses of up to 20 mm, as well as the detection of the same SERRS nanotags through up to 10 mm of tissue sections using a handheld conventional Raman spectrometer. The ability to detect SERRS-active nanotags taken up into *ex vivo* tumour models known as multicellular tumour spheroids (MTS), through depths of 5 mm of tissue was also shown. The advantages of applying multivariate analysis for through barrier detection when discriminating analytes with similar spectral features as the barrier is also clearly demonstrated. To the best of our knowledge, this is the first report of the assessment of the maximum level of through barrier detection using a conventional handheld Raman instrument for SERS applications.

5.2 Introduction

Raman spectroscopy provides sensitive, molecularly specific vibrational information, however it is an inherently weak scattering process.¹ Through the use of molecularly specific Raman reporters adsorbed on the surface of metallic nanostructures, e.g. gold nanoparticles (AuNPs), surface enhanced Raman scattering (SERS) provides a means of enhancing the Raman scattering process by several orders of magnitude.¹ Moreover, by utilising a laser that corresponds to an electronic transition of the analyte, further enhancement can be achieved by surface enhanced resonance Raman scattering (SERRS). Not only has SERRS been reported to produce vibrational fingerprint spectra with enhancements up to 10^{14} , the nanoparticles can also quench the fluorescence that can be an issue with resonant enhancement.^{2,3} Such properties are useful for the purpose of this work where the ability to detect vibrational spectra through barriers is reported.

SERS has been applied in a wide array of biomedical and security applications including the detection of antimicrobial resistant pathogens,³ bacterial spores,⁴ *in vivo* imaging⁵ and in the detection of explosives.⁶ From a security perspective, SERS has been useful in the detection of explosives including dinitrotoluene (DNT)⁷ and trinitrotoluene (TNT).⁶ SERS has been used extensively in applications involving biomedical imaging and nanotags functionalised with biomolecules such as antibodies have assisted in the targeted imaging of numerous cancers *in vivo* including breast,⁸ ovarian⁹ as well as photothermal applications.¹⁰

However, the ability to perform SERS analysis for either security or biomedical applications not only relies upon the effectiveness of the SERS probes themselves, but also on the efficiency and portability of the Raman instrumentation.¹¹ Confocal techniques are frequently applied in order to obtain signal through a barrier, for example plastic or tissue. In this instance, the microscope is focused to a single depth and spectra recorded at each z-plane.¹² It is also possible to use a defocused beam in which a positive and

negative SERS response can be obtained quickly.¹¹ However, such mapping experiments are typically performed using benchtop instruments which are often bulky and lack the portability required to facilitate measurements in the field or clinic. As such, there has been a considerable shift towards advancements in handheld Raman instrumentation in recent years. This is in part due to their ease of use, portability, lower cost and user friendly nature.^{8,13} As a consequence, there has been a substantial increase in the number of portable Raman instruments available on the market.¹⁴

Spatially offset Raman spectroscopy (SORS) is a relatively new technique that is particularly useful for probing through barriers, specifically plastic^{15,16} and tissue.¹⁷ SORS has been used for the detection of ammonium nitrate through 4.5 mm of tissue and in the detection of counterfeit alcohol and also to the transcutaneous,¹⁸ and *in vivo* analysis of bone and bone disease.¹⁹ Using a handheld SORS instrument, we have reported the ability to detect ethanol through up to 21 mm of plastic.¹³ Surface enhanced spatially offset Raman spectroscopy (SESORS) combines SERS and SORS and is useful in the detection of SERS nanotags through considerable thicknesses of tissue.^{20,21} By combining SERS with SORS to yield surface enhanced spatially offset resonance Raman spectroscopy (SESORRS), SERS nanotags present in *ex vivo* breast cancer tumour models were detected through depths of 15 mm of tissue.²² However, in this instance, we aim to demonstrate the powerful capabilities of handheld conventional Raman instrumentation for detecting SERS analytes at significant depth, without the need for SORS techniques.

We have recently reported the use of a handheld conventional Raman instrument for the detection of ethanol through thicknesses of up to 9 mm of plastic.¹³ In combination with multivariate analysis in the form of principal component analysis (PCA), signal was detected through greater depths than could be deconvoluted by eye. Using the same handheld Raman instrument utilised in the work reported here, Van Duyne and co-workers employed SERS for the detection and identification of hair dyes,²³ and in part, for the detection and quantification of intravenous drug therapies.²⁴ Herein we

discuss the use of the same handheld Raman instrument, with back-scattering optics, for the detection of SERRS nanotags through plastic and tissue barriers as well as for the detection of SERRS nanotags taken up into *ex vivo* tumour models. Furthermore, we describe the benefit of using resonant Raman reporters for probing through greater thicknesses. The results presented here are particularly impressive due to the use of a handheld instrument, which unlike microscope-based systems has a fixed focal depth, and in theory, should limit its ability to probe through deeper layers. To the best of our knowledge, this is the first assessment of the use of handheld Raman, rather than SORS, for detecting SERS nanotags through the maximum thickness of plastic and tissue barriers.

5.3 Experimental

5.3.1 Synthesis of SERS nanotags

All chemicals and small molecule Raman reporters were purchased from Sigma Aldrich unless otherwise stated. AuNPs with an average diameter of 78 nm were synthesised using a previously reported method.²² AuNPs were characterised using extinction spectroscopy and had an LSPR of 552 nm. Chalcogenpyrylium-based dyes were synthesized according to previously reported methods.²⁵ Their chemical structures are shown in the supporting information (Figure S1). They are named according to their absorbance maxima. For example, dye823 has an absorbance maxima of 823 nm. Dyes 676, 823 and 959 were prepared by dissolving the solid in anhydrous N,N-dimethylformamide (DMF, 99.8%) to produce a 1 mM stock. Subsequent dilutions were then carried out using DMF and dH₂O (50:50). Raman reporters 1,2-bis(4-pyridyl)ethylene (BPE) and 4,4'-azopyridine (AZPY) were prepared by dissolving the solid in ethanol to produce a 10 mM stock. Subsequent dilutions were carried out using dH₂O. Dyes were characterized using extinction spectroscopy (Agilent Cary 60) to determine their λ_{max} . BPE and AZPY are non-resonant Raman reporters.

Prior to dye addition, NPs were concentrated by centrifugation (1 mL aliquots, 5000 RPM, 10 mins) and resuspended in 500 μL of water. Investigation of the nanotags for SERS applications was carried out by adding each reporter to the AuNPs. The total final volume of each nanotag sample was 1 mL. A final dye concentration of 300 nM was used, keeping the dye concentration as low as possible to exploit the benefit of using a Raman reporter which is in resonance with the laser. The SERS spectra for each of the five Raman reporter molecules is shown in the supporting information, Figure S2.

5.3.2 SERS measurements

All SERS measurements were carried out using a handheld CBEx spectrometer, 785-nm laser excitation wavelength, from Snowy Range Instruments (now Metrohm). Measurements involving plastic were obtained using a 3-s integration time. Tissue experiments were carried out using a 5-s integration time. A point and shoot adaptor with a single element lens and a numerical aperture of 0.5 was fitted for through barrier detection. This gave an average laser power of 43 mW. The focal spot of the CBEx was measured using a beam profiler (BeamMap 2—XYZ scanning slit system 190–2,500 nm, Data-Ray Inc.). The CBEx instrument used in this instance had a spot size of 50–60 microns at a focal distance of 0.5 cm.

5.3.3 Through barrier detection using plastic

Large transparent polyethylene terephthalate (PET) and blue opaque coloured polypropylene (PP) plastic sheets were purchased from a local art shop and then cut up into smaller rectangular pieces (10.5 × 3 cm, thickness 1 mm). The sheets were mounted on a stage and clamped together to create the desired thickness. They were then brought into contact with the laser using the point and shoot adaptor (supporting information, Figure S3). This ensured that there was no air/space between the plastic and instrument. A glass vial containing the nanotags was placed behind the plastic sheets. The glass vials had a 15-mm diameter, 1-mm thickness, and a height of 25 mm (including lid). To determine the maximum thickness of plastic the instruments could detect the SERS nanotags through, measurements were carried out using varying thicknesses of plastic. The thickness of plastic was increased by 1 mm for each set of spectral acquisitions until the maximum thickness at which the instrument could detect the SERS signal from the nanotags was determined.

5.3.4 Cell culture

MCF7 human breast cancer cells were cultured in Rosewell Park Memorial Institute medium (RPMI) supplemented with 1% penicillin/streptomycin

(10,000 units/mL), 1% fungizone, and 10% heat-inactivated fetal bovine serum (FBS). Cells were incubated at 37 °C and 5% CO₂ in a humidified incubator. Cells at a confluence of ca. 90% growing in a T75 flask were incubated overnight with 13.7 pM of AuNP. The following day, cells were trypsinised and re-suspended in medium to give a concentration of ca. 2.4×10^6 cells/mL. Multicellular tumour spheroids (MTS) were grown using a hanging drop technique by pipetting 20 µL drops of this cell suspension onto the lid of a petri dish with ca. 12 mL of medium added to the dish. The lid was placed on the dish and MTS grew over a period of 7 days at 37 °C and 5% CO₂ in a humidified incubator. Medium was removed from the drops and replaced after 2 days.

5.3.5 Through barrier detection using tissue

Pork loin tissue was obtained from a local butcher and cut into sections (roughly 3.5 cm inches x 4 cm with varying thicknesses). Tissue experiments were performed using two approaches. For measurements involving a cuvette, 350 µL of each NP-Dye solution was pipetted into a Suprasil quartz micro cuvette, path length 1 mm, chamber volume 350 µL. Tissue samples of varying thicknesses were then placed in front of the cuvette. The point and shoot adaptor was brought into contact with the tissue samples, thus ensuring there was no space between the instrument and the tissue. The experimental set up is described in the supporting information, Figure S4.

For mapping experiments, MTS models containing the SERRS nanotags were placed directly onto a section of tissue and left to equilibrate for 10 mins. Following this, 5 mm of tissue was then placed on top of the tissue layer containing the MTS models. The two-layer sample was then brought into contact with the laser via the point and shoot adaptor, supporting information, Figure S5. The handheld CBEx instrument was positioned above the tissue samples with the laser pointing down onto the tissue (Figure S3). This set up is more representative of an *in vivo* approach compared to that using the cuvette. An *x-y*-positioning stage was used to enable Raman mapping of either the SERRS active nanotags taken up into MTS through 5

mm of tissue. The stage was moved in 1 mm steps create a 10 x 10 pixel image (total area 1 cm²).

5.3.6 Data processing

All spectra were processed using Matlab software (version 2017a, The MathWorks, Natick, MA, USA). Principal component analysis (PCA) was applied to data involving plastic barriers. Fifteen spectra (five replicates, three samples) of plastic at a given thickness were obtained followed by 15 spectra (five replicates, three samples) of SERS nanotags obscured by plastic of the same thickness. Preprocessing involved truncating and scaling the spectra, before applying the first-order derivative coupled with Savitzky–Golay smoothing. The first-order derivative was used in PCA to remove slight variances in the background, which were found to affect the resulting zero-order PCA plots.²⁶ For mapping experiments, spectra were truncated, baselined and smoothed using Savitzky-Golay filtering before the intensity at 1596 cm⁻¹ at each of the 1 mm steps was plotted as a combination surface/contour false colour 2D heat map.

5.4 Results and discussion

We have previously reported the use of red-shifted chalcogenpyrylium based Raman reporters for both SERS^{1,27,25} and surface enhanced spatially offset Raman spectroscopy (SESORS) applications using NIR Raman excitation.²² By controlling the length of the number of sp² carbons in the aliphatic backbone and the choice of chalcogen atoms in the ring system, it is possible to tune the absorption maximum of the Raman reporter into the near infrared (NIR). More specifically the Raman reporter can be synthesised to be in resonance with the laser wavelength of the Raman instrument, thus making them particularly attractive for SERRS applications. Furthermore, these chalcogenpyrylium dyes have also been shown to outperform commercially available non-resonant Raman reporters including BPE (1,2-bis(4-pyridyl)ethylene) and AZPY (4,4-azopyridine).^{25,22} These studies focused on the attractiveness of these red-shifted chalcogenpyrylium based Raman

reporters for SERS applications in the NIR region, however the results presented here focus on the use of these nanotags for probing through significant depths using conventional handheld Raman. In recent years there has been a shift towards the use of SORS for probing through barriers^{28,29}, however this work explores the use of conventional Raman, rather than SORS, to detect SERS signals at depth through plastic and tissue.

To demonstrate the benefit of using a resonant Raman reporter to probe through large thicknesses of both plastic and tissue, nanotag solutions were prepared by functionalising AuNPs with each of the five Raman reporter molecules, i.e. dye 676 nanotag solution contained AuNPs functionalised with dye 676. The dyes are named according to their absorbance maximum, i.e. dye 676 has a λ_{\max} at 676 nm. Each nanotag solution was initially obscured by plastic barriers and the maximum thickness through which the nanotags could be detected using a handheld Raman instrument, both by eye and using chemometrics, was determined. Figure 5.1 shows the tracking of dye 823 nanotags through thicknesses of up to 21 mm of PET (a) and up to 10 mm of blue PP (b). In both instances the spectrum at the top is the plastic reference spectrum of the barrier and the spectrum at the bottom is of the dye823 nanotags. The handheld instrument used in this work has a laser excitation wavelength of 785 nm, thus nanotags containing dye 823 have an electronic transition close to that of the laser line and are therefore in resonance with the handheld instrument and were expected to generate the largest level of through barrier detection. From previous reports,^{22,25} it was also expected that the off-resonant chalcogenpyrylium-based reporters would also provide superior levels of through barrier detection compared to BPE and AZPY. The PP spectrum is very weak and has a poor signal to noise ratio, with little meaningful spectral characteristics. It is believed that this is due to optical limitations of the handheld instrument, which prevents it from resolving the peaks effectively. However, in this instance, the main aim was not to detect PP peaks, but to use it as a barrier to block SERS signal from the nanotags. As expected, when the thickness of either PET or PP increases, the spectral contribution of dye 823 to the acquired spectrum

diminishes. Through thicknesses of 5 mm PET, dye 823 is clearly observed in the acquired spectrum (1179 and 1596 cm^{-1}). Similar results are observed when dye 823 is tracked through 4 mm of PP. However, as the thickness of plastic is increased, it become difficult to visually detect dye 823. This is particularly true for through barrier detection involving PET, since, although a shoulder that corresponds to that of the dye can be seen in the 1590 to 1600 cm^{-1} region through thicknesses of 10 mm of PET, the dye peak at 1596 cm^{-1} is in close proximity to the plastic peak at 1614 cm^{-1} .

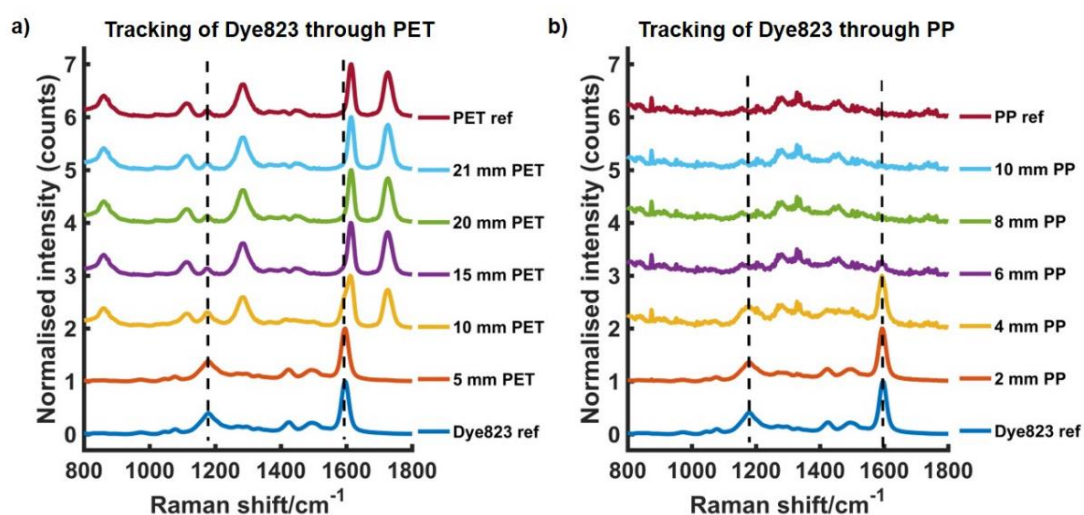


Figure 5.1 – The tracking of dye 823 through PET (a) and PP (b). In both instances, the spectra at the bottom refers dye 823 nanotags and the spectra at the top refers to PET and PP respectively. The dashed line refers to the characteristic dye peaks at 1179 and 1596 cm^{-1} . Spectra were averaged, stacked and normalised for clarity and show the varying contribution of dye 823 and plastic to the acquired spectra as the thickness of the barrier is increased. Measurements were performed using 3 samples, 5 replicates, at a laser excitation wavelength of 785 nm , average laser power 43 mW , and 3-s integration time, five accumulations.

To determine the maximum depth at which dye 823 could be detected, multivariate analysis in the form of PCA was applied. PCA decomposes the spectra into individual components and reduces the dimensionality of the spectroscopic data, thus aiding in the separation of the two layers.^{13,26} Spectra were truncated and scaled, before application of the first order derivative coupled with Savitzky-Golay smoothing.

Figure 5.2 shows the scores plot for the tracking of dye 823 nanotags through 20 mm of clear PET (a) and through 9 mm of blue PP (b). On each of the scores plots, the pink cluster refers to the plastic reference spectra (e.g.

20 mm thick plastic) and the black cluster refers to dye 823 nanotags obscured by plastic of the same thickness, i.e. 20 mm. Convincing separation across PC1 is observed, thus indicating that the instrument is capable of detecting dye 823 SERRS nanotags through 20 mm of clear PET and 9 mm of blue PP using conventional Raman. It is worth noting that as the thickness of plastic increases the score for PC1, which indicates the maximum variance, decreases. This is expected since it demonstrates a decline in variability between reference plastic spectra (e.g. 20 mm thick PET) and spectra obtained of the nanotags obscured by plastic of the same thickness, thus offering further validation that it becomes harder for the instrument to detect SERRS nanotags as the thickness of plastic increases.

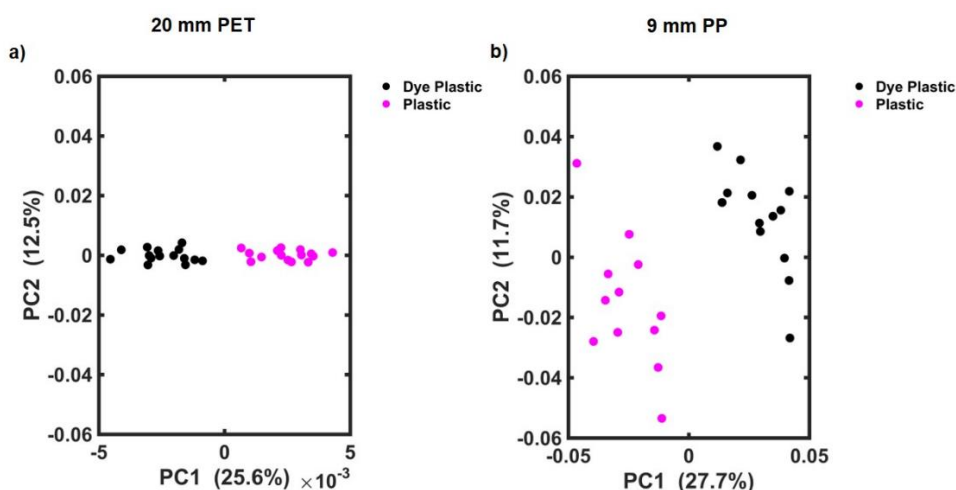


Figure 5.2 – PCA scores plots of the tracking of dye823 through 20 mm of PET and 9 mm of PP using a handheld conventional Raman instrument. In both instances, the pink clusters refer to plastic reference spectra at a given thickness (e.g. 20 mm), and the black cluster refers to a solution of dye 823 nanotags obscured by the same thickness of plastic (e.g. 20 mm). In both instances (PET and PP), clear separation is seen in the score plots indicating that the instrument is capable of detecting a solution of dye 823 nanotags through 20 mm of PET and 9 mm of blue PP.

At thicknesses beyond this, i.e. 21 mm clear PET and 10 mm of blue PP, separation is no longer seen in the scores plot (supporting information, Figure S6), indicating that the Raman instrument is no longer capable of detecting the dye 823 SERRS nanotags through greater barrier thicknesses. Nonetheless, the depth penetration capabilities of this handheld Raman instrument to detect SERRS analytes using a conventional Raman configuration through large thicknesses, without the need for SORS, is

presented. These results suggest that SORS techniques may not always be necessary for probing through barriers. In this instance, using conventional Raman spectroscopy, SERRS nanotags were detected through depths of 20 mm of PET. However, the likelihood that nanotags would need to be tracked through plastic with such a large thickness in a real world situation is slim. Thus, since the majority of plastic containers are only a few mm thick,¹⁵ the results presented here demonstrate the potential of handheld conventional Raman to probe through relevant thicknesses without the need for more complex and expensive optical configuration, such as SORS. In addition, it is clearly demonstrated that using multivariate analysis greatly improves the ability to acquire spectral information and probe through larger thicknesses compared to what can be detected solely by analysing the data by eye.

It is well established that by using a Raman reporter that has an electronic transition that corresponds to the excitation wavelength of the laser, superior enhancement in Raman signal is generated.^{30,31} As already stated, the handheld instrument used in this work has a laser wavelength of 785 nm, thus dye 823 is considered to be in resonance with the laser line. Based on this, dye 676, dye 959, BPE and AZPY are considered to be off resonant reporter molecules. Therefore, taking the signal enhancing benefits of SERRS into account, the ability to detect non-resonant Raman reporters through large thicknesses of plastic was also investigated. In order to demonstrate the advantage of conventional Raman for detection of nanotags functionalised with different Raman reporters at depth, the maximum thickness of plastic through which nanotags functionalised with dye 676, dye 959, BPE and AZPY was determined. The maximum depth that these nanotags could be tracked through was assessed using the same set up used for the assessment of dye 823, i.e. only the choice of Raman reporter differed, and the final concentration of dye was kept constant (300 nM).

The largest thicknesses of clear PET and blue PP that each of the SERS nanotags were detected through using handheld conventional Raman combined with PCA analysis are shown in Table 1. Dye 676, which is absorbs at 676 nm, was successfully detected through 19 mm and 7 mm of

PET and PP respectively. This was followed by dye 959, which absorbs at 959 nm, and was tracked through PET thicknesses of 17 mm and PP thicknesses of 5 mm. Following this, the suitability of the two non-resonant small molecules for through barrier detection applications was also determined. BPE, which has previously been shown to give a good SERS response in the NIR,²⁵ was detectable through 11 mm of PET and 2 mm of PP. This was followed by AZPY which was detected through only 3 mm of PET and 1 mm PP, and thus generated the weakest SERS response through the two barriers.

Table 1 – The maximum thickness of clear PET and blue PP that nanotag solutions of dye 676, dye 823, dye 959, BPE or AZPY were detected through using PCA. Nanotag solutions were prepared by functionalising AuNPs with each of the five Raman reporter molecules, i.e. dye 676 nanotag solution contained AuNPs functionalised with dye 676. The dyes are named according to their absorption maximum, thus dye 823 is resonant at 823 nm and is in resonance with the laser wavelength at 785 nm. Measurements were performed using 3 samples, 5 replicates, at a laser excitation wavelength of 785 nm, average laser power 43 mW, and 3-s integration time, five accumulations.

Raman reporter molecule (300 nM)	Thickness of clear PET (mm)	Thickness of blue PP (mm)
676	19	7
823	20	9
959	17	5
BPE	11	2
AZPY	3	1

The results presented in Table 1 not only demonstrate the advantage of using a resonant Raman reporter for enhanced levels of through barrier detection, but also the benefit of using chalcogenpyrylium-based dyes, over commercially available small molecules, for probing through deeper depths. Overall, superior levels of through barrier detection are achieved when

chalcogenpyrylium-based dyes are used and this supports previous work which has explored the use of the same dyes as SERS nanotags at 1280 nm.²⁵ All three chalcogenpyrylium-based dyes out-perform the commercially available small molecules BPE and AZPY despite dye 676 and dye 959 being off resonant with the 785 nm excitation wavelength. The ability of dye 676 and dye 959 as well as the resonant dye 823 to be detected through large thicknesses of plastic is due to their structural properties in which high polarisability exists. As such, they exhibit large Raman cross sections and are therefore exceptional Raman scatters. Thus, by exploiting these properties to support through barrier detection applications, chalcogenpyrylium-based SERS nanotags were capable of being detected through larger thicknesses of plastic than commercially available reporters. This work demonstrated that in comparison to the commercially available non-resonant Raman reporters BPE and AZPY, chalcogenpyrylium-based dyes are much more effective Raman reporters at longer wavelengths.²⁵ Both these Raman reports have excitation wavelengths that are close to the 785 nm excitation wavelength of the Raman instrument, with dye 823 being closest to resonance. It was observed that both dye 676 and dye 823 generate similar levels of through barrier detection, i.e. they can be detected through similar thicknesses of PET and PP. It is hypothesised that the smaller size of dye 676 compared to dye 823 (one sp² carbon versus three sp² carbons in the aliphatic backbone), means that a greater number of dye molecules can achieve favourable steric arrangements when they interact with the gold surface. Thus, despite dye 676 being further from resonance with the laser excitation wavelength, similar levels of through barrier detection are achieved. Furthermore, it is also worth noting that it was not possible to apply a different point and shoot adaptor lens to the instrument which might afford a greater (or lesser) focal distance. If an adaptor with a longer focal distance was available, it is feasible that through barrier detection would be achieved through even greater thicknesses, particularly with regards to PET since its transparent nature will allow beam penetration to greater depths.

Nonetheless, the work presented here demonstrates the significant potential of handheld Raman to see through large thicknesses of plastic barriers.

Based on these results, it was anticipated that the most suitable Raman reporter for detection of nanotags in through tissue applications would also be dye 823. To confirm this, solutions of each of the five nanotags were held in Suprasil quartz micro cuvette, with a path length 1 mm and a chamber volume 350 μ L. The experimental set up is shown in the supporting information, Figure S4. In keeping with the experiments involving plastic, the final concentration of each of the five Raman reporter molecules was kept at 300 nM. A tissue section (porcine) was placed in front of the nanotags in the cuvette and the point and shoot adapter of the instrument was brought into contact with the tissue. The height of the most intense peak in the spectrum of each of the five Raman reporters was calculated, as well as the relative percentage peak intensity (Figure 5.3). Since dye 823 generated the strongest intensity, it is assigned an intensity value of 100%. The relative peak intensity refers to the peak intensity of nanotags containing dye 676, dye 959, BPE or AZPY obscured by 5 mm of tissue, relative to the peak intensity seen using dye 823. The remaining four peaks are expressed as a percentage relative to that value. As already stated, the handheld Raman instrument has an excitation wavelength of 785 nm, thus the results presented in Figure 5.3 demonstrate that there is a substantial increase in signal with the use of a resonant Raman reporter for probing through tissue barriers, with dye 823 and dye 676 giving the largest signal.

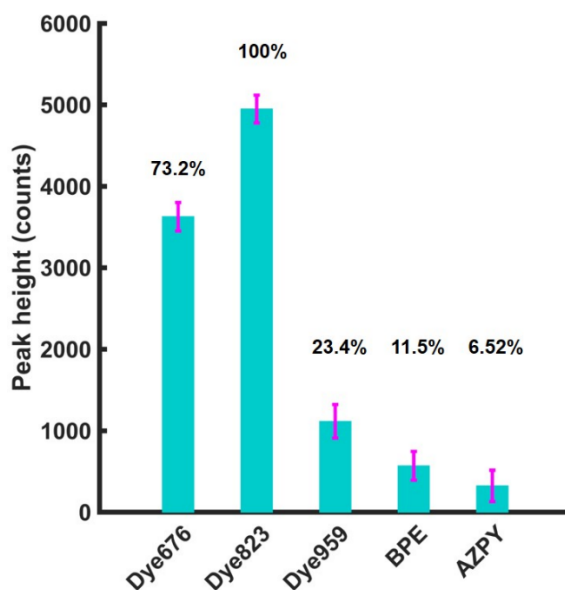


Figure 5.3 - Bar chart showing average peak intensities of dye 676, dye 823, dye 959, BPE and AZPY at 1601, 1596, 1581, 1609 and 1162 cm^{-1} respectively, as well as the relative percentage peak intensity relative to the most intense signal from dye 823, through 5 mm of tissue. Nanotag solutions were held in a cuvette and the cuvette was placed behind tissue samples. Spectra were collected using a handheld CBEx instrument with 785 nm laser excitation. Peak intensities were obtained by scanning 3 replicate samples, 5 times (5 second integration time). The average peak intensity for each of the 5 dyes is shown and error bars represent one standard deviation.

Having established that the resonant dye 823 nanotags gave the most intense SERS response, the maximum thickness of tissue that dye 823 nanotags could be detected through was then investigated. To establish this, the nanotags were held in a cuvette and obscured by varying thicknesses of porcine tissue, Figure 5.4 shows the data obtained through 10 mm of porcine tissue. The characteristic dye peak at 1596 cm^{-1} is clearly visible by eye and thus it can be confidently established that the handheld Raman instrument is capable of detecting the nanotags through 10 mm of tissue. We have previously reported the ability to track the same SERRS nanotags through depths of 25 mm of tissue using a similar experimental set-up using SORS rather than conventional Raman.²² Although the depth penetration achieved here is less than that achieved using the SESORRS technique, the results presented here are impressive for conventional Raman, particularly since the focal distance of the handheld conventional Raman instrument is fixed. It is again anticipated that if a point and shoot adaptor with a longer working

distance was available, dye 823 nanotags could potentially be detected through even greater thicknesses of tissue. Furthermore, these results show the significant potential of handheld Raman for the probing of SERRS nanotags at clinically relevant depths *in vivo*.

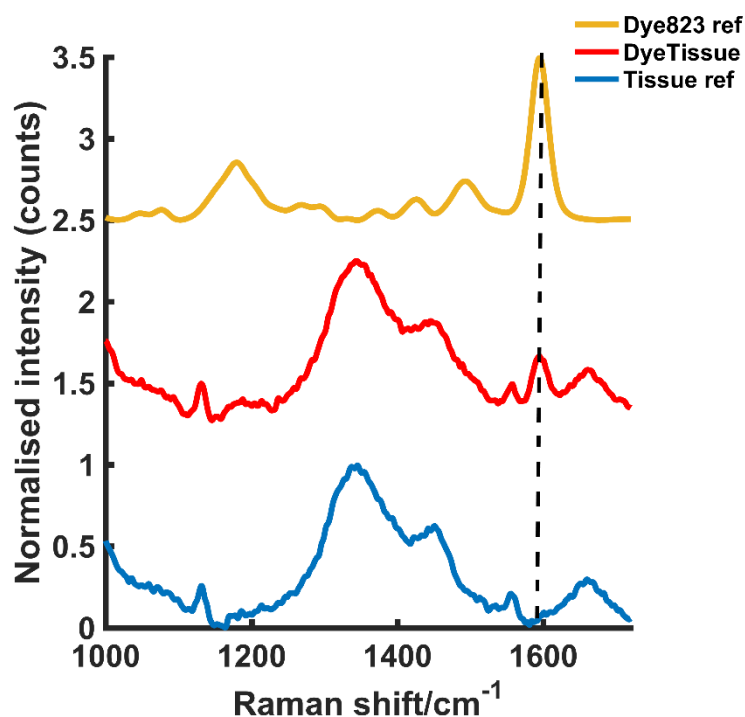


Figure 5.4 – The tracking of dye 823 nanotag solution through 10 mm of tissue. The tissue and dye 823 reference spectra are shown at the bottom and top respectively. The middle spectrum represents the Raman signal collected from the nanotags obscured by 10 mm of tissue. The peak at 1596 cm⁻¹ is easily detectable by eye. Spectra were collected using a handheld CBEx instrument with 785 nm laser excitation, 5 s integration. Peak intensities were obtained by scanning 3 replicate samples, 5 times.

However, detecting the nanotag solution in the confined environment of a cuvette, where the NPs are not dispersed over an area or free to move around does not truly represent a biological system. In this instance the nanotags would be subject to dispersion within the matrix as well as intracellular processes which may limit their uptake into cells, thus ultimately reducing the number of nanoparticles and therefore SERRS signal, at the point of measurement. Whilst this still mimics the potential to use SERRS to

track nanotags in tissue, for example drug release systems where the NPs are embedded in a diffusion system such as a reservoir or matrix device, this is less representative of a system in which the nanotag solution is administered intravenously. Thus, to further mimic the potential to use handheld Raman to detect nanotags *in vivo*, we used multicellular tumour spheroids (MTS) as *ex vivo* breast cancer tumour models. Unlike two dimensional (2D) cell cultures, MTS establish characteristic concentration gradients of oxygen, nutrients and metabolites and thus can be used as an *ex vivo* tumour model as they more closely resemble the 3D *in vivo* environment.^{32,33} Due to the enhanced permeability and retention (EPR) effect, there is potential for NPs to accumulate preferentially in tumours, therefore NPs have potential for use as drug delivery platforms³⁴ and to support imaging applications.³⁵ MTS can provide a model for NP accumulation in tumours *in vivo* without the need for more complex ethical approval and long term experiments associated with such studies.

MTS were used as an *ex vivo* breast cancer model to demonstrate the ability to detect SERRS nanotags at depth using handheld Raman. MCF7 human breast cancer cells were incubated overnight with dye 823 nanotags. MTS were then grown using a hanging drop technique by pipetting 20 μ L drops of MCF7 human breast cancer cell suspension onto the lid of a Petri dish. They were grown over a period of 7 days at 37 C and 5% CO₂ in a humidified incubator to a size <1 mm. No reduction in growth was observed. It is therefore reasonable to assume that the dyes did not cause cell death since cells need to be alive in order to divide and replicate to form MTS models.

Roughly 10 MTS were transferred to a single section of tissue. Following this, another layer of porcine tissue with a 5 mm thickness was then placed on top of the MTS imbedded tissue. The two-layer tissue sample was then transferred to an x-y translational stage and the handheld Raman instrument was positioned perpendicular to the tissue section to enable the Raman mapping of the dye 823 SERRS nanotags taken up into the *ex vivo* breast cancer tumour models through 5 mm off tissue. The experimental set up is described in Figure S5, supporting information. The tissue samples were

moved in steps of 1 mm to create an image of 10 x 10 pixels. It is important to note that the z-direction remained fixed and the point and shoot adaptor, with a working distance of 5 mm was used to probe through the tissue barrier. A false colour 2D SERRS heat map was then constructed, Figure 5.5a. This corresponds to the uptake of dye 823 nanotags into MTS. The map demonstrates clear discrimination between areas where the MTS models were present (i.e. placed onto the tissue section), and areas where they were not. This is confirmed in the spectrum collected at the point of maximum intensity (Figure 5.5b) where the characteristic dye 823 peak at 1596 cm^{-1} is observed. In areas where the MTS containing the SERRS nanotags were not present, no spectral contribution from the dye is seen. In this instance, the observed spectrum corresponds to that of the tissue only. Therefore, since in this model system, the precise location of the spheroids in the tissue is known, control spectra can be generated on the same image but away from the MTS deposition point. It should also be noted that the SERRS-active NPs were contained within the spheroids themselves and therefore their location was known prior to imaging. In comparison to the experimental set up involving a bulk set up, i.e. nanotags held in a vial or a cuvette, the number of NPs present in each MTS was significantly less. Therefore, the results presented here demonstrate the on/off detection of SERRS nanotags in areas where they are present in MTS and where the MTS models are not present by monitoring the peak intensity at 1596 cm^{-1} through thicknesses of 5 mm. These results are particularly impressive since a handheld Raman spectrometer has been utilised to detect the SERRS signal through diffusely scattering turbid media. A previous report has demonstrated the potential to detect the same SERRS nanotags take up into MTS through depths of 15 mm using SESORRS,²² however it is expected that advancements in instrumentation will increase the potential of handheld Raman to probe through clinically relevant depths.

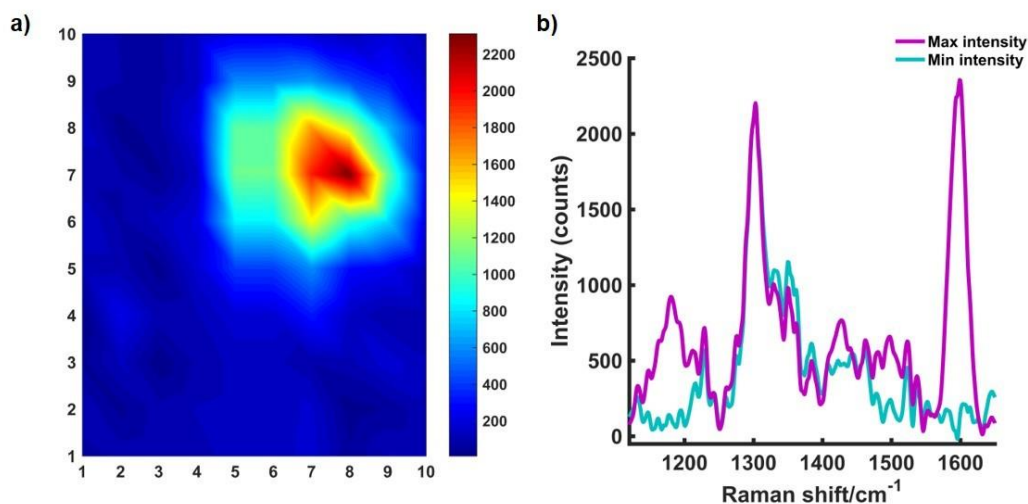


Figure 5.5 - a) A false colour xy-2D heat SERRS map of MTS containing dye 823 through 5 mm of tissue. The map was constructed using the peak intensity at 1596 cm^{-1} . Measurements were carried out using an xy translational stage and moving it in step sizes of 1 mm to create an image of 10 x 10 pixels. Spectra were truncated, baselined and smoothed prior to processing. A combination surface/contour false colour was used to generate a 2D heat map and show the tracking of the MTS through 5 mm of tissue. Clear discrimination is seen between spectra collected at the point of maximum intensity where the nanotags containing MTS models were spotted, and that collected where the MTS were not present. (b) The corresponding maximum and minimum collected through 5 mm of tissue. offset spectra. All measurements were carried out using a 5 s integration time, 785 nm laser excitation wavelength.

5.5 Conclusions

Through utilising the powerful Raman scattering properties of chalcogenpyrylium reporters for SERRS applications, the ability to probe through large thicknesses of plastic and tissue is presented. To the best of our knowledge, this is the first assessment of the maximum thickness that this handheld spectrometer can detect SERRS nanotags through. Furthermore, it is the first assessment of the benefit of using a resonant Raman reporter to probe through the plastic and tissue barriers using SERRS and in addition, the first report of the detection of 3D tumour models through tissue barriers using handheld conventional Raman. In combination with PCA, the ability to detect SERRS nanotags through up to 20 mm of plastic is demonstrated, alongside the tracking of SERRS nanotags through up to 10 mm of tissue using handheld Raman.

Previous work involving the detection of the same SERRS nanotags through tissue has involved benchtop confocal systems. Thus, the results presented here are extremely impressive since a handheld conventional Raman instrument has been utilised for the detection of SERRS nanotags. This work demonstrates the potential to probe through large thicknesses and highlights the advantage of using a resonant Raman reporter for increased chemical specificity to detect SERRS nanotags through plastic or tissue barriers. In addition, it shows that the use of SORS instrumentation to detect SERS nanotags may not always be necessary when probing through barriers, particularly plastic. The instrument used here was designed with security applications in mind, however we envisage that developments in handheld Raman instrumentation for clinical applications will pave the way for the probing of SERRS nanotags through large barriers, specifically tissue. Future development of handheld Raman instrumentation will go hand in hand with increased clinical acceptance of Raman spectroscopy by regulatory bodies worldwide.

5.6 References

- 1 H. Kearns, M. A. Bedics, N. C. Shand, K. Faulds, M. R. Detty and D. Graham, *Analyst*, 2016, **141**, 5062–5065.
- 2 G. McNay, D. Eustace, W. E. Smith, K. Faulds and D. Graham, *Appl. Spectrosc.*, 2011, **65**, 825–837.
- 3 H. Kearns, R. Goodacre, L. E. Jamieson, D. Graham and K. Faulds, *Anal. Chem.*, 2017, **89**, 12666–12673.
- 4 D. Cowcher, Y. Xu and R. Goodacre, *Anal. Chem.*, 2013.
- 5 X. Qian, X.-H. Peng, D. O. Ansari, Q. Yin-Goen, G. Z. Chen, D. M. Shin, L. Yang, A. N. Young, M. D. Wang and S. Nie, *Nat. Biotechnol.*, 2008, **26**, 83–90.
- 6 T. Demeritte, R. Kanchanapally, Z. Fan, A. K. Singh, D. Senapati, M. Dubey, E. Zakar and P. C. Ray, *Analyst*, 2012, **137**, 5041.
- 7 J. M. Sylvia, J. A. Janni, J. D. Klein and K. M. Spencer, *Anal. Chem.*, 2000, **72**, 5834–5840.
- 8 D. L. Ellis, H. Muhamadali, S. A. Haughey, C. . Elliot and R. Goodacre, *Anal. methods*, 2015, **7**, 9401–9414.
- 9 A. Oseledchyk, C. Andreou, M. A. Wall and M. F. Kircher, *ACS Nano*, 2017, **11**, 1488.
- 10 C. Decristoforo, B. Faintuch-Linkowski, A. Rey, E. von Guggenberg, M. Rupprich, I. Hernandez-Gonzales, T. Rodrigo and R. Haubner, *Nucl. Med. Biol.*, 2006, **33**, 945–52.
- 11 S. Laing, L. E. Jamieson, K. Faulds and D. Graham, *Nat. Rev. Chem.*, 2017, **1**, 0060.
- 12 E. Smith and G. Dent, *Modern Raman Spectroscopy: A Practical Approach*, Wiley, 2005.
- 13 F. Nicolson, L. E. Jamieson, S. Mabbott, N. C. Shand, D. Graham and K. Faulds, *J. Raman Spectrosc.*, 2017, **48**, 1828–1838.
- 14 N. C. Shand, *SPIE Eur. Secur. Def.*, 2008, **7119**, 71190J–71190J–12.
- 15 M. Bloomfield, P. W. Loeffen and P. Matousek, *Proc. SPIE*, 2010, **7838**, 783808-1-783808–15.
- 16 K. Buckley, C. G. Atkins, D. Chen, H. G. Schulze, D. V Devine, M. W. Blades and R. F. B. Turner, *Analyst*, 2016, **141**, 1678.
- 17 N. Stone, R. Baker, K. Rogers, A. W. Parker and P. Matousek, *Analyst*, 2007, **132**, 899–905.
- 18 M. V Schulmerich, K. a Dooley, M. D. Morris, T. M. Vanasse and S. a Goldstein, *J. Biomed. Opt.*, 2015, **11**, 060502.

- 19 P. Matousek, E. Draper, A. Goodship, I. Clark, K. Ronayne and A. W. Parker, 2006, **60**, 758–763.
- 20 N. Stone, K. Faulds, D. Graham and P. Matousek, *Anal. Chem.*, 2010, **82**, 3969–3973.
- 21 N. Stone, M. Kerssens, G. R. Lloyd, K. Faulds, D. Graham and P. Matousek, *Chem. Sci.*, 2011, **2**, 776–780.
- 22 F. Nicolson, L. E. Jamieson, S. Mabbott, K. Plakas, N. Shand, M. Detty, D. Graham and K. Faulds, *Chem. Sci.*, 2018, **9**, 3788–3792.
- 23 D. Kurouski and R. Van Duyne, *Anal. Chem.*
- 24 S. Zaleski, K. A. Clark, M. M. Smith, J. Y. Eilert, M. Doty and R. P. Van Duyne, *Anal. Chem.*, 2017, **89**, 2497–2504.
- 25 M. A. Bedics, H. Kearns, J. M. Cox, S. Mabbott, F. Ali, N. C. Shand, K. Faulds, J. B. Benedict, D. Graham and M. R. Detty, *Chem. Sci.*, 2015, **6**, 2302–2306.
- 26 H. J. Butler, L. Ashton, B. Bird, G. Cinque, K. Curtis, J. Dorney, K. Esmonde-white, N. J. Fullwood, B. Gardner, P. L. Martin-Hirsch, M. J. Walsh, M. R. Mcainsh, N. Stone and F. L. Martin, *Nat. Protoc.*, 2016, **11**, 664–687.
- 27 S. Moreton, K. Faulds, N. Shand, M. Bedics, M. Detty and D. Graham, *Nanoscale*, 2015, 6075–6082.
- 28 D. I. Ellis, R. Eccles, Y. Xu, J. Griffen, H. Muhamadali, P. Matousek, I. Goodall and R. Goodacre, *Sci. Rep.*, 2017, **7**, 12082.
- 29 P. Matousek, *TrAC Trends Anal. Chem.*, 2018.
- 30 B. Sharma, R. R. Frontiera, A.-I. Henry, E. Ringe and R. P. Van Duyne, *Mater. Today*, 2012, **15**, 16–25.
- 31 S. Harmsen, M. A. Bedics, M. A. Wall, R. Huang, M. R. Detty and M. F. Kircher, *Nat. Commun.*, 2015, **6**, 6570.
- 32 L. E. Jamieson, D. J. Harrison and C. J. Campbell, *Analyst*, 2015, **140**, 3910–3920.
- 33 L. E. Jamieson, V. L. Camus, P. O. Bagnaninchi, K. M. Fisher, G. D. Stewart, W. H. Nailon, D. B. McLaren, D. J. Harrison and C. J. Campbell, *Nanoscale*, 2016, **8**, 16710–16718.
- 34 E. Blanco, H. Shen and M. Ferrari, *Nat. Biotechnol.*, 2015, **33**, 941–951.
- 35 A. B. Chinen, C. M. Guan, J. R. Ferrer, S. N. Barnaby, T. J. Merkel and C. A. Mirkin, *Chem Rev*, 2015, **115**, 10530–10574.

6 Towards establishing a minimal nanoparticle concentration for applications involving surface enhanced spatially offset Raman spectroscopy (SESORS) in vivo

Intention to submit to Analytical Methods – subject to approval from DSTL

Contributing authors and their roles:

Lauren E. Jamieson¹ – Helped with data processing and preliminary work
Samuel Mabbott¹ – Helped with data processing and preliminary work
Konstantinos Plakas² – Synthesised the dye molecules
Neil C. Shand³ – Provided access to SORS instrumentation and PhD supervisor of FN
Michael R. Detty² – PhD supervisor of Konstantinos Plakas
Duncan Graham¹ – Co-collaborator and PhD supervisor of FN
Karen Faulds¹ – Principal investigator

1. Department of Pure and Applied Chemistry, Technology and Innovation Centre, University of Strathclyde, 99 George Street, Glasgow G1 1RD, UK.
2. Department of Chemistry, University at Buffalo, The State University of New York, New York 14260, USA
3. DSTL, Porton Down, Salisbury, SP4 0JQ, UK.

The supporting information can be found in chapter 9.9

6.1 Abstract

Resonant chalcogenpyrylium nanotags demonstrate an exceptional SERS performance for use in SORS applications. Using SESORS, nanotags containing chalcogenpyrylium dye were observed at concentrations as low as 1 pM through 5 mm of tissue. Calculated limits of detection suggest that these SERRS nanotags can be detected at 104 fM using SESORRS.

6.2 Introduction

The ability to detect low levels of analytes through barriers in a sensitive and non-destructive manner is a challenge faced in both the security and biomedical fields.¹ Raman spectroscopy provides a means to solving this challenge since it provides a unique chemical fingerprint that can distinguish between signals from the barrier and the analyte without the need to destroy the sample, however it is often limited in its ability to detect analytes at depth.² Spatially offset Raman spectroscopy (SORS) is an emerging technique which is capable of providing a unique chemical fingerprint of the analyte under study, even when obscuring barriers such as tissue are present.³ SORS relies on the idea that photons generated at depth undergo multiple diffuse scattering processes, and thus travel laterally upon return to the collection probe.² Unlike conventional 180° backscattering techniques, where excitation and collection typically take places at the same point, SORS makes use of a spatial offset between the point of laser excitation and the point of collection.² Thus, by exploiting the use of a spatial offset between the point of incident light and the point of collection, it is possible to obtain Raman signal of the photons generated at depth, i.e. the analyte obscured by the barrier.⁴

Since first reported by Matousek *et al.*,² SORS has been applied to a number of applications including security,⁴⁻⁷ pharmaceutical analysis,⁸ the detection of counterfeit alcohol⁹ and in the monitoring the quality of red blood cells.¹⁰ Perhaps more importantly, the introduction of SORS has opened up new avenues for medical applications; in particular non-invasive disease diagnostics. Several reports have explore the use of SORS for the assessment of bone¹¹ allowing information on both the inorganic and organic components of bone to be ascertained,³ as well as on subcortical bone tissue in mouse models.¹² In addition, SORS showed promise for the non-invasive assessment of calcifications associated with breast cancer. Ghita *et al.*, reported the detection of calcium hydroxyapatite at clinically relevant

concentrations and depths of 40 mm from tissue mimics thus bringing the SORS technique closer to clinical translation.¹³

Surface enhanced Raman spectroscopy (SERS) is a powerful technique that is useful for overcoming the limitations associated with conventional Raman spectroscopy. By functionalising nanoparticles (NPs) with a molecularly specific Raman reporter, significantly greater enhancement in the inelastic scattering of reporter molecule photons signal can be achieved.¹⁴ As such, SERS has been shown to yield enhancements several orders of magnitude higher than that of conventional Raman spectroscopy.¹⁵ Even further enhancement in Raman signal can be achieved through the use of a Raman reporter with an electronic transition that is close to the laser excitation wavelength. Known as surface enhanced resonance Raman spectroscopy (SERRS),¹⁶ SERRS has been shown to yield enhancements in Raman signal and can produce enhancements in the order of 10^{10} to 10^{14} .¹⁵ SERS has been used in the detection of antimicrobial resistant pathogens,¹⁷ and in security applications, specifically explosives detection.¹⁸ SERS has also been used extensively in biomedical imaging applications and nanotags functionalised with biomolecules such as antibodies have assisted in the targeted imaging of numerous cancers *in vivo* including ovarian¹⁹ and breast.²⁰

As the name suggests, surface enhanced spatially offset Raman spectroscopy (SESORS) encompasses both the SERS and SORS techniques.²¹ Whilst not a completely non-invasive technique since the NPs must be introduced, it does achieve considerable enhancement in Raman signal at greater, more clinically relevant depths. Since it was first reported by Stone *et al.*,²¹ SERS active nanotags have been tracked through depths of up to 50 mm of tissue using a transmission optical approach.²² Using a backscattering geometry, SESORS has been used in glucose sensing,²³ in the tracking of nanotags through 8 mm of bone²⁴ and in the detection of neurotransmitters in the skull.²⁵ Previous work in our group has reported the technique of surface enhanced spatially offset resonance Raman spectroscopy (SESORRS) which demonstrates the benefit of using a

resonant Raman reporter for superior levels of depth penetration.²⁶ In this instance, SERRS active nanotags were detected through 25 mm of porcine tissue and the same nanotags were taken up into *ex vivo* breast cancer models and detected through 15 mm of tissue using a handheld SORS spectrometer.²⁶ Such depth penetration was achieved through the use of chalcogenpyrylium Raman reporters which have tuneable absorption maxima in the near infrared (NIR). Previous reports have shown these reporter molecules to be particularly useful at longer wavelengths including 1280 nm²⁷ and 1550 nm²⁸, outperforming commercially available Raman reporter molecules such as BPE.

In recent years, focus has shifted towards the use of handheld Raman instrumentation, mainly due to their portability, ease of use and typically lower cost.²⁹ Previous work in the SESORS field has typically focused on the depth penetration capabilities of the technique, i.e. the focus has been to probe through significant depth. However, few studies have investigated the minimum nanoparticle (NP) concentration required for detection at a given tissue thickness. This is a key question that needs to be addressed if SESORS is to translate into the clinic. As such, the work presented here explores the benefit of using resonant Raman reporters for superior low level limits of detection of SERRS nanotags through tissue using a handheld SORS instrument.

6.3 Experimental

All chemicals and small molecule Raman reporters were purchased from Sigma Aldrich unless otherwise stated. AuNPs with an average diameter of 78 nm were synthesized using a seeded method and left to stir overnight.³⁰ Briefly, gold seeds of 26 nm were synthesized using the citrate reduction method. Sodium tetrachloroaurate (III) dihydrate (681 μ L, final concentration 0.254M) and sodium citrate trihydrate (528 μ L, final concentration 0.171M) were added to 5.007 ml of 28 nm seeds and made up to 120 ml with dH₂O. The solution was left to stir overnight. NPs were characterized using extinction spectroscopy and had an LSPR of 548 nm.

A chalcogenpyrylium-based dye was synthesized according to previously reported methods.^{27,28,31} Dye 823 was prepared by dissolving the solid in anhydrous N,N-Dimethylformamide (DMF, 99.8%) to produce a 1 mM stock. Subsequent dilutions were then carried out using DMF and dH₂O (50:50). Raman reporter 1,2-bis(4-pyridyl)ethylene (BPE) was prepared by dissolving the solid in ethanol to produce a 10 mM stock. Subsequent dilutions were carried out using dH₂O. Dye 823 was characterized using extinction spectroscopy (Agilent Cary 60) to determine the λ_{max} . BPE is a non-resonant Raman reporter.

Measurements were taken using a handheld Resolve instrument from Cobalt Light Systems (830 nm, average laser power 450 mW). All measurements were carried out using a 2 s integration time, 5 accumulations and an 8 mm offset. The nose cone was fitted to use the instrument in a contact mode setting. The handheld instrument used here has a fixed exposure time. Measurements were carried out using 3 samples. Prior to dye addition, NPs were concentrated by centrifugation (1 mL aliquots, 5000 RPM, 10 mins) and resuspended in 500 μ L of water.

Pork loin tissue was obtained from a local butcher and cut into sections (roughly 3.5 cm inches x 4 cm with varying thicknesses). Pork was chosen as an analogue to human samples due its ability to mimic human tissue greater

than that from avian species.²¹ LOD experiments were performed using quartz cuvettes. 350 μL of each nanotag solution was pipetted into a Suprasil quartz micro cuvette, path length 1 mm, chamber volume 350 μL . Tissue samples of varying thicknesses were then placed in front of the cuvette. The nose cone was brought into contact with the tissue samples, thus ensuring there was no space between the instrument and the tissue. The set up involving the cuvette is shown in Figure 6.1.



Figure 6.1 Experimental set-up using a handheld SORS spectrometer for the detection of nanotags through tissue. Nanotag solutions were held in a cuvette and the cuvette was placed behind tissue samples. The nose cone was brought into contact with the tissue ensuring there was no space between the tissue sample and the instrument.

Investigation of the nanotags for LODs using SESORS carried out by adding each reporter (3 μL , 300 μM) to 500 μL of NPs. The solution was then made up to 1 mL with dH₂O. An initial final dye concentration of 300 nM was used for each nanotag solution, thus by keeping the dye concentration as low as possible the benefit of using a Raman reporter which is in resonance with the laser was exploited. Nanotag solutions were subsequently diluted from 11 pM to 900 fM and SESORS spectra through 5 mm of tissue was obtained. The solutions were diluted using deionised water. The limit of detection (LOD) was calculated to be 3 times the standard deviation of the blank, divided by the gradient of the straight line. Error bars represent one standard deviation resulting from 3 replicate samples and 5 scans of each. All spectra were

processed using Matlab software (Version 2017a, The MathWorks, Natrick, MA, USA). Preprocessing involved truncating and baselining the spectra.

6.4 Results and Discussion

To investigate the advantage of using resonant molecules for improved limits of detection of nanotags, gold nanoparticles (AuNPs) were synthesised according to previously reported methods.²⁷ The resulting particles had an average diameter of 78 nm. AuNPs were functionalised with either a resonant chalcogenpyrylium Raman reporter, dye 823, or the commercially available small molecule reporter 1,2-bis(4-pyridyl)ethylene, BPE to create nanotags. The corresponding SERS spectra and chemical structure of the two Raman reporters are shown in Figure 6.2. A reference spectrum of the tissue is also displayed. Dye 823 is named according to its absorption maximum, i.e. it absorbs at 823 nm. By controlling the number of sp^2 carbons in the aliphatic backbone, and the choice of chalcogen atoms in the ring systems, the wavelength of absorption can be tuned to the NIR to be resonant with the wavelength of the incident laser light, in this instance 830 nm.^{28,27} BPE is a non-resonant small molecule which is often used in SERS applications. It has previously been shown that when a solution of nanotags are obscured by a tissue barrier, superior SERS signal is generated through the use of resonant Raman reporter molecules compared to non-resonant small molecule such as BPE.²⁶ Here, solutions of the nanotags were held in a quartz microcuvette and obscured by 5 mm of porcine tissue. The peak intensity of the most intense peak that corresponded to the reporter molecule in the offset spectra was measured. Significant enhancement in signal was generated through the use of a resonant Raman reporter compared to off resonant molecules. BPE however was shown to offer improved SERS signal through the tissue barrier in comparison to another commercially available off-resonant small molecule, azopyridine (AZPY). Therefore, in order to demonstrate the advantage of using a resonant Raman reporter molecule over a non-resonant reporter for improved limits of detection (LOD) using SESORS, the ability to detect nanotag solutions containing either BPE or dye 823 at varying concentrations was explored.

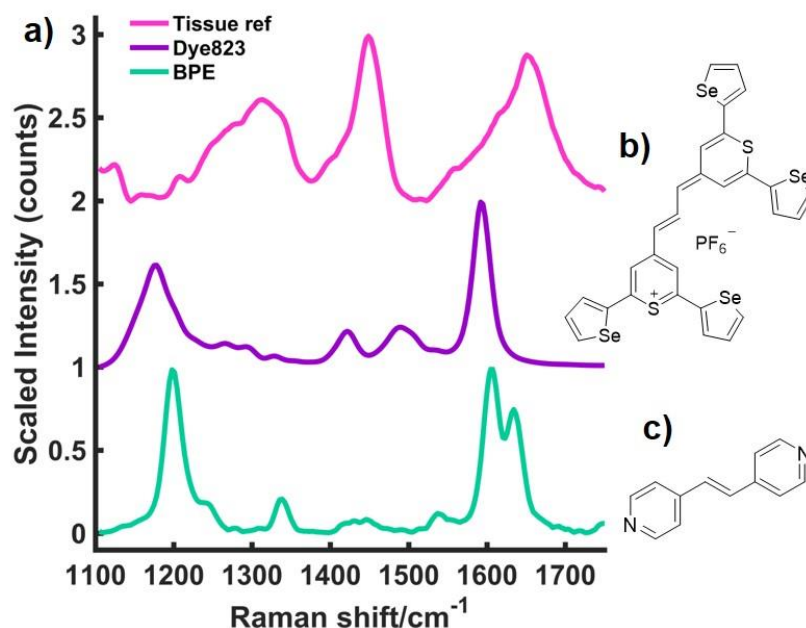


Figure 6.2 – (a) SERS spectra of the two Raman reporters used in this work, BPE (bottom) and dye 823 (middle), as well as a Raman spectrum of the tissue as a reference (top). Dye 823 is a resonant chalcogen based Raman reporter and BPE is commercially available non-resonant small molecule Raman reporter. Spectra were obtained using the SORS instrument in a conventional Raman mode. All measurements were carried out using a 2 s integration time, 5 accumulations, 830 nm laser excitation wavelength. Chemical structure of dye 823 (b) and BPE (c).

Particle dilution studies were conducted in order to calculate a limit of detection for both nanotag solutions through 5 mm of tissue using SESORS. Each of the two Raman reporters were added to AuNPs to create nanotag solutions with a final dye concentration of 300 nM. The aim was to keep the dye concentration as low as possible by exploiting the benefit of using a Raman reporter that is in resonance with the laser. It should be noted that in these studies no inorganic salt was added to the nanotags to enhance the SERS response. The concentration of the nanotag solution was calculated to be 11.1 pM and subsequent dilutions of the nanotags were carried out using deionised water until no SORS signal from either of the reporter molecules was observed. All measurements were carried out using a handheld SORS instrument using a total exposure time of 10 seconds (2 s integration time, 5 accumulations). The nose cone was fitted to use the instrument in a contact mode setting. The handheld instrument used here has a fixed maximum exposure time, therefore it should be noted that if longer acquisition times

were used, the signal to noise ratio may be improved and greater limits of detection could potentially be achieved. To investigate the LOD for each of the two nanotags, solutions with each reporter were held in a quartz microcuvette. Porcine tissue samples of a 5 mm thickness were placed in front of the cuvette and brought into contact with the laser leaving no space between the nose cone and the sample (Figure 6.1). The peaks at 1204 cm^{-1} and 1592 cm^{-1} were used to calculate the LODs for BPE and dye 823 nanotags respectively since these were the strongest peaks. Spectra were acquired at an 8 mm spatial offset and truncated and baselined and the peak height at either 1204 cm^{-1} or 1592 cm^{-1} was measured at each concentration.

The potential of BPE or dye 823 nanotags for use in *in vivo* applications was then assessed. Figure 6.3 a shows the tracking of BPE nanotags through 5 mm of tissue at a concentration of 11 pM (middle spectrum) using an 8 mm offset. The BPE and tissue reference spectra are shown at the top and bottom respectively. As shown, spectral features that correspond to BPE can be seen at this concentration, specifically the peak at 1204 cm^{-1} . However, when the particles were diluted further, i.e. to a concentration of 10 pM, they failed to produce a SERS response and the resulting spectra corresponded to that of the tissue. Therefore, it was only possible to state an observable LOD of 11 pM through 5 mm of tissue using BPE nanotags. The sensitivity of BPE nanotags were then compared to nanotags containing dye 823. Figure 6.3b shows the particle dilution study of dye 823 nanotag solution through 5 mm of tissue. The LOD was calculated over a range of 6 to 1 pM using the peak height at 1592 cm^{-1} . Figure 6.3b shows that a linear response was followed and the observable LOD is therefore 1 pM. The theoretical LOD was calculated to be 104fM. This was achieved by multiplying the standard deviation of the blank three times and dividing it by the gradient of the straight line which can be observed in Figure 6.3b. Tissue spectra collected at an 8 mm offset were used as the blank, supporting information (Figure S1). Offset spectra were used as the blank to account for poorer resolution and signal to noise when using spectra collected at an 8 mm offset. The peak intensity at 1592 cm^{-1} is also plotted in Figure 6.3c and shows the decline in

peak intensity as the concentration of the nanotag is reduced. Therefore, it can be stated that the observable limit of detection of nanotags through 5 mm of tissue using SESORS containing dye 823 is eleven times higher than nanotags containing BPE, i.e. 1 pM (dye 823) compared to 11 pM (BPE).

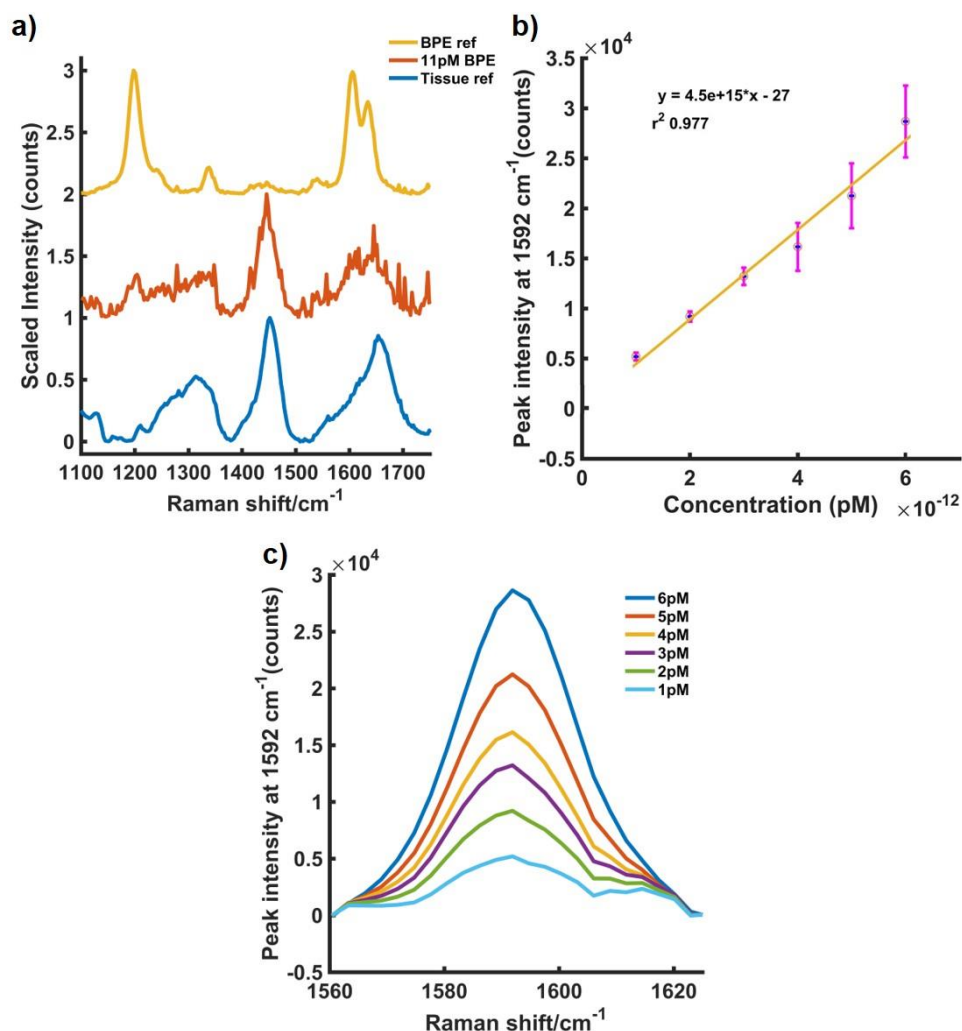


Figure 6.3(a) – The tracking of BPE nanotag solution through 5 mm of tissue. The middle spectrum shows 8 mm offset spectra of BPE nanotags at a concentration of 11 pM obscured by 5 mm of tissue. The tissue and BPE reference spectra are shown at the bottom and top respectively. The middle spectrum represents the Raman signal collected at an 8 mm offset through 5 mm of tissue. **(b)** SERS particle dilution study for dye 823 nanotags obscured by 5 mm tissue over the concentration range of 6pM to 1 pM. From the graph, the observed limit of detection of nanotags containing dye 823 is 1 pM. The theoretical limit of detection was calculated to be 104 fM. The limit of detection was determined by calculating the peak intensity at 1592 cm⁻¹ in the 8 mm offset spectra. Nanotags were obscured by 5 mm of tissue and held in a quartz microcuvette. **(c)** The peak intensity at 1592 cm⁻¹ at concentrations of 6 – 1 pM. Peak intensities were obtained by scanning 3 replicate samples, 5 times. The average peak intensity for each of the 5 dyes is shown and error bars represent \pm one standard deviation. All measurements were carried out using a 2 s integration time, 5 accumulations, 830 nm laser excitation wavelength.

The chalcogen nanotag, which is in resonance with the laser wavelength of 830 nm, produces highly intense SERRS spectra due to its highly aromatic structure. Thus, by making use of the SORS technique, it is possible to obtain a vibrational fingerprint of dye 823 nanotags at low concentrations, even when obscuring tissue barriers are present. Figure 6.4(a) shows the 8 mm offset spectra of BPE nanotags (green) and dye 823 nanotags (purple) at a concentration of 11 pM. As shown, there is a clear difference in the signal to noise ratio between the two nanotags. The resonant Raman reporter produces clear spectra with excellent signal to noise. This is in contrast to the spectra collected of the BPE nanotags at the same concentration through 5 mm of tissue, in which several spectral features correspond to that of the tissue (supporting information, Figure S1). The relative peak intensities of the most intense peak that corresponds to that of either nanotag, 1592 cm^{-1} (dye 823) and 1204 cm^{-1} (BPE), are also shown, Figure 6.4b. Dye 823 generated the strongest intensity, and is therefore assigned an intensity value of 100%. The relative peak intensity refers to the peak intensity of nanotags containing BPE obscured by 5 mm of tissue, relative to the peak intensity seen using dye 823, expressed as a percentage. As shown, there is almost a 100% increase in signal when a resonant Raman reporter is used at a nanotag concentration of 11 pM. Thus, the benefit of red-shifted chalcogenpyrylium Raman reporters for ultra-sensitive SESORS applications, is further demonstrated.

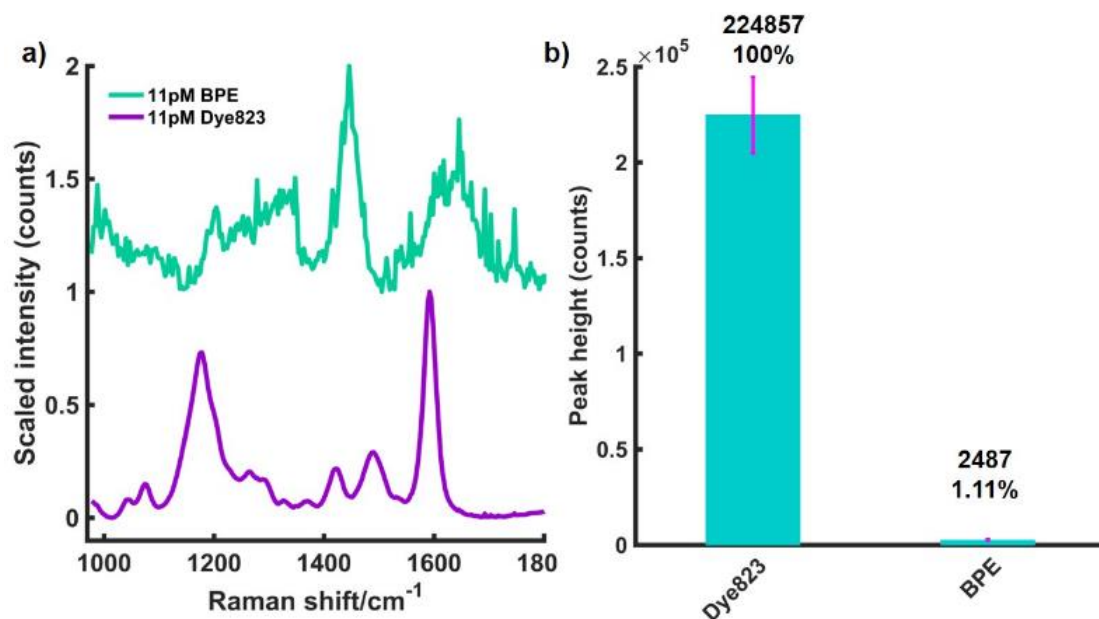


Figure 6.4 – (a) Scaled 8 mm offset spectra of 11 pM BPE nanotags (green) and dye 823 nanotags (purple) obscured by 5 mm of tissue. (b) Bar chart showing average peak intensities of dye 823 and BPE at 1592, and 1204 cm⁻¹ respectively, as well as the relative percentage peak intensity relative to the most intense signal from dye 823, through 5 mm of tissue. Nanotag solutions were held in a cuvette and the cuvette was placed behind tissue samples. Peak intensities were obtained by scanning 3 replicate samples, 5 times and error bars represent one standard deviation. All measurements were carried out using a 2 s integration time, 5 accumulations, 830 nm laser excitation wavelength.

6.5 Conclusion

By utilising a resonant chalcogenpyrylium Raman reporter for SESORRS applications, superior limits of detection can be achieved in contrast to commercially available non-resonant small molecules. The observable limits of detection for nanotags containing dye 823 are eleven times higher than what is seen when nanotags containing BPE are obscured by 5 mm of tissue, i.e 1 pM in comparison to 11 pM respectively. The work presented here explores the benefit of using resonant Raman reporters for superior low level limits of detection of SERRS nanotags using the SORS technique. It demonstrates the suitability of red-shifted nanotags for biomedical imaging applications where it may be important to keep the nanotag concentration as low as possible. Furthermore, if nanoparticles were used to target a tumour, their accumulation within the tumour would also be low, particularly if they are administered systemically. Therefore, it is important to understand the number of nanoparticles that can be detected at a given depth and also to establish the minimum concentration of nanotags required for SERRS response at a given depth using SORS. Future work will focus on establishing the minimum concentration of dye 823 nanotags required to produce a SERRS response at larger, more clinically relevant depths using SORS as well as investigating the use of red shifted nanomaterials for SESORRS applications.

6.6 References

- 1 P. Matousek, *Chem. Soc. Rev.*, 2007, **36**, 1292–1304.
- 2 P. Matousek, I. P. Clark, E. R. C. Draper, M. D. Morris, a E. Goodship, N. Everall, M. Towrie, W. F. Finney and A. W. Parker, *Appl. Spectrosc.*, 2005, **59**, 393–400.
- 3 P. Matousek, E. Draper, A. Goodship, I. Clark, K. Ronayne and A. W. Parker, 2006, **60**, 758–763.
- 4 C. Eliasson, N. a Macleod and P. Matousek, *Anal. Chem.*, 2007, **79**, 8185–9.
- 5 M. Bloomfield, P. W. Loeffen and P. Matousek, *Proc. SPIE*, 2010, **7838**, 783808-1-783808–15.
- 6 B. Zachhuber, C. Gasser, E. T. H. Chrysostom and B. Lendl, *Anal. Chem.*, 2011, **83**, 9438–9442.
- 7 F. Nicolson, L. E. Jamieson, S. Mabbott, N. C. Shand, D. Graham and K. Faulds, *J. Raman Spectrosc.*, 2017, **48**, 1828–1838.
- 8 J. Griffen, A. Owen and P. Matousek, *J. Pharm. Biomed. Anal.*, 2015, **115**, 277–282.
- 9 D. I. Ellis, R. Eccles, Y. Xu, J. Griffen, H. Muhamadali, P. Matousek, I. Goodall and R. Goodacre, *Sci. Rep.*, 2017, **7**, 12082.
- 10 K. Buckley, C. G. Atkins, D. Chen, H. G. Schulze, D. V Devine, M. W. Blades and R. F. B. Turner, *Analyst*, 2016, **141**, 1678.
- 11 K. Sowoidnich, J. H. Churchwell, K. Buckely, A. E. Goodship, A. W. Parker and P. Matousek, *Analyst*, 2017, **142**, 3219.
- 12 G. Feng, M. Ochoa, J. R. Maher, H. A. Awad and A. J. Berger, *J. Biophotonics*, 2017, **10**, 990–996.
- 13 A. Ghita, P. Matousek and N. Stone, *J. Biophotonics*, , DOI:10.1002/jbio.201600260.
- 14 R. Goodacre, D. Graham and K. Faulds, *TrAC - Trends Anal. Chem.*, 2018, **102**, 359–368.
- 15 B. Sharma, R. R. Frontiera, A.-I. Henry, E. Ringe and R. P. Van Duyne, *Mater. Today*, 2012, **15**, 16–25.

- 16 R. J. Stokes, A. Macaskill, P. Johan Lundahl, W. Ewen Smith, K. Faulds and D. Graham, *Small*, 2007, **3**, 1593–1601.
- 17 H. Kearns, R. Goodacre, L. E. Jamieson, D. Graham and K. Faulds, *Anal. Chem.*, 2017, **89**, 12666–12673.
- 18 T. Demeritte, R. Kanchanapally, Z. Fan, A. K. Singh, D. Senapati, M. Dubey, E. Zakar and P. C. Ray, *Analyst*, 2012, **137**, 5041.
- 19 A. Oseledchyk, C. Andreou, M. A. Wall and M. F. Kircher, *ACS Nano*, 2017, **11**, 1488.
- 20 T. R. Nayak, C. Andreou, A. Oseledchyk, W. D. Marcus, H. C. Wong, J. Massagué and M. F. Kircher, *Nanoscale*, 2017, **9**, 1110–1119.
- 21 N. Stone, K. Faulds, D. Graham and P. Matousek, *Anal. Chem.*, 2010, **82**, 3969–3973.
- 22 N. Stone, M. Kerstens, G. R. Lloyd, K. Faulds, D. Graham and P. Matousek, *Chem. Sci.*, 2011, **2**, 776–780.
- 23 K. Ma, J. M. Yuen, N. C. Shah, J. T. Walsh, M. R. Glucksberg and R. P. Van Duyne, *Anal Chem*, 2011, **83**, 9146–9152.
- 24 B. Sharma, K. Ma, M. R. Glucksberg and R. P. Van Duyne, *J. Am. Chem. Soc.*, 2013, **135**, 17290–17923.
- 25 A. S. Moody, P. C. Baghernejad, K. R. Webb and B. Sharma, *Anal. Chem.*, 2017, **89**, 5688–5692.
- 26 F. Nicolson, L. E. Jamieson, S. Mabbott, K. Plakas, N. Shand, M. Detty, D. Graham and K. Faulds, *Chem. Sci.*, 2018, **9**, 3788–3792.
- 27 M. A. Bedics, H. Kearns, J. M. Cox, S. Mabbott, F. Ali, N. C. Shand, K. Faulds, J. B. Benedict, D. Graham and M. R. Detty, *Chem. Sci.*, 2015, **6**, 2302–2306.
- 28 H. Kearns, M. A. Bedics, N. C. Shand, K. Faulds, M. R. Detty and D. Graham, *Analyst*, 2016, **141**, 5062–5065.
- 29 N. C. Shand, *SPIE Eur. Secur. Def.*, 2008, **7119**, 71190J–71190J–12.
- 30 W. Leng, P. Pati and P. J. Vikesland, *Environ. Sci. Nano*, 2015, **2**, 440–453.
- 31 S. Harmsen, M. A. Bedics, M. A. Wall, R. Huang, M. R. Detty and M. F. Kircher, *Nat. Commun.*, 2015, **6**, 6570.

7 Conclusions

In the fields of security and biomedical imaging there is a significant need to probe through barriers, e.g. plastic, glass or tissue in a non-invasive manner. Raman spectroscopy provides chemically specific sample evaluation in a non-destructive manner however it is limited in part by its inability to probe through significant depth, particularly with regards to turbid media. SORS provides a means to overcoming these challenges by utilising a different optical approach to a CR set-up in order to collect Raman scattered photons from the deeper, sub-surface layers. Through the use of functionalised NPs, significant enhancement in Raman signal can be generated through the use of SERS. Furthermore, by combining the depth penetration benefits of SORS with the signal enhancing capabilities of SERS, SESORS is capable of achieving sample interrogation at even greater depth. Therefore, the focus of this research was to probe through barriers, specifically plastic and tissue, using both handheld CR and SORS instruments. The ability of both techniques to detect Raman and SERS analytes through barriers was explored and compared for applications involving security and biomedicine.

Initially, the potential of both techniques to detect ethanol through clear PET and blue PP barriers was investigated using handheld CR and SORS instrumentation. It was found that by using SORS, ethanol could be detected through 21 mm of PET compared to only 9 mm of PET using CR techniques. To further assess the potential of handheld SORS and CR for through barrier detection, the detection of ethanol through opaque blue PP was investigated using the same approach. It was found that ethanol could be detected through 9 mm of PP using SORS but only 2 mm using CR. The advantage of using multivariate analysis in the form of PCA was also presented as a method to probe through larger depths than could be detected by visual inspection of the data. This was particularly useful when both the barrier and analyte spectra contained peaks with similar spectral features.

Interestingly, with regards to probing through clear barriers such as PET, CR is in fact a useful technique. PET is commonly used in the manufacture of plastic bottles which are typically only a few millimetres thick. As such, the results presented here suggest that the use of SORS techniques may not always be necessary since ethanol was detected through thicknesses of 9 mm clear PET using CR. However, when opaque barriers, such as blue PP are used, the benefit of using SORS over CR techniques is clearly shown. The SORS technique has been deployed across several airports worldwide through the use of benchtop instruments where it is used for the screening of liquids and medicines before passengers board an aircraft. In this instance it may not be feasible to transfer the samples under scrutiny to clear plastic bottles, thus the benefit of SORS over CR techniques to probe through turbid samples is clearly shown. Furthermore, the work presented here highlights the performance of small, handheld portable instruments, with back-scattering optical configurations, to detect a Raman analyte through plastic barriers.

Using gold NPs functionalised with a Raman reporter molecule to create a nanotag, the ability to detect nanotags was investigated using the SESORS technique. This work highlighted the benefit of using a resonant Raman reporter for probing through even greater depths. SERRS active nanotags were tracked through up to 25 mm of tissue and the same SERRS nanotags were taken up into *ex vivo* tumour models and detected through 15 mm of tissue using back-scattering SORS. This large depth penetration was due to the use of red-shifted chalcogenopyrylium-based Raman reporters to demonstrate the novel technique of surface enhanced spatially offset resonance Raman spectroscopy (SESORRS) for the first time.

Since MTS resemble the 3D *in vivo* environment of a tumour more closely they were chosen over using 2D monolayer cell cultures. The high sensitivity of the SESORRS technique to detect MTS models through 15 mm was demonstrated here since the MTS themselves are less than 1 mm in size. Thus, if the MTS models, or tumour in the case of *in vivo* imaging applications was larger, it may have been possible to detect the nanotags

through even greater thicknesses. This hypothesis is substantiated through the detection of the same SERRS active nanotags held in a cuvette through 25 mm of tissue. To date, this is the largest thickness that SERRS nanotags have been detected at using a back-scattering optical set up. Previous reports using a transmission geometry have demonstrated the ability to detect nanotags through up to 50 mm of tissue.¹ However, the results presented here demonstrate the ability to detect SERS nanotags through the same total thickness using handheld SESORRS in a back-scattering approach. Since the incident photons must travel through 25 mm of tissue to reach the nanotags and are then the scattered photons must return to the collection optics through the same thickness, i.e. 25 m of tissue, the total thickness that the photons must travel through is therefore 50 mm of tissue. Furthermore, these experiments were carried out using a handheld SORS spectrometer which although portable and extremely user friendly, has a fixed exposure time. Thus, it is envisaged that if a benchtop instrument was used, larger depth penetration and better signal to noise ratios may have been achieved. Nonetheless, this work represents a significant step forward in the detection of vibrational fingerprints through tissue samples and is an important step towards the use of handheld back-scattering SESORRS for potential clinical applications including non-invasive tumour detection.

In addition to non-invasive tumour detection, the ability to multiplex and to simultaneously detect multiple targets *in vivo* is a significant challenge. Multiplex detection offers the potential to sample a number of disease conditions in the same organ, at the same time, and has the potential to be used in new methodologies for enhanced personalised treatment. Although the ability to detect up to ten SERS nanotags has previously been reported using confocal techniques,² the use of SESORS presents an opportunity to detect multiple analytes simultaneously through tissue at clinically relevant depths. Using a handheld SORS instrument, MTS containing a singleplex of each of three different SERRS nanotags and a triplex containing equal ratios of the three nanotags was detected through 10 mm of tissue. In this instance, three resonant chalcogenpyrylium-based Raman reporters were used as it

was shown that resonant reporter molecules facilitate better depth penetration, it was therefore envisaged that this would also offer improved spectral discrimination between the three single dyes at depth. Since strong spectral similarity exists between the spectra from the three individual SERRS nanotags and the triplex, principal component analysis was used to discriminate between each singleplex and triplex.

Previous reports using SESORS for multiplex applications have utilised a spatial approach where the individual nanotags, with significantly different spectral fingerprints, were each injected into four corners of a tissue section. The authors were able to assign a specific peak in each of the four spectra to enable the spatial multiplex detection through 20 mm of tissue using SESORS. However, using MTS to facilitate the uptake of all three nanotags simultaneously, the work presented here demonstrates the first co-localised multiplex using SESORRS. Thus, the ability to not only analyse a tissue sample containing SERRS-active nanotags at depth, but also the ability to simultaneously classify a sample containing multiple nanotags is shown. Furthermore, the depth penetration achieved here rivals traditionally used benchtop instruments, since the incident photons have travelled through the 10 mm tissue sample before they are subsequently scattered back through the same tissue section, thus the total thickness that the photons must travel through is therefore 20 mm. In addition, this work highlights the performance of a small, handheld portable instrument, to detect and discriminate between multiple SERRS analytes in *ex vivo* tumour models through tissue barriers and shows the potential of handheld instruments for clinical applications.

In keeping with the aims of this thesis (through barrier detection), the ability of CR to detect SERS analytes through both plastic and tissue barriers was also investigated. These results explore the use of a handheld CR instrument to probe through barriers. The instrument in question has a fixed focal depth, which unlike microscope-based systems cannot be focused, and in theory should therefore be limited in its ability to probe through deeper layers. However, by exploiting the use of chalcogenpyrylium-based Raman

reporters, particularly one that is in resonance with the laser wavelength, significant depth penetration can be achieved. As such, nanotags containing a resonant Raman reporter molecule were detected through up to 20 mm of clear PET and 9 mm blue PP. The results also highlight the benefit of using the highly Raman active chalcogenpyrylium-based reporter molecules over non-resonant small molecules for probing through barriers using CR. SERRS nanotags held in a cuvette were detected through 10 mm of tissue and the same SERRS nanotags, taken up in to *ex vivo* tumour models, were detected through 5 mm of tissue.

These results suggest that SESORS techniques may not always be necessary for detecting SERS nanotags through barriers, particularly plastic. However, it is evident from these results that the SORS technique is extremely useful for probing through tissue barriers, since the same *ex vivo* tumour models were detected through 15 mm of tissue using SESORRS, compared to only 5 mm using SERRS. In spite of this, it is envisaged that advances in instrumentation may facilitate better depth penetration using CR, through the development of a point and shoot adaptor with a greater focal depth. This would be particularly useful for applications involving turbid media such as tissue. Therefore, it is reasoned that developments in handheld Raman instrumentation for clinical applications will pave the way for the probing of SERRS nanotags through large barriers, specifically tissue using CR. Of course, financial investment in the development of handheld Raman instrumentation will go hand in hand with increased clinical acceptance of the use of NPs for *in vivo* applications and Raman spectroscopy, by regulatory bodies worldwide.

The work in this thesis explored the use of CR and SORS to detect Raman and SERS analytes through plastic and tissue barriers. In these instances, the minimum concentration of analyte required to generate a response through a given thicknesses was not investigated. Since it was repeatedly shown that nanotags containing resonant Raman reporters consistently outperform commercially available non-resonant small molecules, a limit of detection was carried out through 5 mm of tissue using SESORS. The

observable limit of detection for nanotags containing the resonant chalcogenpyrylium-based Raman reporter molecule (dye 823) was eleven times higher than nanotags containing BPE, i.e 1 pM in comparison to 11 pM respectively. The calculated LOD for dye 823 was 104 fM. Thus, the results clearly demonstrate the benefit of using a resonant chalcogenpyrylium Raman reporter over commercially available non-resonant small molecules for SESORRS applications in order to achieve superior limits of detection. With regards to *in vivo* applications, localisation of NPs within the tumour is likely to be low, particularly if the NPs are administered systemically. It is therefore important to understand the minimum concentration of nanotag needed to provoke a SERS response using SORS, as the ultimately nanotag concentration should be kept as low as possible for clinical applications.

Overall, this thesis demonstrates the use of both handheld conventional Raman and SORS instruments for through barrier detection involving both tissue and plastic barriers. The benefit of using of Raman reporters with tuned resonances into the NIR region is clearly demonstrated for through barrier detection applications and thus the technique of surface enhanced spatially offset Resonance Raman spectroscopy (SESORRS) is introduced for the first time. By exploiting the resonance effect, superior depth penetration can be achieved, therefore generating lower limits of detection as well as improved signal to noise ratios. In addition, the multiplex capabilities of SESORRS opens up the potential to detect multiple targets in the same organ at clinically relevant depth. Furthermore, applicability of handheld instruments for through barrier detection applications, specifically SORS for clinical applications is clearly demonstrated. This work, provides the basis for future investigation in a number of fields, most significantly in the field of biomedical imaging and disease detection.

- 1 N. Stone, M. Kerssens, G. R. Lloyd, K. Faulds, D. Graham and P. Matousek, *Chem. Sci.*, 2011, **2**, 776–780.
- 2 C. L. Zavaleta, B. R. Smith, I. Walton, W. Doering, G. Davis, B. Shojaei, M. J. Natan and S. S. Gambhir, *Proc. Natl. Acad. Sci. U. S. A.*, 2009, 106, 13511–13516.

8 Future work

The aim of this thesis was to investigate the use of handheld instrumentation to probe through depth using either CR or SORS approaches. Thus, the work presented here demonstrates the use of both techniques for applications involving through barrier detection.

With regards to the use of CR for through barrier detection involving both plastic and tissue barriers, it would be interesting to investigate whether the use of point and shoot adaptor with a longer working distance would facilitate even greater depth penetration. It is envisaged this would lead to improved levels of through barrier detection, i.e. signal from Raman and SERS analytes would be detected through even greater thicknesses. However, to date such piece of equipment does not exist.

From a security perspective, it would be useful to compare the use of CR or SORS for the through barrier detection of explosives or drugs of abuse in SERS based assays. In these instances, the ability to detect either explosives or drugs of abuse using a SERS based assay through varying barriers and thicknesses would be investigated. These two instruments would be particularly suited to these studies as they are portable and were designed primarily for security applications. It is reasoned that SORS would outperform CR techniques due to its ability to effectively probe through diffusely scattering media.

The potential of handheld SESORRS to detect signal from nanotags at clinically relevant depths has been clearly demonstrated. This thesis provides a fundamental understanding on the ability of a handled SORS instrument detection to detect nanotags through tissue. It is envisaged that in the future, significant advancements can be achieved based on these results. This work explored the use of *ex vivo* tumour models to demonstrate the clinical application of SESORRS however, future work should focus on targeted SESORRS in animal models, i.e. the use of nanoparticles functionalised with a Raman reporter and a biomolecule to specifically target a diseased organ

in vivo. In addition, the ability to carry out multiplex detection using the same *ex vivo* tumour models using SESORRS has been shown, thus future work should also investigate the multiplex detection of numerous targets *in vivo*. Moreover, investigation of tumour depth location is also of vital importance. This can in part be achieved through establishing the minimum number of NPs required to generate a SERS signal at a given depth. Depth profiling experiments could also help facilitated this understanding, and could be achieved by building a profile based on the SERRS intensity in the offset spectrum versus the depth location of the tumour/NPs. The creation of this SERRS intensity profile will allow for a better understanding of tumour location *in vivo*.

9 Appendix

9.1 Materials and Methods

All materials were purchased from Sigma Aldrich unless otherwise stated.

9.2 Instrumentation

9.2.1 Extinction Spectroscopy

All extinction spectroscopy was carried out on a Agilent Carry 60 UV-visible spectrophotometer in combination with Cary WinUV software. The instrument was left to warm up and equilibrate for at least 10 minutes. The range of wavelengths scanned was 400-800 nm.

9.2.2 Dynamic Light Scattering

A Malvern Zetasizer Nano ZS was used to carry out all size measurements along with Zetasizer μ V and APS version 6.20 software. Approximately 1 ml of sample was run in a disposable plastic cuvette with a standard Malvern Dip cell.

9.2.3 NanoSight

A NanoSight LM20 and accompanying NTA software was used to determine the concentration of Cabot nanotags.

9.2.4 SEM Measurements

Samples were analysed using a Sirion 200 Shottky field emission electron microscope operating at an accelerating voltage of 30 kV and a magnification of 82197. Briefly, 10 μ L of a sample of AuNPs were spotted onto the silicon wafer and left to dry.

9.2.5 Raman and SERS Measurements

All Raman and SERS measurements were performed using a CBEx handheld Raman instrument from Snowy Range Instruments with a 785 nm

laser excitation wavelength and an average laser power of 43 mW. A point and shoot adaptor was used to enable the instrument to be used in a contact mode.

9.2.6 SORS and SESORS Measurements

All SORS and SESORS measurements were performed using a handheld Resolve from Cobalt Light Systems, now part of Agilent. The nose cone was fitted for all measurements to enable the instrument to be used in a through barrier detection mode.

9.3 Data Analysis

All data was processed in Matlab (version 2016a, The MathWorks, Natick, MA, USA) unless otherwise stated. Typically, spectra were truncated prior to processing. Spectra were baselined using asymmetric least squares and smoothed using Savitzky Golay smoothing.

For SORS spectra scaled subtraction was also applied. Briefly, spectra were truncated and baselined using asymmetric least squares. Following this, the surface spectrum (i.e., the signal detected at the zero position) was removed from the subsurface spectrum (i.e., signal detected at the offset position). The resulting spectra was then scaled using the most intense peak in the offset spectra. Data were subsequently smoothed.

PCA was carried out using customised Matlab scripts. Pre-processing involved truncating and scaling the spectra, before applying the first-order derivative coupled with Savitzky–Golay smoothing. The first-order derivative was used in PCA to remove slight variances in the background, which were found to affect the resulting zero-order PCA plots.

False colour heat maps were produced in Matlab using a specific peak intensity at a given wavenumber and plotted as a combination surface/contour false colour 2D heat map.

9.4 Experimental

9.4.1 Nanoparticle Synthesis

AuNPs with an average size of 80 nm were synthesised in two parts. Firstly, using a hotplate, 20 nm AuNPs were synthesised in a conical flask by adding sodium tetrachloroaurate (10.5 mg) to distilled water (100 mL). The solution was heated until boiling. Then, sodium citrate (75 mg dissolved in 7.5 ml dH₂O) was added and boiling maintained for 15 minutes. The solution was left to cool. Continuous stirring was maintained throughout via the use of a magnetic stirrer bar.

Large AuNPs were produced by adding sodium tetrachloroaurate (III) dihydrate (681 μ L, final concentration 0.254M) and sodium citrate trihydrate (528 μ L, final concentration 0.171M) to 5.007 ml of 28 nm seeds. The solution was made up to 120 ml with dH₂O in a conical flask. The solution was left to stir overnight using a magnetic stirrer bar.

9.4.2 Dye Preparation

Dyes 676, 823 and 959 were prepared by dissolving the solid in anhydrous N,N-Dimethylformamide (DMF, 99.8%) to produce a 1 mM stock. Subsequent dilutions were then carried out using DMF and dH₂O (50:50). Raman reporters 1,2-bis(4-pyridyl)ethylene (BPE) and 4,4-azopyridine (AZPY) were prepared by dissolving the solid in ethanol to produce a 10 mM stock. Subsequent dilutions were carried out using dH₂O.

9.4.3 Nanoparticle Functionalisation

Prior to dye addition, NPs were concentrated by centrifugation (1 mL aliquots, 5000 RPM, 10 mins) and resuspended in 500 μ L of water. Investigation of the nanotags for SERS applications was carried out by adding each reporter to the AuNPs (3 μ L, 300 μ M) to 500 μ L of NPs. The solution was then made up to 1 mL with dH₂O. The total final volume of each nanotag sample was 1 mL. A final dye concentration of 300 nM was used in all instances.

9.4.4 Raman and SORS Measurements Involving Plastic Barriers

Large transparent polyethylene terephthalate (PET) and blue opaque coloured polypropylene (PP) plastic sheets were purchased from a local art store and then cut up into smaller rectangular pieces (10.5 × 3 cm, thickness 1 mm). The sheets were mounted on a stage and clamped together to create the desired thickness. They were then brought into contact with the laser using either the point and shoot adaptor (CR spectrometer; Figure 9.1a) or the nose cone (SORS spectrometer; Figure 9.1b). This ensured that there was no air/space between the plastic and instrument. A glass vial containing ethanol was placed behind the plastic sheets. The glass vials had a 15-mm diameter, 1-mm thickness, and a height of 25 mm (including lid).

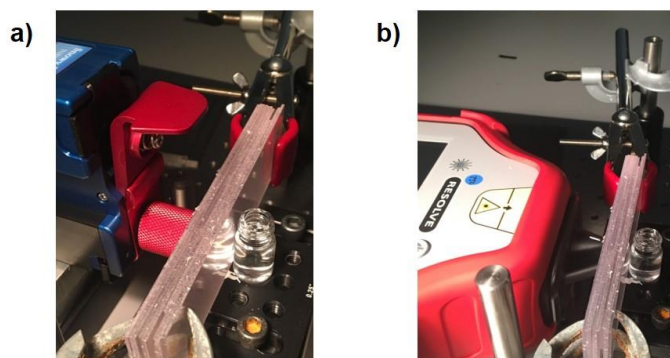


Figure 9.1 - Experimental set up using plastic sheets as a barrier using (a) CR spectrometer with point and shoot adaptor and (b) a SORS spectrometer with nose cone on. In both instances, using either a CR or SORS set up, there was no space between the instrument and the barrier.

9.4.5 Raman and SORS Measurements Involving Tissue Barriers

Pork loin tissue was obtained from a local butcher and cut into sections (roughly 3.5 cm inches x 4 cm with varying thicknesses). Tissue experiments were performed using either a quartz cuvette or by spotting the MTS models directly on to the tissue samples. For measurements involving a cuvette, 350 μ L of each NP-Dye solution was pipetted into a Suprasil quartz micro cuvette, path length 1 mm, chamber volume 350 μ L. Tissue samples of

varying thicknesses were then placed in front of the cuvette. The nose cone was brought into contact with the tissue samples, thus ensuring there was no space between the instrument and the tissue. The set up involving the cuvette is shown in Figure 9.2.



Figure 9.2 - Experimental set-up using a handheld SORS spectrometer for the detection of nanotags through tissue. Nanotag solutions were held in a cuvette and the cuvette was placed behind tissue samples. The nose cone was brought into contact with the tissue to ensure there was no space between the tissue sample and the instrument.

For mapping experiments, the MTS models containing the SERRS nanotags were placed directly onto a section of tissue and left to equilibrate for 10 mins. Following this, tissue of varying thicknesses was then placed in on top of the tissue layer containing the MTS models. The two-layer sample was then brought into contact with the laser via the nose cone. The handheld SORS instrument was positioned above the tissue samples with the laser pointing down onto the tissue, Figure 9.3. In comparison to previous work involving the cuvette, the tissue section was laid flat on the stage and the handheld instrument mounted above the sample. This set up is more representative of an *in vivo* approach compared to that using the cuvette. An x-y-positioning stage was used to enable Raman mapping of the MTS containing SERRS nanotags through tissue.

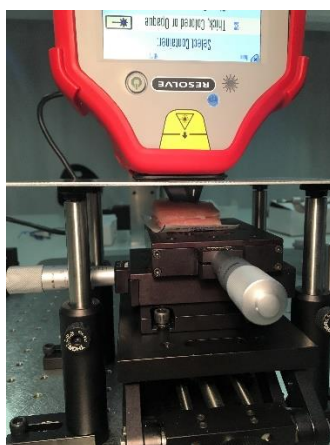


Figure 9.3 - The experimental set-up involved mounting the instrument above the tissue samples. The sample was then brought into contact with the laser via the nose cone

9.4.6 Cell culture and Nanoparticle Incubation

All cell culture was carried out by Dr Lauren Jamieson. MCF7 human breast cancer cells were cultured in Rosewell Park Memorial Institute medium (RPMI) supplemented with 1% penicillin/streptomycin (10,000 units/mL), 1% fungizone, and 10% heat-inactivated foetal bovine serum (FBS). Cells were incubated at 37 °C and 5% CO₂ in a humidified incubator. Cells at a confluence of ca. 90% growing in a T75 flask were incubated overnight with the AuNP. The following day, cells were trypsinised and re-suspended in medium to give a concentration of ca. 2.4 to 3.7 × 10⁶ cells/mL (depending on batch of cells used). Multicellular tumour spheroids (MTS) were grown using a hanging drop technique by pipetting 20 µL drops of this cell suspension onto the lid of a petri dish with ca. 12 mL of medium added to the dish. The lid was placed on the dish and MTS grew over a period of 6 to 9 days at 37 °C and 5% CO₂ in a humidified incubator. Medium was removed from the drops and replaced after 3 days.

9.5 Supporting information - Through Barrier Detection of Ethanol using Handheld Raman Spectroscopy - Conventional Raman versus Spatially Offset Raman Spectroscopy (SORS)

Experimental

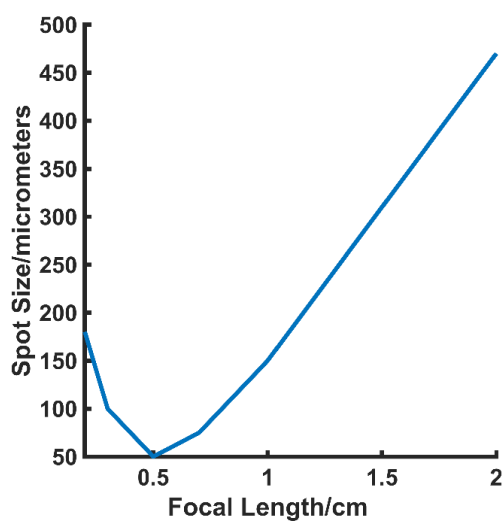


Figure S1 – The influence of focal length on spot size. The instrument in question has a spot size of 50 – 60 microns at a focal distance of 0.5 cm.

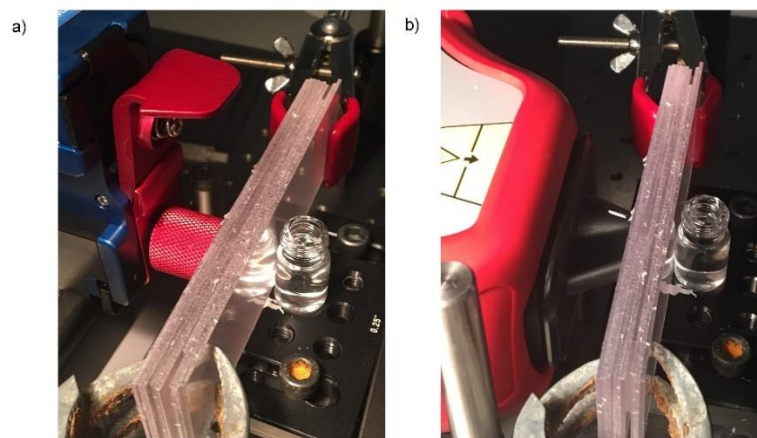


Figure S2 – Experimental set up (a) CR spectrometer with point and shoot adaptor (b) SORS spectrometer with nose cone on.

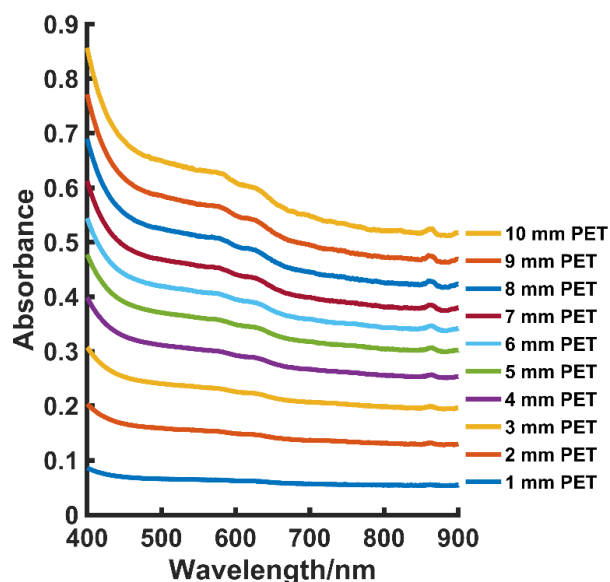


Figure S3 – Stacked absorption spectra of PET. Little difference in absorption is seen at 830 nm and 785 nm. As thickness increases absorbance also increases thus indicating that not all the laser light is being transmitted to the ethanol sample. Performed using an Agilent Cary 60 UV-Vis spectrometer.

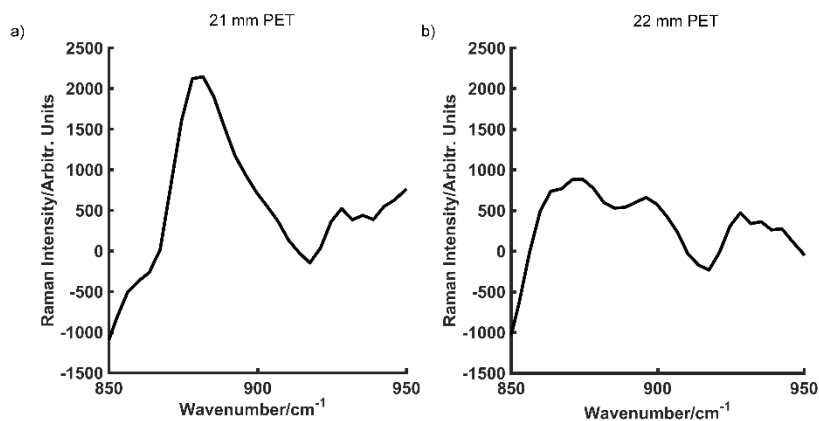


Figure S4 – Scaled subtractions at 21 mm thick PET (a) and 22 mm thick PET (b).

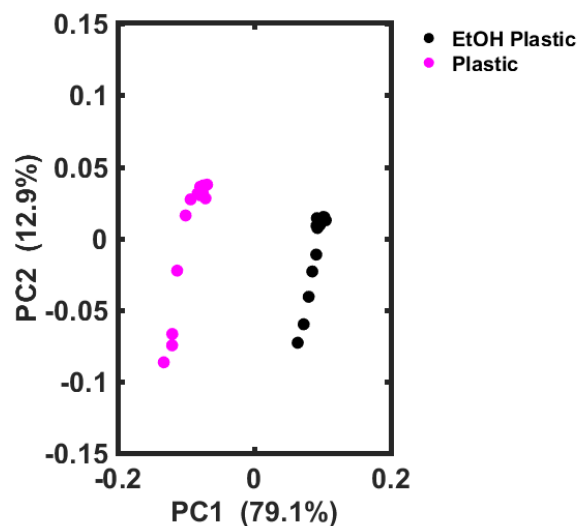


Figure S5 – PCA scores plots at a PP thicknesses of 2 mm.

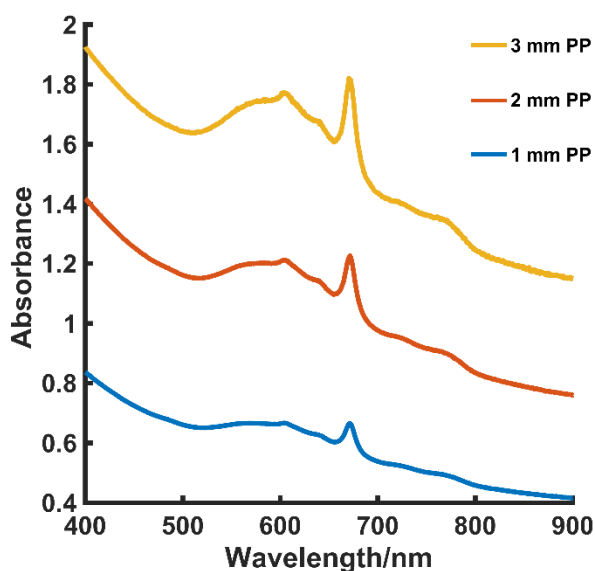


Figure S6– The absorption spectra of blue PP at thicknesses of 1 – 3 mm. The maximum absorption occurs at 670 nm. As expected, when the thickness of PP is increased, absorbance also increases. A shoulder begins to emerge at 767 nm and is most prominent at a thickness of 3 mm. Performed using an Agilent Cary 60 UV-Vis spectrometer.

Using a SORS instrument in a CR mode

CR was performed at 830 nm using the SORS instrument in a CR mode at both the highest and lowest powers (450 mW and 60 mW). Using a CR mode

on the SORS instrument, spectra were taken of ethanol obscured by plastic at each thickness, as well as reference spectra of the plastic of the same thickness. At 450 mW, through barrier detection of ethanol is possible through both plastics (PET and PP) up to thicknesses of 4 mm (Fig. S7 (a,b)). When the laser power is reduced to 60 mW, ethanol detection is achieved up to thicknesses of 3 mm (Fig. S7 (c,d)). Interestingly, the thickness to which ethanol detection takes place at each respective laser power, is the same, i.e. the colour of the plastic does not influence what thicknesses the instrument can detect ethanol through. This is most likely due to the nature of the beam, which it is hypothesised as having a short focal distance, and thus focuses mainly on the barrier. This is ideal for a SORS set up as it ensures maximum discrimination between the signal collected at the surface and that collected at the offset. Such setup is particularly useful in the scanning of plastic bottles, since the thickness of a typical plastic bottle is relatively thin, thus ensuring that the analyte (i.e. the contents inside the bottle) do not contribute to the spectra collected at the zero position (plastic). This is further confirmed when the laser power is increased to 450 mW in a CR mode since increasing the laser power does not considerably increase the thickness to which through barrier detection takes place. In addition, a higher laser power has a greater chance of detecting the analyte, however, this approach also increases the probability of detecting the plastic signal and therefore explains why detection levels are not significantly increased at 450 mW.

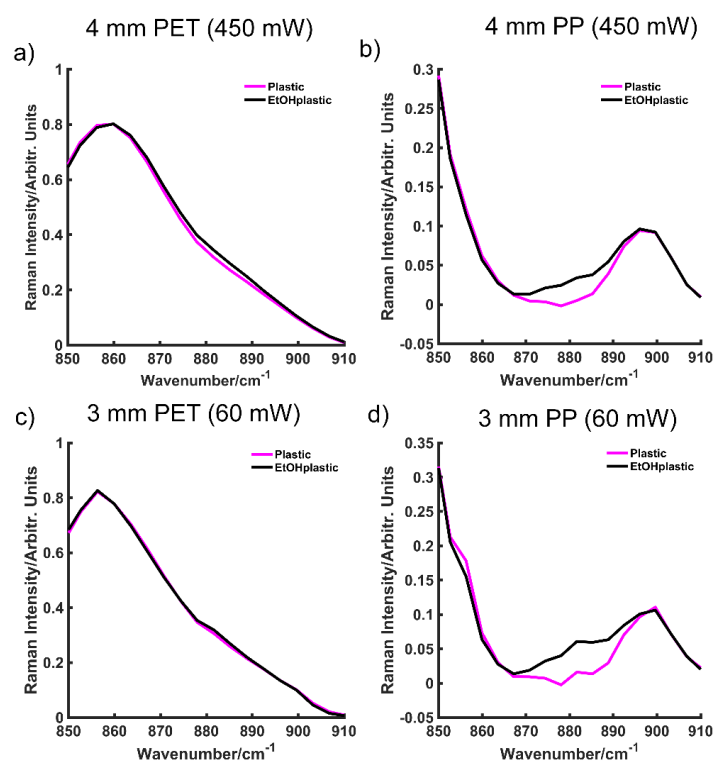


Figure S7 – Detection of ethanol through plastic using the Resolve SORS instrument in a CR mode. At 450 mW, ethanol can be detected up to thicknesses of 4 mm for PET (a) and PP (b). At 4 mm PET, a small shoulder can be seen at 882 cm⁻¹. Similarly, greater spectral intensity can be seen in spectra containing ethanol obscured by 4 mm PP (b) at 882 cm⁻¹. This is also the case when the laser power is lowered to 60 mW, where ethanol detection is possible through 3 mm PET (c) and 3 mm pp (d). Measurements were performed at a laser excitation wavelength of 830 nm with 3 s integration time, 5 accumulations. Spectra were averaged and baselined and normalised.

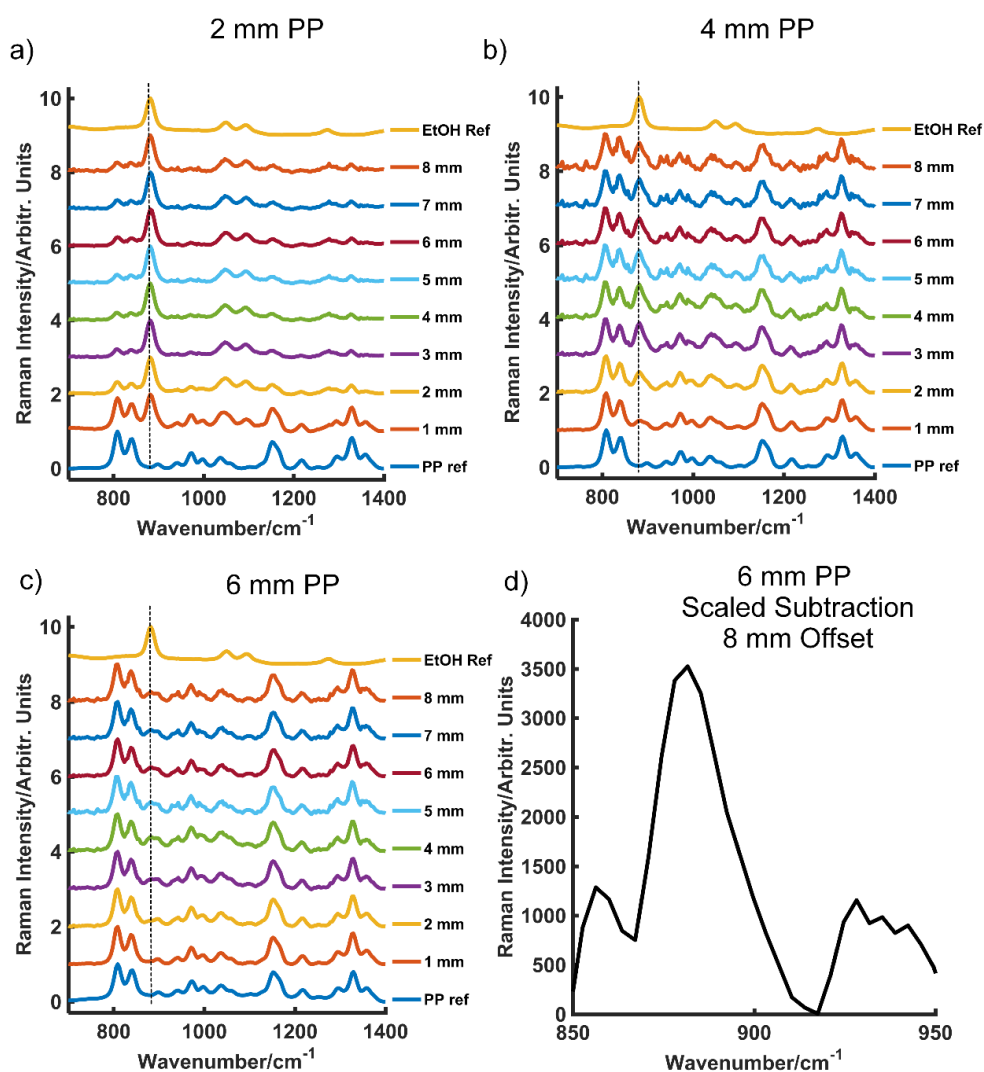


Figure S8 – Normalised, stacked SORS spectra at blue PP thicknesses of 2 mm (a) 4 mm (b) and 6 mm (c) and SORS scaled subtraction at 6 mm thick blue PP (d). The spatial offset was increased from 1 mm to 8 mm in 1 mm increments and the offset spectra recorded. Spectra are normalised and stacked for clarity. As thickness increases, the spatial offset required to obtain the analyte signal (ethanol) also increases. At a thickness of 2 mm ethanol makes a spectral contribution at an offset of 1 mm. At a thickness of 4 mm, ethanol contributes slightly to the spectra at a 1 mm offset. The ethanol specific peak at 882 cm⁻¹ is difficult to distinguish at a thickness of 6 mm however, following a scaled subtraction there is a clear peak at this wavenumber (d). This approach removes the signal obtained at the zero position (plastic) from that acquired at an 8 mm offset (plastic and ethanol).

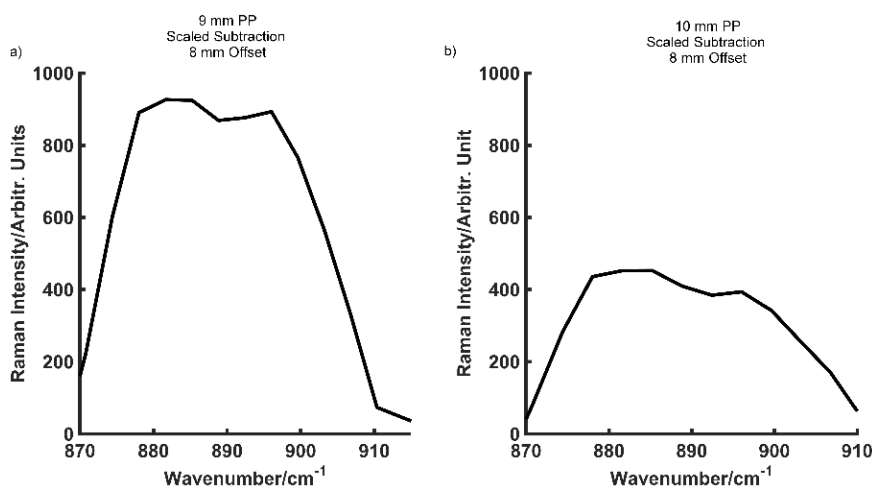


Figure S9 – Scaled subtractions at 9 mm thick blue PP (c) and 10 mm thick blue PP (d).

Reduced laser power SORS

SORS was also performed at 60 mW (the lowest laser power possible), Fig.S10. As before, spectra were collected at the zero position (plastic) and the offset position (EtOH plastic). Ethanol was detected through PET at a thickness of 13 mm and through PP at 6 mm. Since a lower laser power was used, the resulting spectral resolution was lower and thus generated a higher signal to noise ratio, particularly with regards to spectra collected at the offset. As a result, it was difficult to separate the spectra using PCA since the spectra became separated based on variations in noise rather than due to the presence of ethanol in the offset spectra. Therefore, this is the maximum thickness to which ethanol can confidently be detected using SORS at a lower laser power. Nonetheless, despite the use of a slightly higher laser power than what was for CR experiments at 785 nm, the results further demonstrate that the SORS approach has an advantage over CR for through barrier detection.

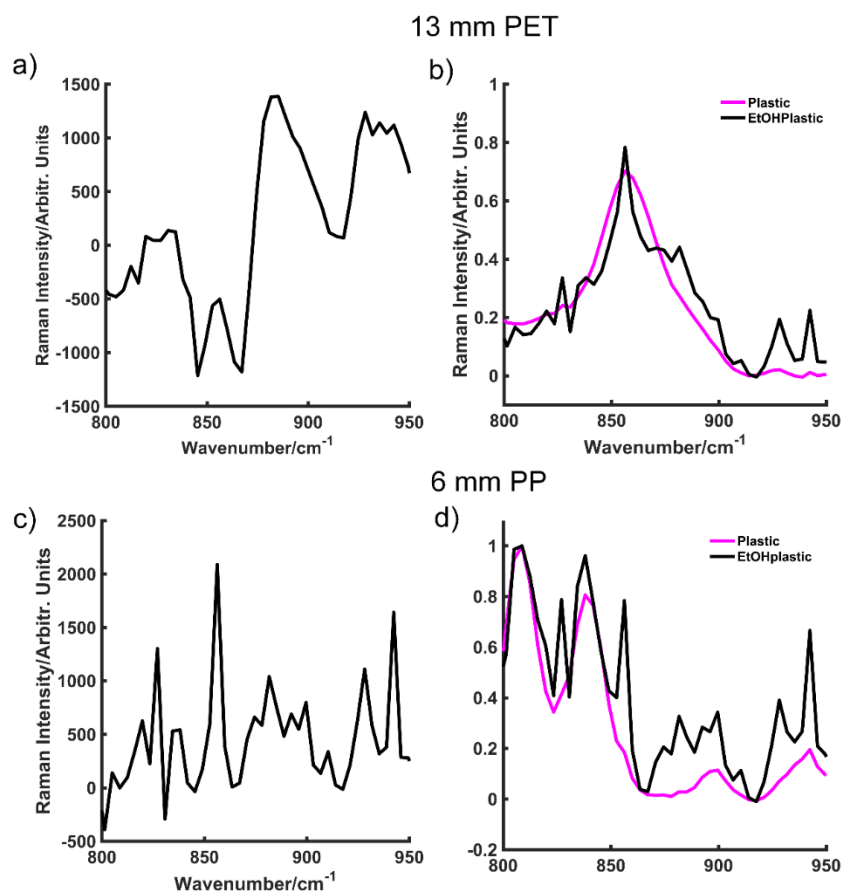


Figure S10 – Scaled subtracted spectra using SORS at 60 mW of 13 mm PET (a) and 6 mm PP (c). Overlaid spectra collected at the zero position (plastic) and 8 mm offset position (EtOHplastic) at thicknesses of 13 mm PET (b) and 6 mm PP (d). The ethanol peak at 882 cm⁻¹ is distinguishable at these thicknesses, both in the scaled subtraction and baseline overlaid spectra.

9.6 Supporting information - Through Tissue Imaging of a Live Breast Cancer Tumour Model Using Handheld Surface Enhanced Spatially Offset Resonance Raman Spectroscopy

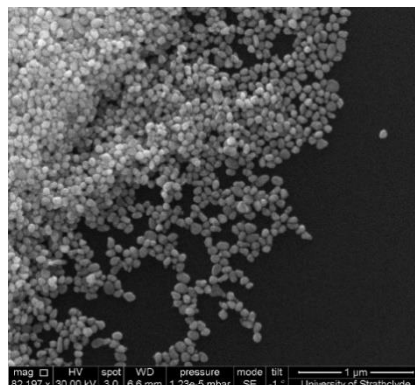


Figure S1 – SEM image of nanoparticles used in SESORS experiments.

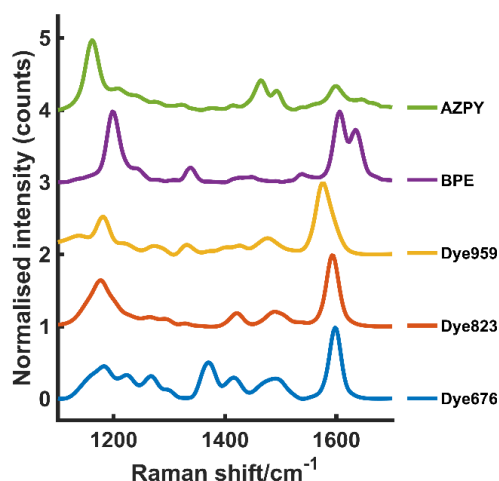


Figure S2 – SERS spectra of the five Raman reporters used in this work. Dyes 676, 823 and 959 are chalcogen based reporters BPE and AZPY are commercially available. Spectra were obtained using the SORS instrument in a conventional Raman mode. Dyes 1 – 3 are resonant at 676, 823 and 959 nm respectively. BPE and AZPY are non-resonant molecules. All measurements were carried out using a 2 s integration time, 5 accumulations, 830 nm laser excitation wavelength.

Experimental set up

Pork loin tissue was obtained from a local butcher and cut into sections (roughly 3.5 cm inches x 4 cm with varying thicknesses). Pork was chosen as

an analogue to human samples due its ability to mimic human tissue greater than that from avian species.⁵ Tissue experiments were performed using either a quartz cuvette or by spotting MTS models directly on to the tissue samples. For measurements involving a cuvette, 350 μL of each NP-Dye solution was pipetted into a Suprasil quartz micro cuvette, path length 1 mm, chamber volume 350 μL . Tissue samples of varying thicknesses were then placed in front of the cuvette. The nose cone was brought into contact with the tissue samples, thus ensuring there was no space between the instrument and the tissue. The set up involving the cuvette is shown in Figure S3.



Figure S3 – Experimental set-up using a handheld SORS spectrometer for the detection of nanotags through tissue. Nanotag solutions were held in a cuvette and the cuvette was placed behind tissue samples. The nose cone was brought into contact with the tissue ensuring there was no space between the tissue sample and the instrument.

For mapping experiments, the MTS models containing the SERRS nanotags were placed directly onto a section of tissue (Figure S4a) and left to equilibrate for 10 mins. Following this, 15 mm of tissue was then placed in on top of the tissue layer containing the MTS models (Figure S4b). The two-layer sample was then brought into contact with the laser via the nose cone. The handheld SORS instrument was positioned above the tissue samples with the laser pointing down onto the tissue (Figure S4b). As shown, in

comparison to previous work involving the cuvette, the tissue section was laid flat on the stage and the handheld instrument mounted above the sample. All measurements were performed using an 8 mm offset. This set up is more representative of an *in vivo* approach compared to that using the cuvette. An x-y-positioning stage was used to enable Raman mapping of the MTS containing SERRS nanotags through 15 mm of tissue. The SORS technique utilises the properties of photon diffusion in turbid media⁶, thus when the scattered photons are returned to the collection probe they will undergo multiple scattering processes and are more likely to migrate laterally. This explains why there is larger area of maximum intensity (compared to actual size of the spheroids). The same principle of diffuse scattering also applies to the laser photons that must reach the MTS models in the first instance.

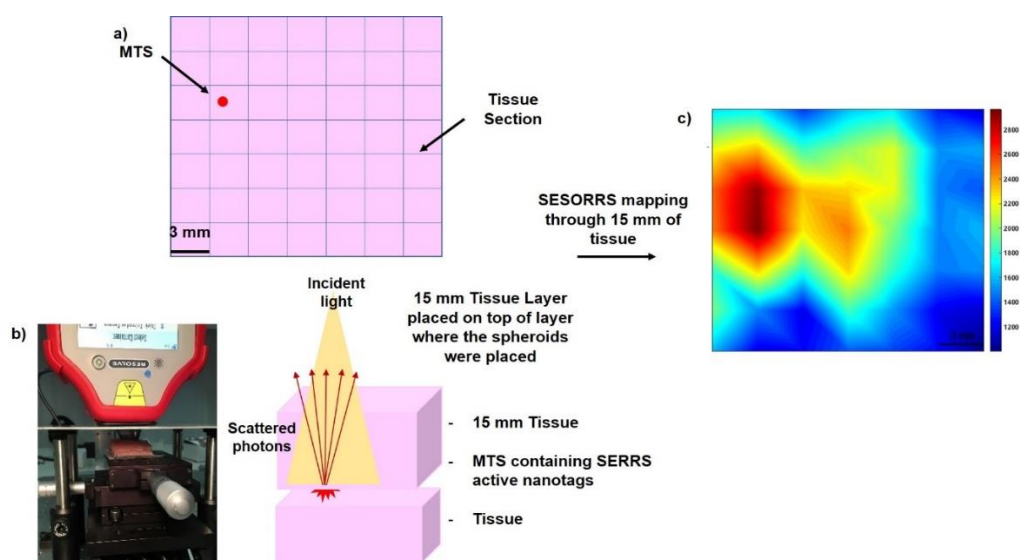


Figure S4 – Correlation of the MTS position on the underlying tissue layer (a,b) to the heat intensity observed in the false colour 2D heat map (c). MTS were placed onto a section of tissue (a). A 15 mm section of porcine tissue was then placed on top of the tissue layer upon which the MTS models were positioned. The experimental set-up involved mounting the instrument above the tissue samples. The sample was then brought into contact with the laser via the nose cone (b). Detection of SERRS nanotags through 15 mm of tissue was measured in a 7 x 7 grid, pixel size 3 mm. All spectra were collected at an 8 mm offset. In the region where the MTS models were present, the largest SERRS intensity is observed (c). The map was constructed using the peak intensity at 1178 cm^{-1} . Measurements were carried out using an xy translational stage in step sizes of 3 mm to create an image of 7 x 7 pixels. This shows the tracking of MTS models through 15 mm of tissue. All measurements were carried out using a 2 s integration time, 5 accumulations, 830 nm laser excitation wavelength.

Data processing

All spectra were processed using Matlab software (Version 2017a, The MathWorks, Natrick, MA, USA). Preprocessing involved truncating and baselining the spectra. A scaled subtraction was also applied in some instances. Briefly spectra were truncated and baselined. Following this, the surface spectrum (i.e. the signal detected at the zero position) was removed from the subsurface spectrum (i.e. signal detected at the offset position) using a scaled subtraction. Data was subsequently smoothed using Savitzky-Golay filtering. Mapping experiments were performed using an x-y positioning stage to enable Raman mapping of the SERRS nanotags through 15 mm of tissue. All measurements were performed using a 8 mm offset. Spectra were truncated, baselined and smoothed using Savitzky-Golay filtering before the intensity at 1178 cm^{-1} at each of the 3 mm steps was plotted as a combination surface/contour false colour 2D heat map.

A scaled subtraction was applied (Figure S5) which aims to show the presence of the analyte obscured by the barrier. The scaled subtraction removed the spectral contribution from the tissue and revealed the peaks at 1178 cm^{-1} and 1592 cm^{-1} , characteristic of resonant dye 823. This further demonstrates the detection of dye 823 through 25 mm of tissue using SESORRS in a back-scattering configuration.

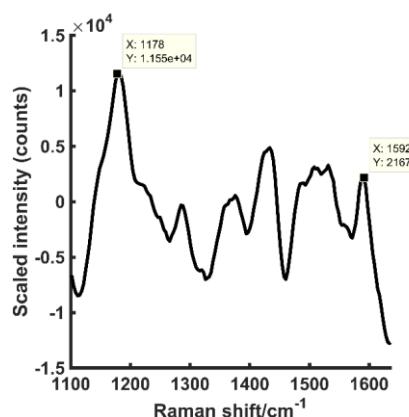


Figure S5. The tracking of dye 823 nanotag solution through 25 mm of tissue following a scaled subtraction. The peaks at 1178 cm^{-1} and 1592 cm^{-1} are revealed. This approach removes signal collected at the zero position (tissue) from that collected at the 8 mm offset (tissue and dye). All measurements were carried out using a 2 s integration time, 5 accumulations, 830 nm laser excitation wavelength.

References

- 1 W. Leng, P. Pati and P. J. Vikesland, *Environ. Sci. Nano*, 2015, **2**, 440–453.
- 2 M. A. Bedics, H. Kearns, J. M. Cox, S. Mabbott, F. Ali, N. C. Shand, K. Faulds, J. B. Benedict, D. Graham and M. R. Detty, *Chem. Sci.*, 2015, **6**, 2302–2306.
- 3 H. Kearns, M. A. Bedics, N. C. Shand, K. Faulds, M. R. Detty and D. Graham, *Analyst*, 2016, **141**, 5062–5065.
- 4 S. Harmsen, M. A. Bedics, M. A. Wall, R. Huang, M. R. Detty and M. F. Kircher, *Nat. Commun.*, 2015, **6**, 6570.
- 5 N. Stone, K. Faulds, D. Graham and P. Matousek, *Anal. Chem.*, 2010, **82**, 3969–3973.
- 6 P. Matousek and N. Stone, *Chem. Soc. Rev.*, 2016, **45**, 1794–1802.

9.7 Supporting information - Multiplex Imaging of Live Breast Cancer Tumour Models Through Tissue Using Handheld Surface Enhanced Spatially Offset Resonance Raman Spectroscopy (SESORRS)

Experimental set up

Pork loin tissue was obtained from a local butcher and cut into sections (roughly 3.5 cm inches x 4 cm with varying thicknesses). Tissue experiments were performed using either a quartz cuvette or by spotting the MTS models directly on to the tissue samples.

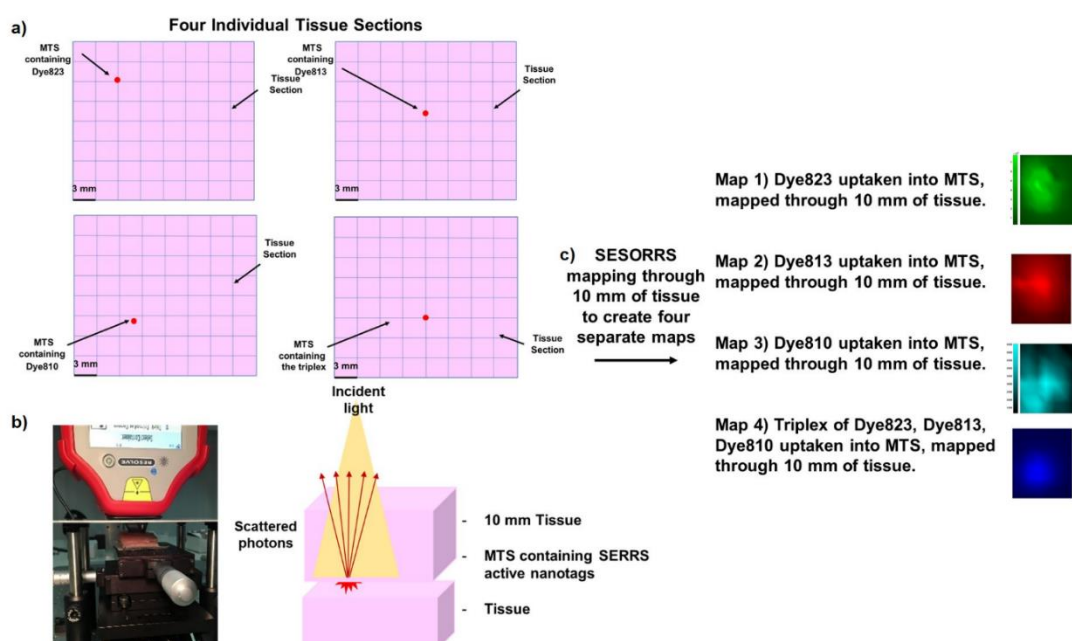


Figure S1 – MTS containing either the single nanotags (dye823, dye813 and dye810) or the triplex of the three SERS nanotags were placed onto four separate sections of tissue (a). A 10 mm section of porcine tissue was then placed on top of each of the tissue layers upon which the MTS models were positioned. The experimental set-up involved mounting the instrument above the tissue samples. The samples were then brought into contact with the laser via the nose cone (b). Detection of each of the four MTS models containing the varying SERS nanotags (single nanotags or triplex) through 10 mm of tissue was measured in a 8 x 8 grid, pixel size 3 mm. This created four individual SERS heat intensity maps (c). Measurements were carried out using an xy translational stage in step sizes of 3 mm to create an image of 7 x 7 pixels. This shows the tracking of MTS models through 15 mm of tissue. All measurements were carried out using a 2 s integration time, 5 accumulations, 830 nm laser excitation wavelength.

For measurements involving a cuvette, 350 μL of each NP-Dye solution was pipetted into a Suprasil quartz micro cuvette, path length 1 mm, chamber volume 350 μL . Tissue samples of varying thicknesses were then placed in front of the cuvette. The nose cone was brought into contact with the tissue samples, thus ensuring there was no space between the instrument and the tissue. The set up involving the cuvette is shown in Figure S2.



Figure S2 - Experimental set-up using a handheld SORS spectrometer for the detection of nanotags through tissue. Nanotag solutions were held in a cuvette and the cuvette was placed behind tissue samples. The nose cone was brought into contact with the tissue to ensure there was no space between the tissue sample and the instrument.

Data processing

All spectra were processed using Matlab software (Version 2017a, The MathWorks, Natick, MA, USA). Pre-processing involved truncating and baselining the spectra. Mapping experiments were performed using an x-y positioning stage to enable Raman mapping of the SERRS nanotags through 15 mm of tissue. All measurements were performed using an 8 mm offset. Spectra were truncated, baselined and smoothed using Savitzky-Golay filtering before the intensity at 1178 cm^{-1} (dye823) 1181 cm^{-1} (dye813), 1185 cm^{-1} (dye810) and 1181 cm^{-1} (triplex) was plotted as a combination surface/contour false colour 2D heat map.

Principal component analysis (PCA) was applied to develop a multiplexed imaging technique. The solution multiplex was performed by collecting 15 spectra (5 replicates, 3 samples) through 10 mm of tissue of each of the four nanotag solutions, i.e. dye823, dye813, dye810 and the triplex containing the three dyes. PCA was performed on spectra obtained at an offset of 8 mm through 10 mm of tissue. The same was applied for the multiplex detection of MTS models through 10 mm of tissue. 15 spectra were collected at the point where the MTS models containing each of the four nanotag solutions, i.e. dye823, dye813, dye810 and the triplex containing the three dyes was located. The spectra collected at an 8 mm offset through 10 mm of tissue was then used to perform PCA. Pre-processing involved truncating and scaling the spectra, before applying the first order derivative coupled with Savitzky-Golay smoothing. The first order derivative was used in PCA to remove slight variances in the background which were found to affect the resulting zero order PCA scores plots.⁵

References

- 1 W. Leng, P. Pati and P. J. Vikesland, *Environ. Sci. Nano*, 2015, 2, 440–453.
- 2 M. A. Bedics, H. Kearns, J. M. Cox, S. Mabbott, F. Ali, N. C. Shand, K. Faulds, J. B. Benedict, D. Graham and M. R. Detty, *Chem. Sci.*, 2015, 6, 2302–2306.
- 3 H. Kearns, M. A. Bedics, N. C. Shand, K. Faulds, M. R. Detty and D. Graham, *Analyst*, 2016, 141, 5062–5065.
- 4 S. Harmsen, M. A. Bedics, M. A. Wall, R. Huang, M. R. Detty and M. F. Kircher, *Nat. Commun.*, 2015, 6, 6570.
- 5 H. J. Butler, L. Ashton, B. Bird, G. Cinque, K. Curtis, J. Dorney, K. Esmonde-white, N. J. Fullwood, B. Gardner, P. L. Martin-Hirsch, M. J. Walsh, M. R. Mcainsh, N. Stone and F. L. Martin, *Nat. Protoc.*, 2016, 11, 664–687.

9.8 Supporting information - Point and Shoot – The Benefit of Resonant Raman Reporters for Probing Through Plastic and Tissue Barriers Using Handheld Surface Enhanced Raman Spectroscopy (SERS)

Experimental

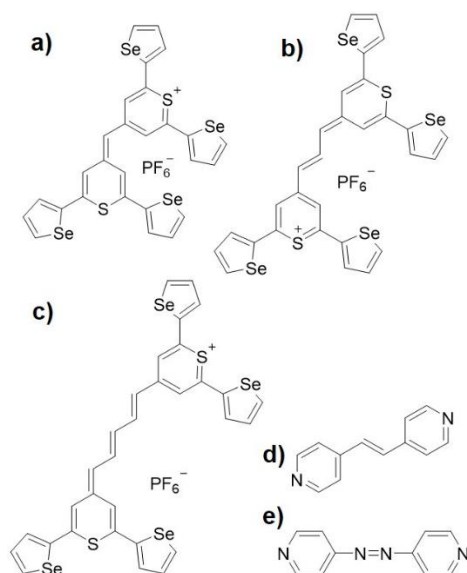


Figure S1 – Chemical structure of dye 676 (a), dye 823 (b), dye 959 (c), BPE (d) and AZPY (e)

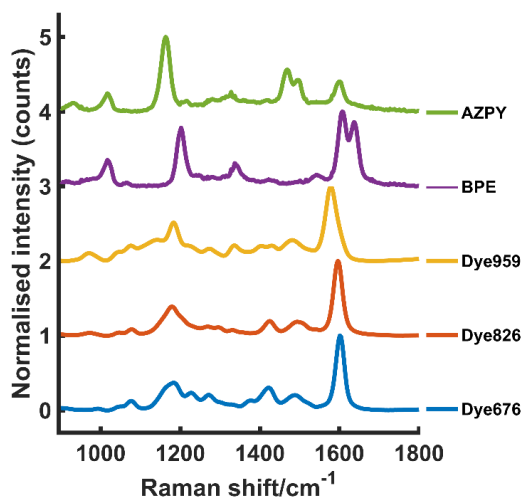


Figure S2 – SERS spectra of dye 676, dye 823, dye 959, BPE and AZPY. Reference SERS measurements of the unobscured nanotags were performed using a handheld CBEx instrument from Snowy Range Instruments, 785 nm wavelength, 1 s acquisition.

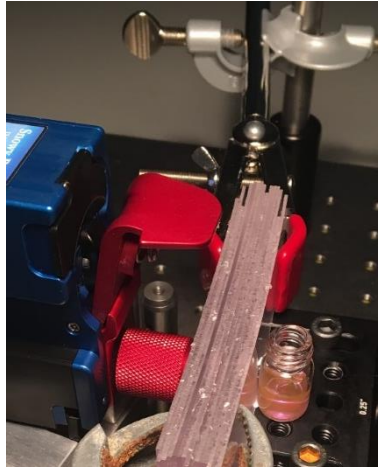


Figure S3 – Experimental set up. The point and shoot adaptor was brought into contact with the plastic barrier and the nanotags placed behind the plastic in a vial.



Figure S4 – Experimental set up involving the tracking of nanotags through tissue. The nanotags were held in a microcuvette and obscured by the tissue. The point and shoot adaptor was used to bring the tissue into contact with the instrument, thus ensuring there was no space between the tissue and the instrument.

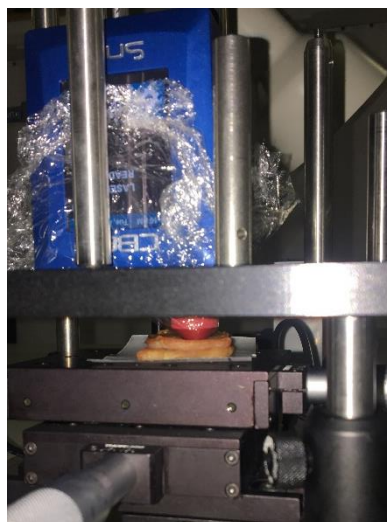


Figure S5 – Mapping of SERRS nanotags through 5 mm of tissue. The experimental set-up involved mounting the instrument above the tissue samples. The sample was then brought into contact with the laser via the point and shoot adaptor. MTS models containing the SERRS active nanotags were also placed onto a section of tissue. They were then obscured by a sample of tissue with a thickness of 5 mm. Using an x-y translational stage, the SERRS nanotags were mapped through 5 mm of tissue (10 × 10 grid, step size 1 mm).

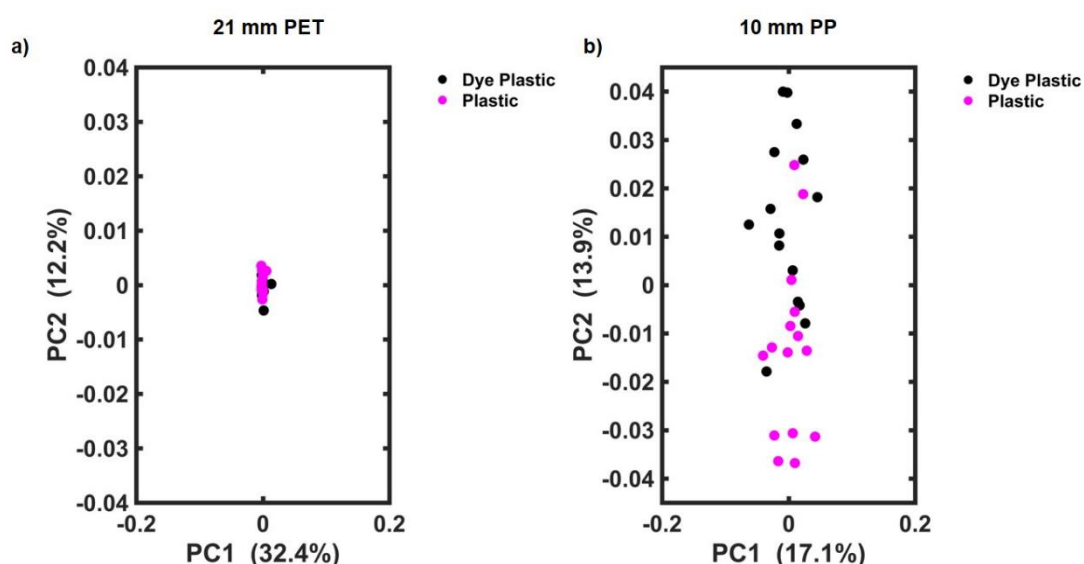


Figure S6 – PCA scores plots of the tracking of dye823 through 21 mm of clear PET and 10 mm of blue PP using a handheld conventional Raman instrument. In both instances, the pink clusters refer to plastic reference spectra at a given thickness (e.g. 21 mm), and the black cluster refers to a solution of dye 823 nanotags obscured by the same thickness of plastic (e.g. 21 mm). In both instances (PET and PP), no separation is seen in the scores plots across both PC1 and PC2 which have the maximum variance. Thus, the instrument is no longer capable of detecting a solution of dye 823 nanotags at thicknesses of 21 mm of PET and greater as well as thicknesses equal to and greater than 10 mm of blue PP.

9.9 Supporting information - Towards establishing a minimal nanoparticle concentration for applications involving surface enhanced spatially offset Raman spectroscopy (SESORS) *in vivo*

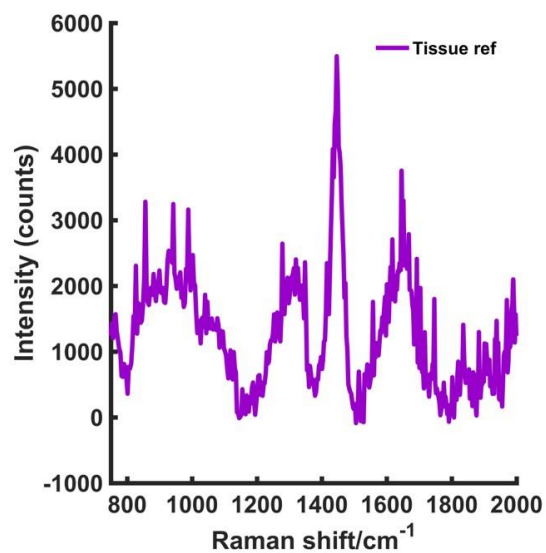


Figure S1 – Reference spectra of the tissue, with no nanotags behind, collected at an 8 mm offset. All measurements were carried out using a 2 s integration time, 5 accumulations, 830 nm laser excitation wavelength.

10 Publications and Presentations

Oral Presentations

1. *Tracking of Reporter Functionalised Nanoparticles in Tissue using Handheld Surface Enhanced Spatially Offset Raman Spectroscopy*, WestCHEM Research Day, University of Glasgow, UK, Dec 2017 (**Best Oral Presentation**)
2. *Tracking of Reporter Functionalised Nanoparticles in Tissue using Handheld Surface Enhanced Spatially Offset Raman Spectroscopy (SESORS)*, SciX 2017, Reno, USA, Oct 2017 (**Wiley Raman Student Award**)
3. *Through Barrier Detection Using Surface Enhanced Spatially Offset Raman Spectroscopy (SESORS)*, University of Strathclyde Bionanotechnology and Analytical Section Meeting, Glasgow, Aug 2017
4. *The Development and Applications of Surface Enhanced Spatially Offset Raman Spectroscopy*, SciX 2016, Minneapolis, USA, Sept, 2016

Poster Presentations

1. *Tracking of Reporter Functionalised Nanoparticles in Tissue using Handheld Surface Enhanced Spatially Offset Raman Spectroscopy (SESORS)*, Faraday Discussion on SERS, University of Strathclyde, UK, Aug 2017 – (**Selected for Flash Presentation**)
2. *Through Barrier Detection Using Portable Surface Enhanced Spatially Offset Raman Spectroscopy (SESORS)*, RSC Analytical Research Forum (ARF), Burlington House, London, UK, July 2017 – (**Prize Winner**)
3. *The Development and Applications of Surface Enhanced Spatially Offset Raman Spectroscopy*, IRDG 214 and 14th Martin and Willis Prize meeting, Sheffield Hallam University, UK, Sept 2016
4. *The Development and Applications of Surface Enhanced Spatially Offset Raman Spectroscopy*, RSC Early Careers Symposium, University of Strathclyde, UK, June 2016

Peer Reviewed Publications

1. "Through Barrier Detection of Ethanol – Conventional Raman versus Spatially Offset Raman Spectroscopy (SORS)"
F. Nicolson, L.E. Jamieson, S. Mabbott, N.C. Shand, D. Graham and K. Faulds, *J. Raman Spectrosc.*, **48**, 1828–1838
2. "Through Tissue Imaging of a Live Breast Cancer Tumour Model Using Handheld Surface Enhanced Spatially Offset Resonance Raman Spectroscopy"
F. Nicolson, L.E. Jamieson, S. Mabbott, K. Plakas, N.C. Shand, M.R. Detty, D. Graham, and K. Faulds, *Chem. Sci.*, 2018, **9**, 3788-379
3. "Multiplex Imaging of Live Breast Cancer Tumour Models Through Tissue Using Handheld Surface Enhanced Spatially Offset Resonance Raman Spectroscopy (SESORRS)" **F. Nicolson**, L.E. Jamieson, S. Mabbott, K. Plakas, N.C. Shand, M.R. Detty, D. Graham, and K. Faulds, *Chem. Commun.*, 2018, **54**, 8530-8533